Public

Report

Document ID	Version	Status	Reg no	Page
1469524	1.0	Approved		1 (81)
Author Jan Hernelind/5T Engineering AB			Date 2015-02-24	
Reviewed by Lisette Åkerman (QA)			Reviewed date 2015-02-27	
Approved by Jan Sarnet			Approved date 2015-02-27	

Modelling and analysis of BWR-canister and buffer for earthquake induced rock shear with copper corrosion

Overview

This report is one in a series of reports that together address the response of the buffer and the canister in a KBS-3 repository to shear movements in fractures intersecting deposition holes. In this report the main focus is the copper shell and how stresses and strains are affected if the thickness is reduced to half of the thickness in the reference design.

Rock shear movements to analyse are given as design requirements derived from previous safety assessments. Mechanical properties of the buffer are determined in laboratory tests that are interpreted into a buffer material model with parameter values for the calculations. Mechanical data for the canister insert and copper shell are obtained from laboratory tests yielding canister material models.

The mechanical impact on the buffer and on the canister insert and copper shell by shear movements are determined by finite element modelling. The calculated canister stresses and strains are propagated to *i*) an assessment of plastic deformation against failure criteria for the copper shell, *ii*) an analysis of the damage tolerance of the insert and *iii*) an assessment of the margin to global collapse of the insert.

Abstract

Existing fractures crossing a deposition hole may be activated and sheared by an earthquake. The effect of such a rock shear has been investigated by finite element calculations.

The buffer material in a deposition hole acts as a cushion between the canister and the rock, which reduces the effect of a rock shear substantially. Lower density of the buffer yields softer material and reduced effect on the canister. However, at the high buffer density that is suggested for a repository the stiffness of the buffer is rather high. The stiffness is also a function of the rate of shear, which means that there may be a substantial damage on the canister at very high shear rates.

In this theoretical study the impact of rock shear is studied for a copper shell thickness of 2.5 cm. The rock shear has been modelled with finite element calculations with the code ABAQUS. A three-dimensional finite element mesh of the buffer and the canister has been created and simulation of a rock shear has been performed.

The rock shear is assumed to be perpendicular to the canister axis at either 90% of the insert height or at the insert steel lid. According to previous reports (SKBdoc 1339902 and 1403930), this is the shear positions that provide the greatest impact on the copper shell.

The shear calculations have been driven to at least a total shear of 5 cm and more if possible without convergence difficulties.

Svensk Kärnbränslehantering AB
Swedish Nuclear Fuel and Waste Management Co
PO Box 925, SE-572 29 Oskarshamn
Visiting address Gröndalsgatan 15
Phone +46-491-76 79 00 Fax +46-491-76 79 30
www.skb.se
556175-2014 Seat Stockholm

In accordance with current design criteria for the canister, plastic strain in the copper shell was used as a failure mechanism and criterion when evaluating the results.

The conclusion is that the canister will maintain its mechanical integrity for the shear load case even with half of the copper shell thickness, i.e. a thickness of 2.5 cm.

Sammanfattning

Befintliga sprickor som skär deponeringshål kan aktiveras och skjuvas genom ett jordskalv. Inverkan av en sådan bergskjuvning har analyserats med finita element beräkningar.

Bentonitbufferten i ett deponeringshål fungerar som en kudde mellan kapseln och berget, vilken avsevärt reducerar inverkan av en bergskjuvning - ju lägre densitet desto mjukare buffert och desto mindre påverkan på kapseln. Vid de höga densiteter som föreslås för bufferten i ett slutförvar är den däremot ganska styv. Styvheten är också en funktion av skjuvhastigheten, vilket medför att kapseln kan skadas avsevärt vid mycket höga skjuvhastigheter.

Denna rapport redovisar resultat från beräkningar av effekten av skjuvning på en kapsel med ett 2.5 cm tjockt kopparhölje Bergskjuvningen har modellerats och beräknats med finita-element-koden ABAQUS. Ett tredimensionellt elementnät som modellerar bufferten och kapseln har skapats och simulering av bergskjuvningar har utförts.

Bergskjuvningen antas ske vinkelrätt mot kapselaxeln antingen vid 90 % av insatsens höjd eller vid insatsens stållock. Enligt tidigare analyser (SKBdoc 1339902 respektive 1403930) är detta de skjuvpositioner som ger den största påverkan på koppahöljet.

Skjuvberäkningarna har genomförts för en total skjuvrörelse upp till minst 5 cm och mer om inte konvergensproblem uppstått.

I enlighet med gällande konstruktionsförutsättningar för kapseln har plastisk töjning i kopparhöljet använts som kriterium vid utvärdering av resultaten.

Slutsatsen är att kopparhöljet kommer att vidmakthålla sin mekaniska integritet för skjuvlastfallet även vid halverad tjocklek på kopparhöljet, det vill säga för en tjocklek på 2,5 cm.

Contents

1 Introduction

1.1 Background

The Swedish Radiation Safety Authority (SSM) has in a letter (SSM 2014) requested additional analyses concerning the impact on the canister of the combination of copper shell corrosion and rock shear.

The Design analysis of the canister is based on the canister reference geometry, described for example in section 5 of Raiko et al. (2010). In section 7.6 of Raiko et al. (2010) an uncertainty analysis of the deformation in the copper shell during shear load is presented. This uncertainty analysis does not address the case of a copper wall thickness less than the reference design. SSM consider that SKB should supplement the investigation with an uncertainty analysis for different thicknesses of the copper shell when the shear load occurs. The uncertainty analysis should evaluate different copper wall thicknesses <5 cm to illustrate how the integrity of the copper shell can be maintained for the combination of corrosion and shear load.

The purpose of this study is to analyse the impact of rock shear for a reduced thickness of the copper shell in order to respond to the request by SSM.

According to the design premises set out by SKB, see Table 1-1 in SKB (2010), the copper corrosion barrier should remain intact after a 5 cm shear movement at a velocity of 1 m/s for buffer material properties of a Ca-bentonite with the saturated density 2,050 kg/m^3, for all locations and angles of the shearing fracture in the deposition hole, and for temperatures down to 0°C. The insert should maintain its pressure-bearing properties to isostatic loads.

Based on the design premises, a potential failure mechanism for the canister is fractures in the copper shell due to excessive plastic deformation. The design criterion is that the effective strain should not exceed 80 % in the copper shell according to Raiko et al. (2010, Section 3.3). Therefore, this study focuses on evaluating this failure criterion for the corroded copper shell.

1.1.1 Context of this report

To illustrate the impact of a corroded copper canister, a copper thickness of 2.5 cm is applied in the calculations in this report. This is half of the reference design thickness of 5 cm. This reduced thickness was chosen to provide sufficient response in the investigations since the postulated reduction is significant.

A sequence of analyses has previously been performed for earthquake induced rock shear. The analyses “Shearing of copper canister at top and base” (SKBdoc 1403930) and “Global simulation of copper canister-final deposition” (SKBdoc 1339902) were identified as the most severe cases for the copper shell and were, therefore, employed for this investigation. The horizontal shear plane at 90 %-distance from the base of the insert was identified as the position that provide the greatest impact on the copper shell (SKBdoc 1339902). However, shearing at the insert lid also leads to significant plastic deformation in the copper shell (SKBdoc 1403930).

One important function of the buffer material in a deposition hole in a repository for nuclear waste disposal is to reduce the damage of rock movements on the canister. The worst case of rock movements is a very fast shear that takes place along a fracture and occurs as a result of an earthquake.

The consequences of such rock shear have been investigated earlier, both by laboratory tests (laboratory simulations in the scale 1:10) (Börgesson et al. (2003) and finite element modelling (Börgesson and Hernelind 2006, Börgesson et al. 1995). Those investigations were focussed on a base case with a horizontal shear plane and Na-bentonite as buffer material.

Since it is very probable that the Na-bentonite will be transformed to Ca-bentonite or that Ca-bentonite might be used as buffer material, the calculations are based on material properties of Ca-bentonite instead of Na-bentonite.

2 Geometry definitions and meshes

2.1 General

The geometry used for the analyses of earthquake induced rock shear consists of the insert (made of nodular cast iron), the insert lid (made of steel) and the copper shell surrounded by buffer material (bentonite). The geometry is based on CAD-geometries received from SKB "Ritningsförteckning för kapselkomponenter" (SKBdoc 1203875) and should therefore correspond to the current design.

Due to symmetry only one half of the system has been modelled. The mesh is then generated by 3-dimensional solid elements, mainly 8-noded hexahedral (most of them using full integration technique) and a few 6-noded wedge.

The model size is defined by about 325,000 elements and 431,000 nodes (total number of variables about 1,094,000).

A sequence of quasi static analyses has been performed studying the effect of reduced copper shell thickness (the analysis is performed assuming that the copper shell thickness is half of the reference design thickness). Also two different material models for copper have been compared.

Two shearing planes are used for rock shear perpendicular to the axis of the canister, one at 90% of the insert height and one at the insert lid, Figure 2-1. Figure 2-2 shows detail of the mesh at the insert upper corner.

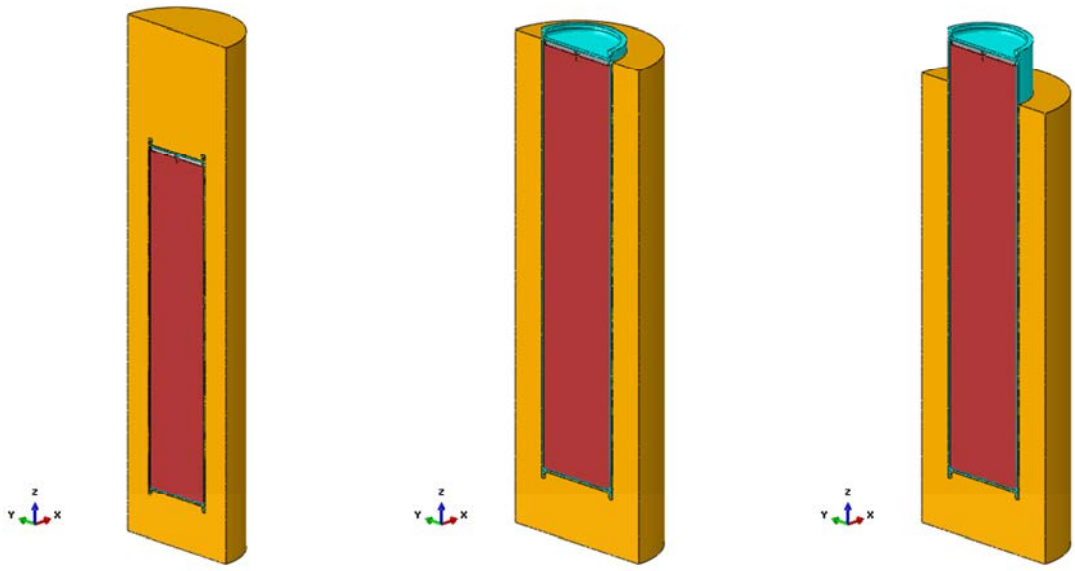

Figure 2-1. *Geometry for rock shear perpendicular to the axis of the canister (left), bentonite removed for illustration purposes above shearing at the lid (mid) and bentonite removed for illustration purposes above shearing at 90 % height of the insert (right).*

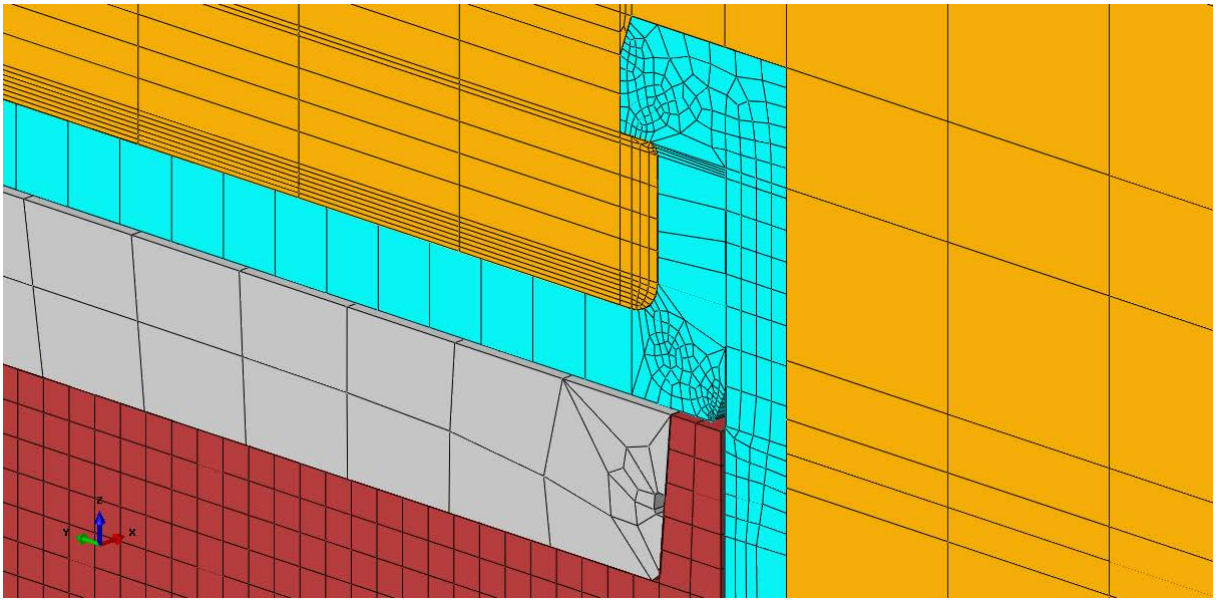

Figure 2-2. *Details of the top corner showing bentonite (orange), copper shell (cyan), insert lid (grey) and insert (red).*

2.2 Geometry of parts

2.2.1 Deposition hole

The model of the deposition hole has a diameter of 1.75 m and a length of 6.9 m. The canister is placed about 0.5 m above the bottom and about 1.5 m below the top of the deposition hole. Buffer material (bentonite) surrounds the canister and will fill out the deposition hole. The rock shear is then simulated by prescribing boundary conditions at the buffer envelope.

2.2.2 Insert (BWR)

The insert is made of nodular cast iron and has been simplified regarding the square tubes which are assumed to be tied to the cast iron insert and thus these contribute as added material to the insert. This simplification will probably overestimate stresses and strains in this region.

The insert is modelled as one part including the steel channels with 3D solids, see Figure 2-3.

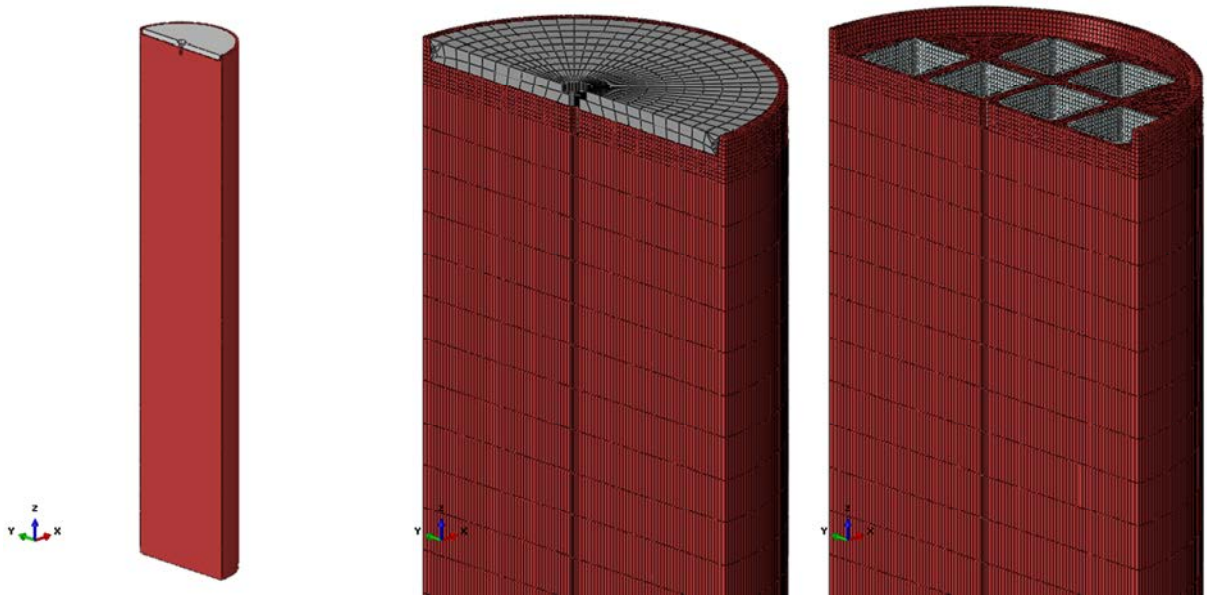

Figure 2-3. *Insert BWR geometry (left), mesh with insert lid (mid) and without insert lid (right).*

2.2.3 Insert lid

The insert lid is made of steel and is modelled with 3D solids, see Figure 2-4.

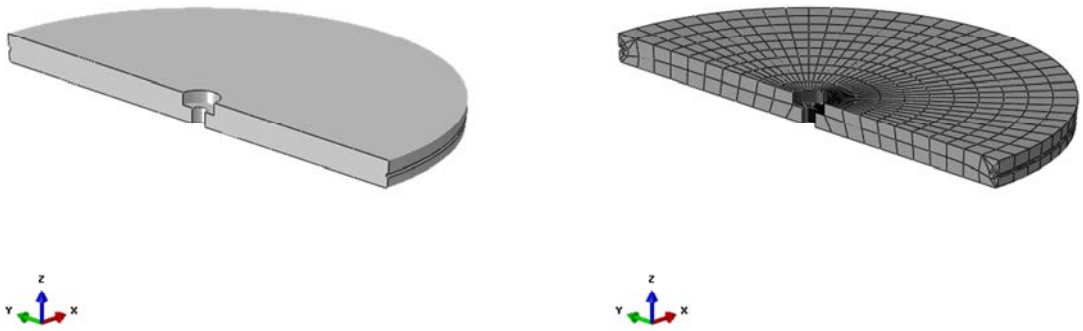

Figure 2-4. *Insert lid geometry (left) and mesh (right).*

2.2.4 Copper shell

The copper shell surrounds the insert and interacts with the buffer and the insert. The canister has been modelled rather accurately in order to catch “hot spots” where large strains are expected, e.g. the fillets at the base and top (the lid). The lid is welded to the flange and lid and canister will act as one part, see Figure 2-5. The copper shell wall thickness of 2.5 cm is applied in this report.

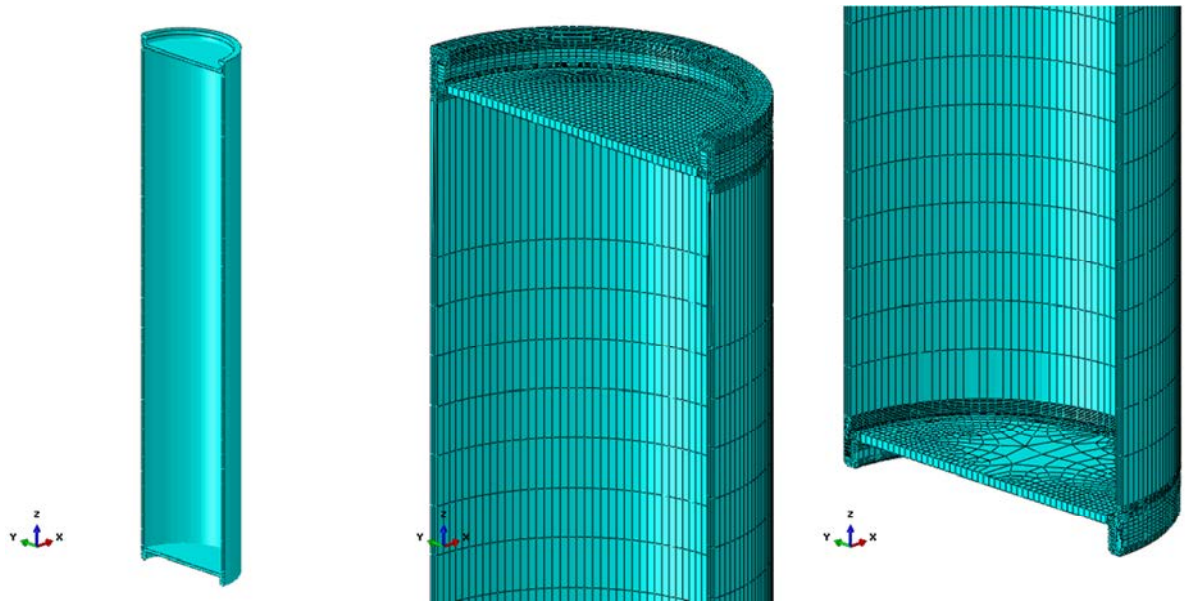

Figure 2-5. *Copper shell geometry (left), mesh top (mid) and mesh base (right).*

2.2.5 Buffer (Bentonite)

The copper shell is surrounded by the buffer made by Ca-bentonite with density 2050 kg/m^3.The buffer interacts with the copper shell. The shearing zones have been modelled with 20 cm thickness, see Figure 2-6.

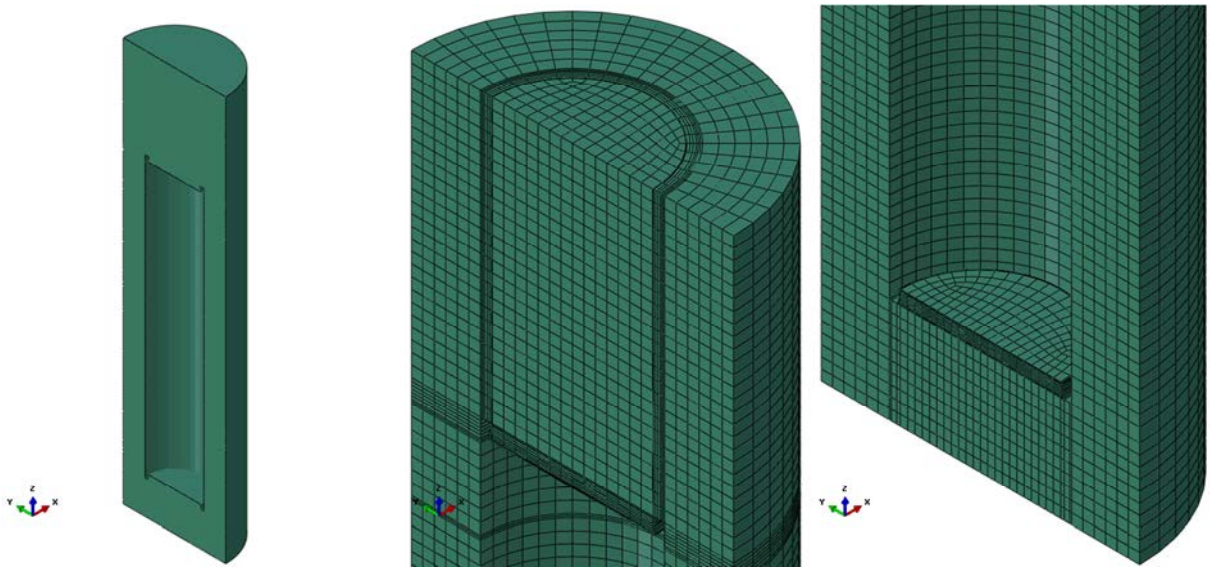

Figure 2-6. *Buffer geometry (left), mesh top (mid) and mesh base (right).*

3 Material models

The finite element code ABAQUS was used for the calculations. The materials have been modelled as elastic-plastic with stress-strain properties that correspond to each material and the applied shear load induced strain rate, when applicable.

All analyses have the same material model for the buffer, steel channels and insert lid. The insert has the same material properties as in previous calculations (Hernelind 2010) except for the reference models (SKBdoc 1339902) where the yield surface is about 10% higher. Since this study focus on the copper shell and the copper has low yield stress and the nodular cast iron in the insert essentially has an elastic response, this difference have marginal influence on the copper shell response.

For the copper shell, the same material model is used as in previous calculations (Hernelind 2010) except for the analyses where this material model is compared with the material model suggested by Unosson (SKBdoc 1393179).

3.1 Nodular cast iron (used for the insert)

The material model for the nodular cast iron, "Dragprovning av gjutjärn" (SKBdoc 1201865) is based on elastic behaviour defined by Young's modulus and the Poisson's ratio. The plastic behaviour is defined through von Mises yield surface (true stress) versus plastic strain (using logarithmic strain), see Table 3-1 and Figure 3-1.

The experiments were performed at 0^{o} C.

Table 3-1. True stress-true strain definition for the insert.

Plastic strain (%)	Stress (MPa) Strain rate= 0 1/s	Stress (MPa) Strain rate= 2×10^{-4} 1/s	Stress (MPa) Strain rate= 0.5 1/s	Strain rate factor (--) at strain rate= 0.5 1/s
0	293	293	348	1.19
1	324	324	367	1.13
2	349	349	385	1.10
3	370	370	406	1.10
4	389	389	423	1.09
5	404	404	438	1.09
6	418	418	451	1.08
7	428	428	464	1.08
8	438	438	474	1.08
9	447	447	483	1.08
10	456	456	490	1.07
11	465	465	498	1.07
12	472	472	504	1.07
13	478	478	510	1.07
14	484	484	516	1.07
15	488	488	520	1.07

The strain rate dependency is defined by assuming that the yield surface is proportional to the strain rate factor (at the strain rate 0.5 1/s the factor 1.08 has been chosen and at strain rate 0 1/s the factor is 1.0).The instantaneous strain rate factor is then linearly interpolated between 1 and 1.08 using the instantaneous strain rate.

Furthermore, Young's modulus E = 166 GPa and Poisson's ratio $\nu = 0.32$ (Raiko et al. 2010).

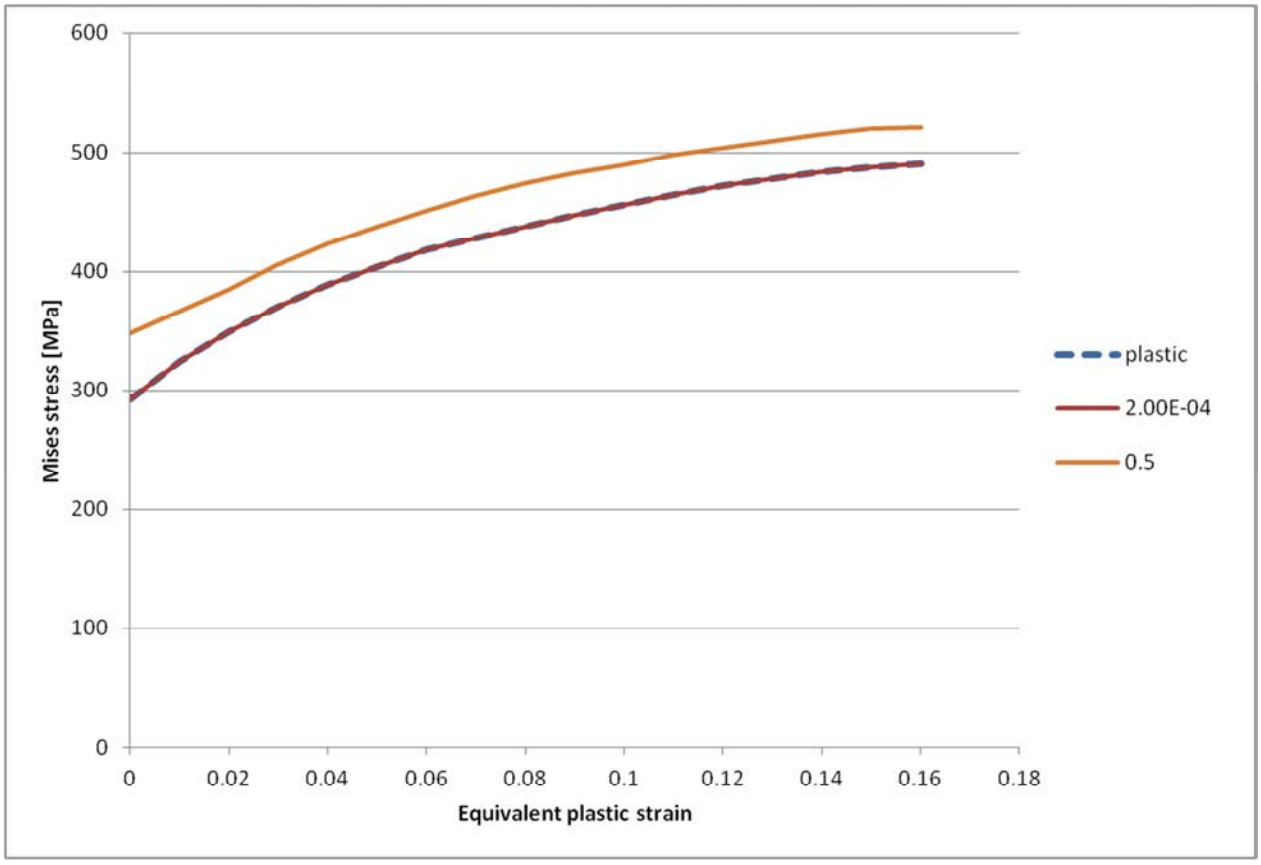

Figure 3-1. *True strain – stress curves for the nodular cast iron. Mises stress [MPa] versus logarithmic equivalent plastic strain for different plastic strain rates. Note that the base (plastic) is defined to coincide with strain rate=2×10^{-4} [1/s].*

3.2 Steel (used for the channel tubes in the insert)

The material model for the channel tubes in the insert is based on elastic behaviour defined by Young's modulus and the Poisson's ratio. The plastic behaviour is defined through von Mises yield surface (true stress) versus plastic strain (using logarithmic strain) using isotropic hardening.

The steel channel tubes are manufactured by steel S355J2H, for example Domex 355 MC B. SKB has earlier supplied test data for the yield point of their material, however no stress-strain data to be used in a plastic analysis. The stress-strain curve for Domex 355 MC B (SSABDirect 2008) can be scaled using the yield stress and tensile ultimate strength measured by SKB, Re = 412 MPa (yield stress) and Rm = 511 MPa (ultimate stress). With this procedure a simplified stress-strain curve is obtained as shown in Table 3-2 and Figure 3-2.

Table 3-2. Stress-strain definition for channel tubes used for the insert.

Strain (%)	Stress (MPa)	Log Strain (%)	True Stress (MPa)	Equivalent plastic strain (%)
0	0	0	0	0
0.196	412	0.196	412	0
15	509	14.3	587	14.0
20	511	18.5	613	18.2

Furthermore, Young's modulus E = 210 GPa and Poisson's ratio ν = 0.3 according to Raiko et al. (2010, Table 3-3).

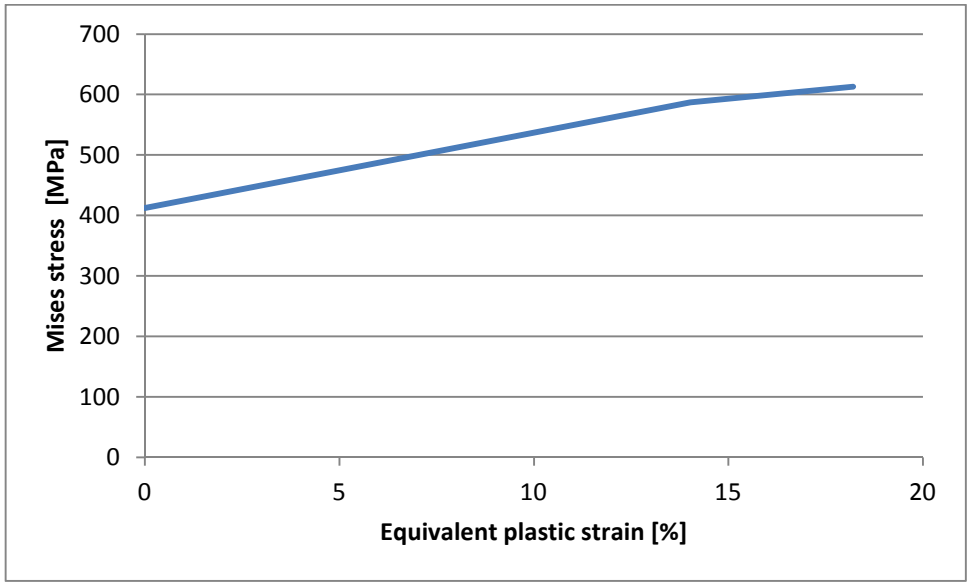

Figure 3-2. *Channel tube yield surface, true stress [MPa], as a function of the logarithmic equivalent plastic strain.*

The data with the lowest value from the experiment has been chosen for the yield surface. However, the plasticity definition for the steel channel tubes has very minor influence on the overall results. Furthermore the obtained results from the performed analyses are within the range of available material data.

3.3 Steel (used for the insert lid, support plates, bottom plates and screws)

The material model for the insert lid is based on elastic behaviour defined by Young's modulus and the Poisson's ratio. The plastic behaviour is defined through Mises yield surface (true stress) versus plastic strain (calculated as logarithmic strain) with isotropic hardening.

Manufacturing drawings for the lid specify steel S355J2G3. Strain versus stress for steel Domex 355 MC B with *Re* = 389 MPa (yield stress) and *Rm* = 484 MPa (ultimate stress) can be found from SSABDirekt (2008). According to SS-EN 10025-2:2004, the material S355 with nominal thickness 40-63 mm has *Re* = 335 MPa (yield stress) and *Rm* = 470-630 MPa (ultimate stress). Scaling stress-strain curves for Domex 355 by the minimum values given in SS-EN 10025-2:2004 implies the simplified material definition (engineering data) shown in Table 3-3 and Figure 3-3.

Table 3-3. Stress-strain definition for the insert lid.

Strain (%)	Stress (MPa)	Log Strain (%)	True Stress (MPa)	Equivalent plastic strain (%)
0	0	0	0	0
0.1595	335	0.1593	335	0
15	470	13.98	540	13.7
20	470	18.2	564	17.9

Furthermore, Young's modulus E = 210 GPa and Poisson's ratio ν = 0.3 according to Raiko et al. (2010, Table 4-3).

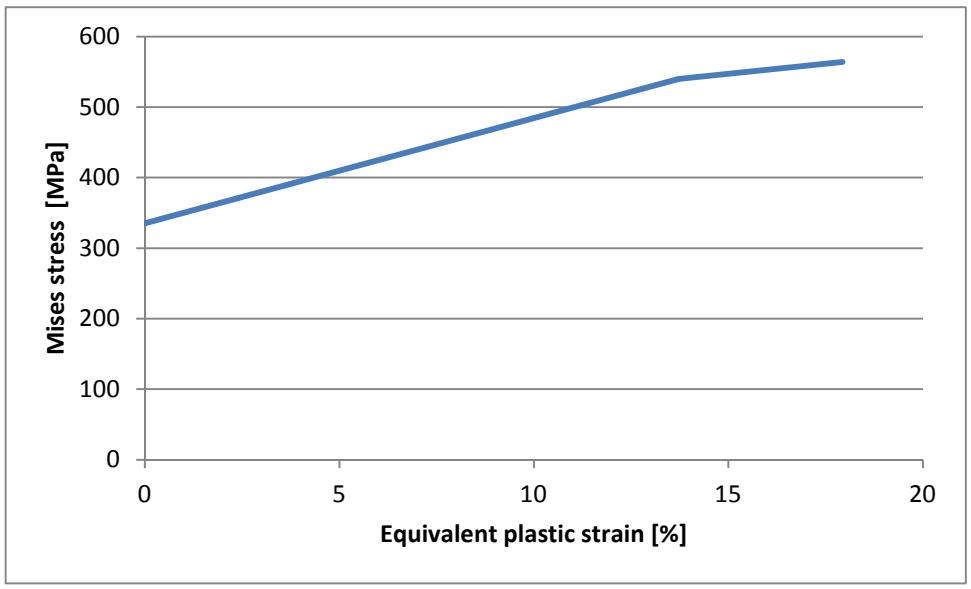

Figure 3-3. *Insert lid yield surface, true stress [MPa], as a function of the logarithmic equivalent plastic strain.*

The data with the lowest value from the experiments (SS-EN 10025-2:2004) has been chosen for the yield surface. However, the plasticity definition for the insert lid has very minor influence on the overall results. Furthermore, the obtained results are within the range of available material data.

3.4 Bentonite model (used for the buffer)

The bentonite is modelled based on experiments, see Börgesson et al. (2010) and adapted to the actual density of the bentonite. The bentonite buffer is modelled using only total stresses that do not include the pore water pressure, the reason being the very fast compression and shear.

Two types of material models have been used in previous calculations. In the first calculations (Börgesson 1988), a total stress model that did not consider the pore water pressure was applied. In the later calculations (Börgesson 1992) the effective stress concept was applied. According to the effective stress concept the effective stress (the total stress minus the pore water pressure) is controlling the stress strain behaviour of a soil. A general experience regarding clays, which also is valid for swelling clays, is that the total stress concept is applicable for fast or un-drained conditions while the effective stress is necessary to apply at drained processes that take place over longer times. The difference is mainly that the effective stress theory is required when there is time enough for the pore water to move in the clay and thus change the state of the clay.

The experience from the previous calculations was that the total stress approach, applied for the calculations of the model tests (Börgesson 1988), was well fitted for the fast shear movements used in these tests. The effective stress approach was motivated for the combined slow shear and creep studies made for the full-scale simulations (Börgesson 1992), but was also more complicated and more difficult to run.

Since the aim of this study is to study the effect of the fastest possible shear, the conclusion is that the total stress approach is the best model for these calculations.

The most important properties of the bentonite for the rock shear are the stiffness and the shear strength. These properties vary with bentonite type, density and rate of strain. Ca-bentonite has higher shear strength than Na-bentonite and the shear strength increases with increasing density and strain rate. Since it cannot be excluded that the Na-bentonite MX-80 will be ion-exchanged to Ca-bentonite the properties of Ca-bentonite is used in the modelling.

The material model is in ABAQUS expressed with the von Mises stress σ_{Mises} that describes the effective stress in three dimensions according to Equation 3-1.

$$\sigma_{Mises}=(((\sigma_1- \sigma_3)^2 + (\sigma_1- \sigma_2)^2 + (\sigma_2- \sigma_3)^2)/2)^{1/2} \quad (3\text{-}1)$$

where

σ_1, σ_2 and σ_3 are the principal stress components.

The material model defines the relation between the stress and the strain and is partitioned in elastic and plastic parts. For details regarding definition of the shear strength and the influence of density, pressure and rate of shear, see Börgesson et al. (1995, 2004).

Rate dependent elastic-plastic stress-strain relation

The elastic-plastic stress strain relations used for the three different densities are derived according to the description above in an identical way as the relations used in all previous calculations.

The bentonite is modelled as linear elastic combined with the von Mises yield surface and isotropic hardening - Table 3-4 shows the elastic constants. The plastic hardening curve is made a function of the strain rate of the material. The reason for the latter relation is that the shear strength of bentonite is rather sensitive to the strain rate. It increases with about 10% for every 10 times increase in strain rate. Since the rock shear at an earthquake is very fast (1 m/s) the influence is strong and the resulting shear strength will be different at different parts of the buffer. Figure 3-4 shows the material model. The stress-strain relation is plotted at different strain rates.

Table 3-4. Elastic material data for the Na-bentonite buffer converted to Ca-bentonite.

Density (kg/m^3)/Swelling pressure (MPa)	Elastic part	
	E **(MPa)**	**ν**
High - 2050/12.3	462	0.49

The experiments (Börgesson et al. 2010) show that also Young's modulus *E* is dependent on strain rate but in the calculations this has been neglected and a representative stiffness based on typical strain rates for the analyses has been chosen (sensitivity analyses did show minor changes of the results when varying Young's modulus between maximum and minimum values achieved from the experiments).

From the performed analyses it's obvious that the bentonite gets plastic strains outside the defined range for material data. However, other studies, "Earthquake induced rock shear through a deposition hole – Part 2. Additional calculations of the influence of inhomogeneous buffer on the stresses in the canister." (SKBdoc 1407337), show that this doesn't affect the results significantly.

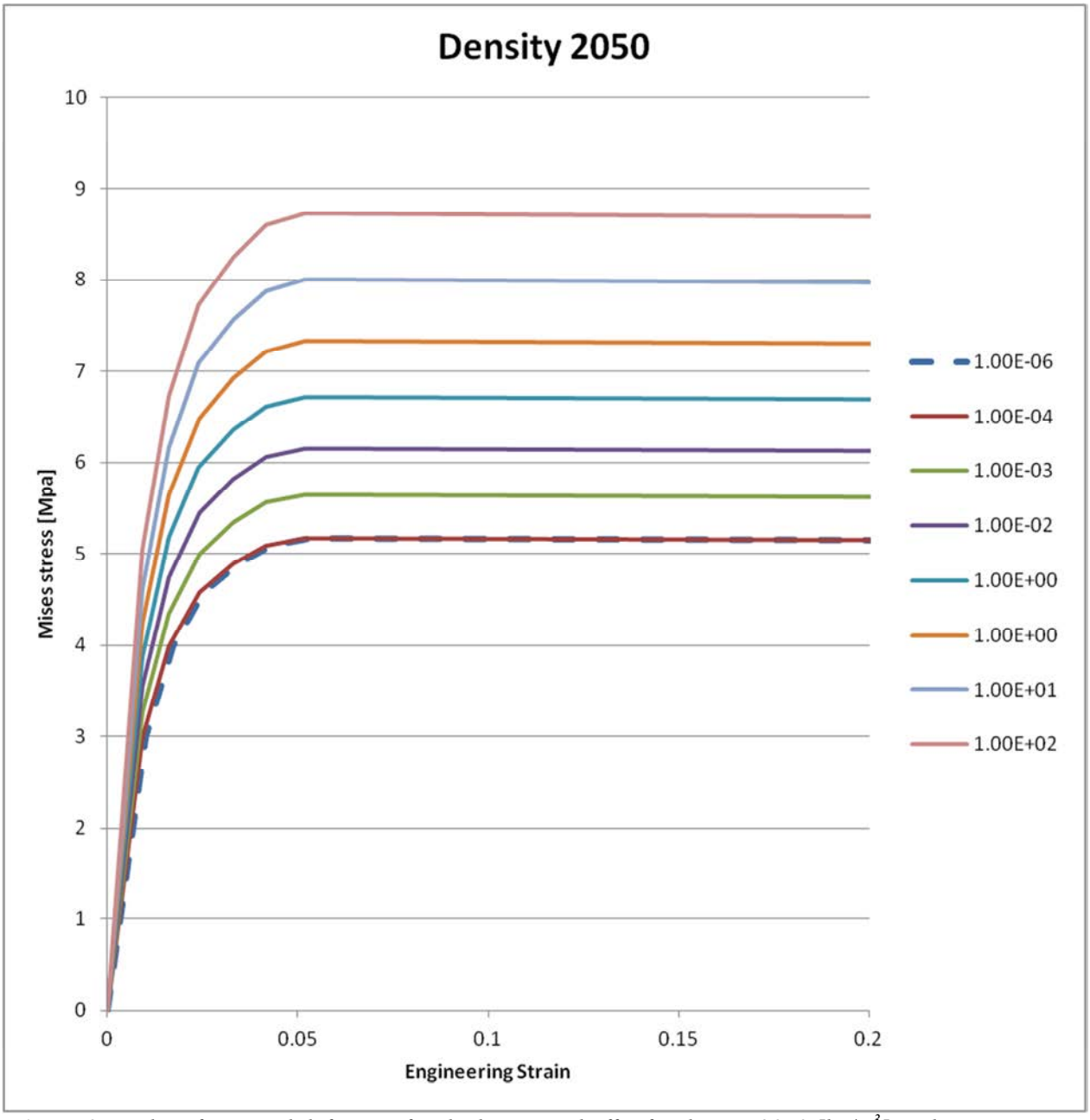

Figure 3-4. *Plot of material definition for the bentonite buffer for density 2050 [kg/m^3] and strain rates [1/s]. Mises stress [MPa] versus engineering strain (nominal strain).*

3.5 Copper material model (used for the copper shell)

3.5.1 Kimab material

The material model used for copper for most of the analyses is described below.
The stress-strain properties of the copper in the copper shell were investigated by Swerea Kimab and the results are represented by a creep material model developed by Rolf Sandström, see Sandström and Andersson (2008), Jin and Sandström (2008) and Sandström et al. (2009).

The material model for the short duration rock shear analysis, used for all analyses in this study and also in previous studies for short duration rock shear analyses (Hernelind 2010) and "Global simulation of copper canister – final deposition" (SKBdoc 1339902), is based on a simplified elastic-plastic material model, see Table 3-5, using data from the creep model assuming a strain rate of 5×10^{-3}/s.

The flow curve data has been calculated from Sandström et al. (2009) wherein eq.(17) has been used together with the parameter values defined in the corresponding Table 3-5, as well as $m = 3.06$, $\alpha = 0.19$, $\omega = 14.66$.

The copper model data is shown in Figure 3-5. Data is available up to 50% equivalent plastic strain and covers the range of obtained results.

Table 3-5. Elastic-plastic material data for the copper at strain rate 5×10^{-3}/s.

Elastic part		Plastic part: von Mises stress σ_j (MPa) at the following plastic strains (ε_p)					
E (MPa)	v	0	0.10	0.20	0.30	0.40	0.50
$1.2\cdot10^5$	0.308	72	178	235	269	288	300

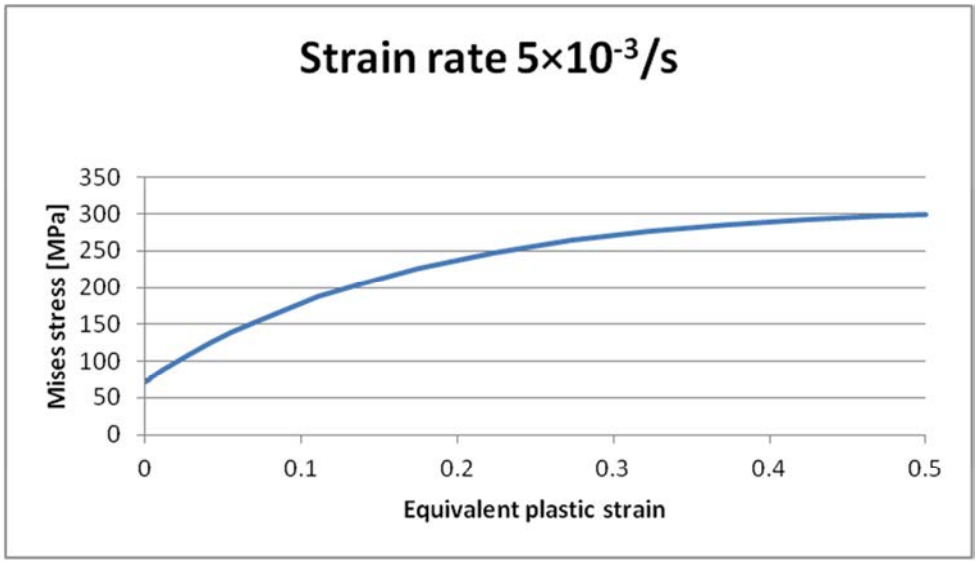

Figure 3-5. *Copper shell yield surface, true stress, [MPa] as a function of the logarithmic equivalent plastic strain.*

3.5.2 Copper material with kinematic hardening combined with texture damage/rotation

A material model based on a modified Mises theory where the shear stresses have more influence than the direct stress components has been suggested by Unosson (SKBdoc 1393179). A local material direction is defined to follow the principal strain directions. The model is described in "A constitutive model for texture dependent deformation hardening and pressure dependent" (SKBdoc 1393179). Figure 3-6 shows the material model and below a short summary taken from SKBdoc 1393179 is used as illustration.

$$\sigma_{jmf} = \sqrt{1.5(s_{xx}^2 + s_{yy}^2 + s_{zz}^2 + \alpha(s_{yz}^2 + s_{xz}^2 + s_{xy}^2))}$$
$$\alpha = 2(1 + 0.1\varepsilon_{jmf})$$

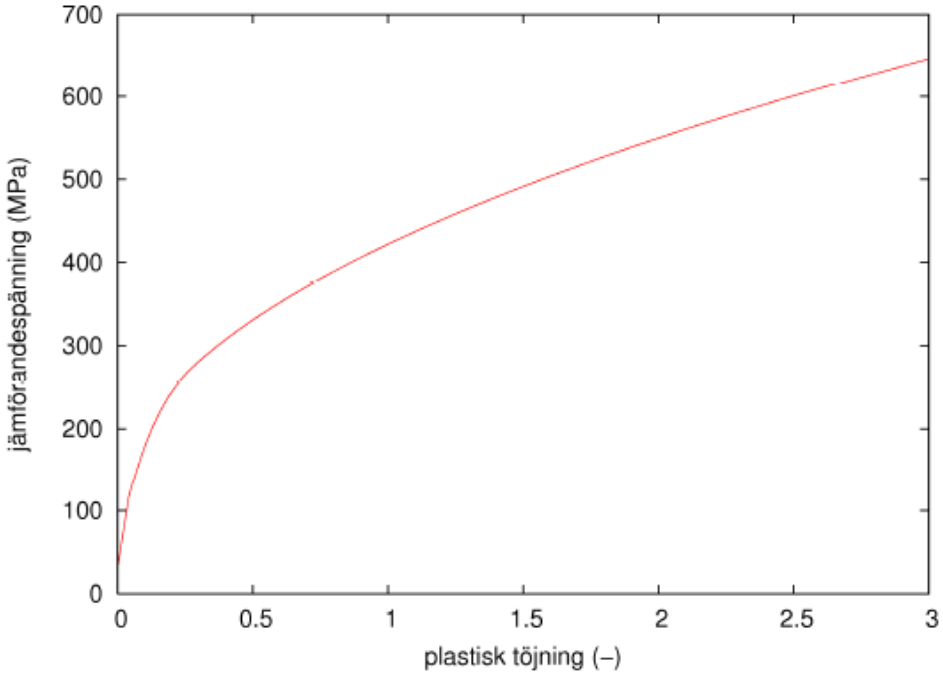

Figure 3-6. *Mises stress versus plastic strain.*

4 Contact definitions

All the boundaries of the buffer, the copper shell, the insert and the insert lid interact through contact surfaces allowing finite sliding. All contact surfaces have friction at sliding with no cohesion and the friction coefficient 0.1, i.e. the friction angle (ϕ) is 5.7˚ and the cohesion (c) is 0 kPa.

The contact is released when the contact pressure is lost.

A few contact pairs are tied together (tied means that the surfaces are constrained together and will not allow for opening/closing or sliding) in order to improve the numerical convergence rate. This applies at the contact pairs between the insert and insert lid and also at the base of insert and copper shell bottom.

The interaction between the buffer and the rock (not modelled) is assumed to be tied through prescribed boundary conditions and will not allow for opening/closing or sliding.

5 Initial conditions

Initial conditions are defined as:

- Total pressure for the buffer (17.3 MPa) is based on the swelling pressure (12.3 MPa for bentonite with density 2,050 kg/m^3) plus 500 meter water pressure (5 MPa) when using elastic-plastic material model without pore pressure (the repository is located approximately 500 meter below the surface for the Forsmark site). To achieve a total pressure of approximately 17.3 MPa at the start of the rock shearing analysis, an initial condition for pressure in the bentonite is given as 40.2 MPa. This value (40.2) is determined by one additional analysis where the initial pressure in the bentonite is plotted versus pressure on the outer surface of the copper shell. Note that the total pressure can only be defined as an initial condition if the complete system is in equilibrium and in the current analyses only the bentonite has initial stresses defined which imply that the copper shell (and the insert) deforms and the stresses in the bentonite decreases.

- Another observation is that the calculated swelling pressure will vary both in the axial and radial direction which means that it's not possible to have the correct swelling pressure without using elements with pore pressure as a degree of freedom (ABAQUS have those elements but the material model is tuned to total stresses (pore pressure + effective pressure) and not effective stresses (effective stress for soils corresponds to mean stress).

6 Boundary conditions

Symmetry conditions have been specified for the symmetry plane (displacements in the normal direction to the symmetry plane prescribed to zero), see Figure 6-1.

The surrounding rock has been simulated by prescribing the corresponding displacements at the outer surface of the buffer and depends also on type of simulation.

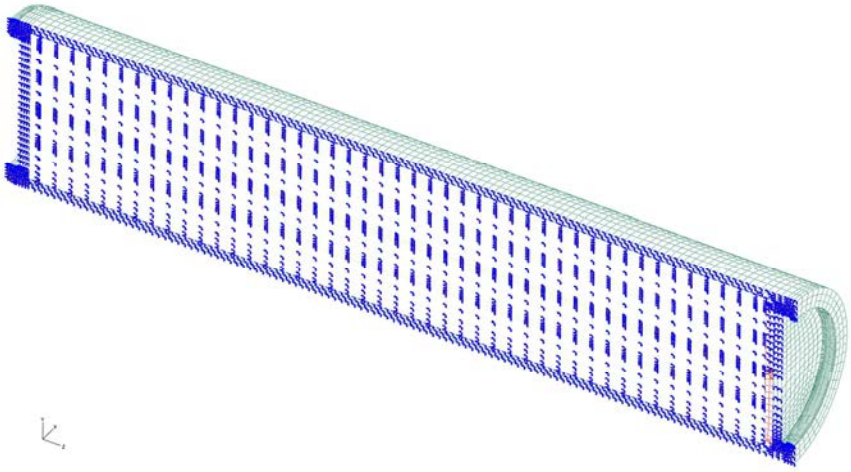

Figure 6-1. *Prescribed symmetry conditions.*

7 Calculations

7.1 General

7.1.1 Rock shear calculation cases

The reference case for BWR is based on Na-bentonite converted to Ca-bentonite with buffer density 2050 kg/m^3.

rock shear perpendicular to the axis of the canister

- At 90% of the height from the base:
  - model6g_corrosion_90b – Kimab copper material model as in previous calculations (Hernelind 2010, SKBdoc 1339902). The copper shell with wall thickness of 2.5 cm.
  - model6g_corrosion_90b_MU - copper material model suggested by Unosson in SKBdoc 1393179. The copper shell with wall thickness of 2.5 cm
  - N31b_finer_1sekm - reference model (Hernelind 2010, SKBdoc 1339902) with nominal copper thickness. Kimab copper material model. Used for comparison with model6g_corrosion_90b.
- at the insert lid:
  - model6g_corrosion_lidb – Kimab copper material model, as in previous calculations (Hernelind 2010, SKBdoc 1339902). The copper shell with wall thickness of 2.5 cm
  - model6g_corrosion_lidb_MU - copper material model suggested by Unosson in SKBdoc 1393179. The copper shell with wall thickness of 2.5 cm
  - N34b_finer_1sekm_quasi - reference model (Hernelind 2010, SKBdoc 1339902) with nominal copper thickness. Kimab copper material model. Used for comparison with model6g_corrosion_lidb.

7.1.2 Analysis approach

The numerical calculations are performed using the FE-code ABAQUS version 6.13 (ABAQUS 2013) assuming non-linear geometry and material definitions. This means that all non-linearities defined by the input will be considered such as large displacements, non-linear interactions (contact) and non-linear materials. All non-linear contributions will be used when forming the equations to be solved for each equilibrium iteration.

The short term analyses are based on quasi-static response but the results will depend on the time used for the simulation since rate-dependent material data is used.

The code will choose suitable time-increments for the loading based on (in most cases) default convergence tolerances.

7.2 Short term analyses

The short term analyses (few seconds with 1 m/s as shearing velocity) consist of three steps where the shearing is prescribed by boundary conditions.

In the first step, initial stresses corresponding to the swelling pressure (12.3 MPa for bentonite with density 2,050 kg/m^3) plus 5 MPa hydrostatic pressure (the deposition is made about 500 meters below the surface) in the bentonite is applied, see also in chapter “Initial conditions”.

In the second step, 5 cm is used for the shearing magnitude and finally the third step defines additional 5 cm shearing. The results for BWR are shown in Appendix 1-4 for the buffer density 2,050 kg/m^3.

8 Results

For each analysis, a large amount of results are available. However, only a few parameters are reported since it is enough for the evaluation of the analyses. The results are focused on the effect for the copper shell and are compared with results from previous analyses with twice as thick copper shell. The copper shell is divided in regions for output purposes, see Figure 8-1. Region 4 (discontinuity at the top) contains one row of elements at the discontinuity which has deformed to have an almost singular Jacobian matrix which makes the results in this region non-representative. For this reason this row of elements has been removed before creating contour plots of PEEQ.

Output regions

The numbers in Tables 8-2 to 8-5 are from six regions in the copper shell, as defined in Figure 8-1, and should be used with care and in combination with the corresponding plots in the enclosed appendixes. Region 4, 7 and 8 is excluded from the tables – region 4 since this region contain too distorted elements which makes a comparison doubtful and region 7 and 8 since these regions have much lower magnitudes and is not affecting the conclusions.

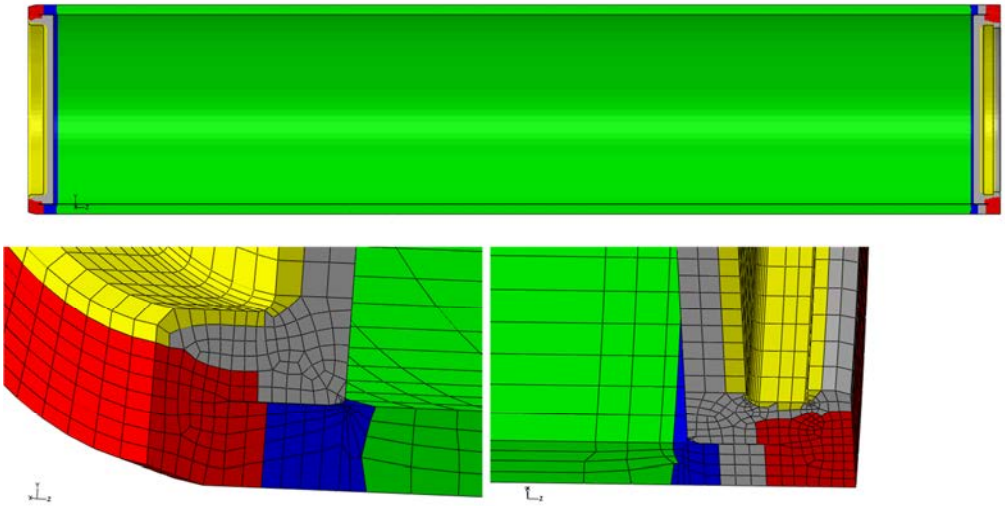

Figure 8-1. *Output regions for copper shell. Region 1 - mid canister (green). Region 2 – top weld (red, lower right). Region 3 – base weld (red, lower left). Region 4 – top discontinuous geometry (blue, lower right). Region 5 – base discontinuous geometry (blue, lower left). Region 6 – top fillet (yellow, lower right). Region 7 – base fillet (yellow, lower left). Region 8 – top reminding (grey, lower right). Region 9 – base reminding (grey, lower left)*

8.1 Results for rock shear

For the short term rock shear analyses the peak values for Mises stress and equivalent plastic strain PEEQ according to (ABAQUS 2013) are summarized in Tables 8-1 to 8-5. The equivalent plastic strain PEEQ is defined below:

PEEQ

Equivalent plastic strain. This identifier also provides a yes/no flag (1/0 on the output database) telling if the material is currently yielding or not (AC YIELD: "actively yielding"; that is, the plastic strain changed during the increment).

The equivalent plastic strain is defined as $\bar{\varepsilon}^{pl}|_0 + \int_0^t \dot{\bar{\varepsilon}}^{pl} dt$, where $\bar{\varepsilon}^{pl}|_0$ is the initial equivalent plastic strain.

The definition of $\dot{\bar{\varepsilon}}^{pl}$ depends on the material model. For classical metal (Mises) plasticity $\dot{\bar{\varepsilon}}^{pl} = \sqrt{\frac{2}{3}\dot{\boldsymbol{\varepsilon}}^{pl} : \dot{\boldsymbol{\varepsilon}}^{pl}}$.

8.1.1 Shearing at the insert lid

Figures 8-2 to 8-4 show comparisons for the reference case, N34b_finer_1sekm_quasi, and model6g_corrosion_lidb at 8 cm shearing. Mises stresses are similar even though some differences can be observed which to some extent can be explained by a finer mesh for model6g_corrosion_lidb (Figure 8-3). The plastic strains are almost zero for the insert (Figure 8-4).

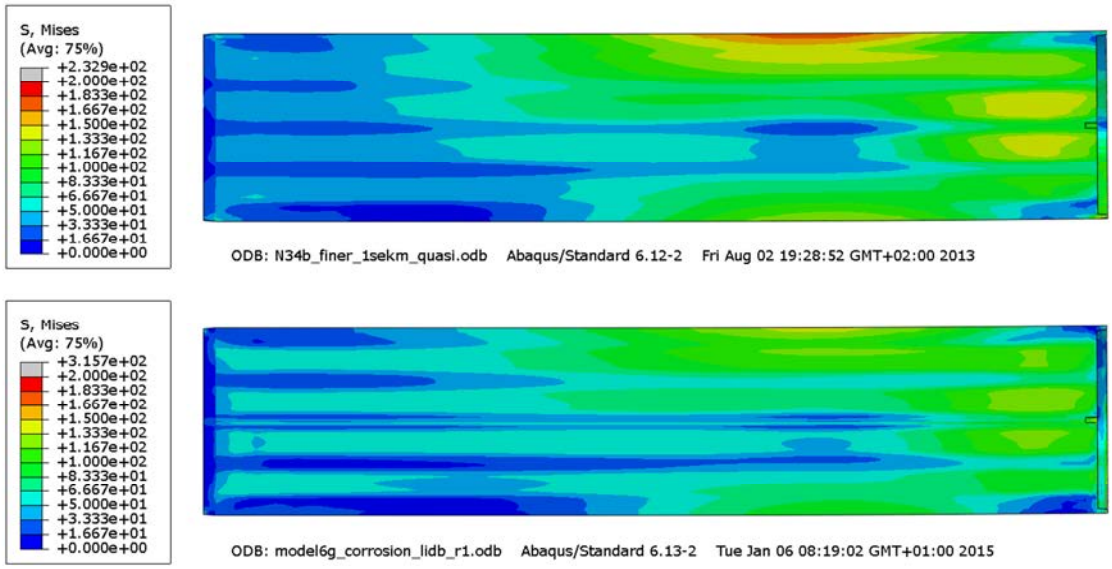

Figure 8-2. *Mises stress in the insert at 8 cm shearing for reference model, N34b_finer_1sekm_quasi (upper) and model6g_corrosion_lidb (lower)*

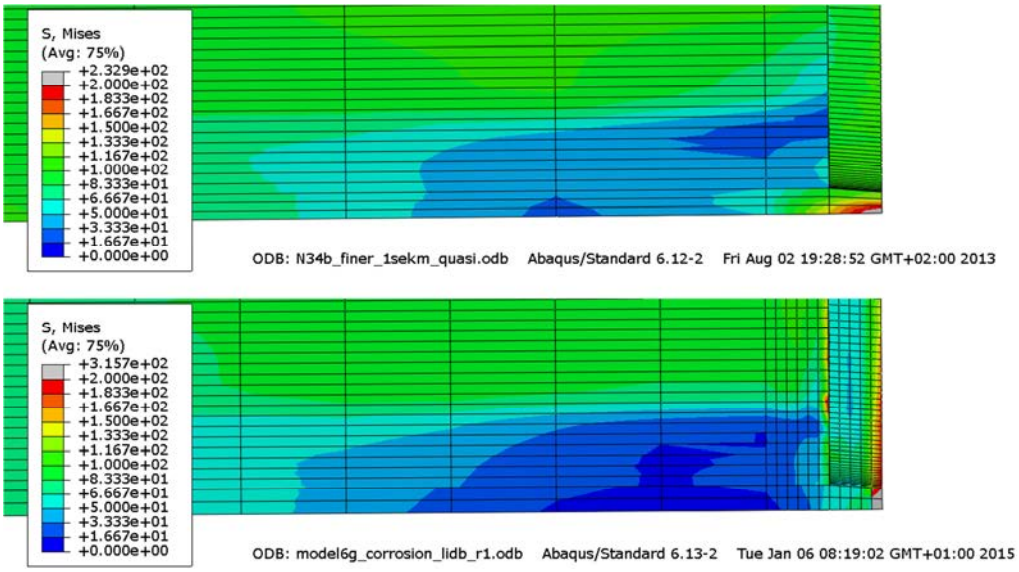

Figure 8-3. *Mises stress in the insert at 8 cm shearing for reference model, N34b_finer_1sekm_quasi (upper) and model6g_corrosion_lidb (lower) at the top corner*

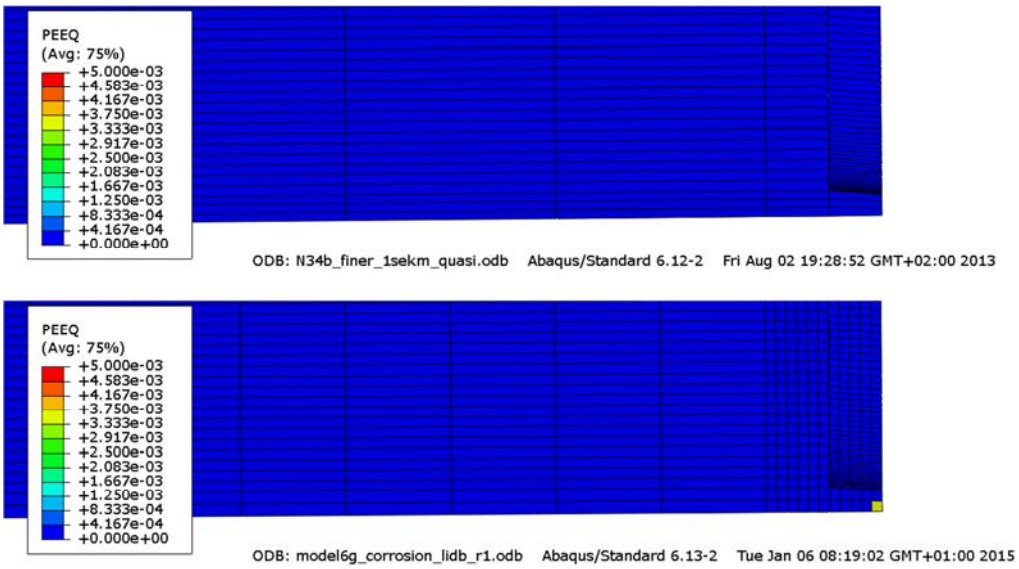

Figure 8-4. *Equivalent plastic strain (PEEQ) in the insert at 8 cm shearing for reference model, N34b_finer_1sekm_quasi (upper) and model6g_corrosion_lidb (lower) top right corner*

Figures 8-5 to 8-7 shows comparisons for equivalent plastic strains (PEEQ) for reference model N34b_finer_1sekm_quasi and model6g_corrosion_lidb. The maximum values differs a lot, 24% for the reference model and 48% for model6g_corrosion_lidb.

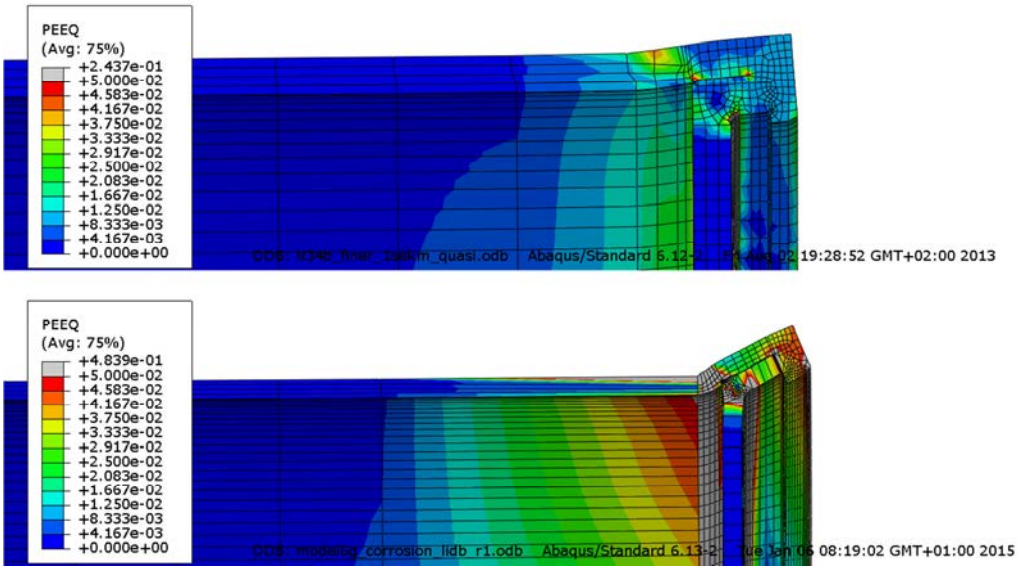

Figure 8-5. *Equivalent plastic strain (PEEQ) in the copper shell at 8 cm shearing for reference model, N34b_finer_1sekm_quasi (upper) and model6g_corrosion_lidb (lower) top left corner*

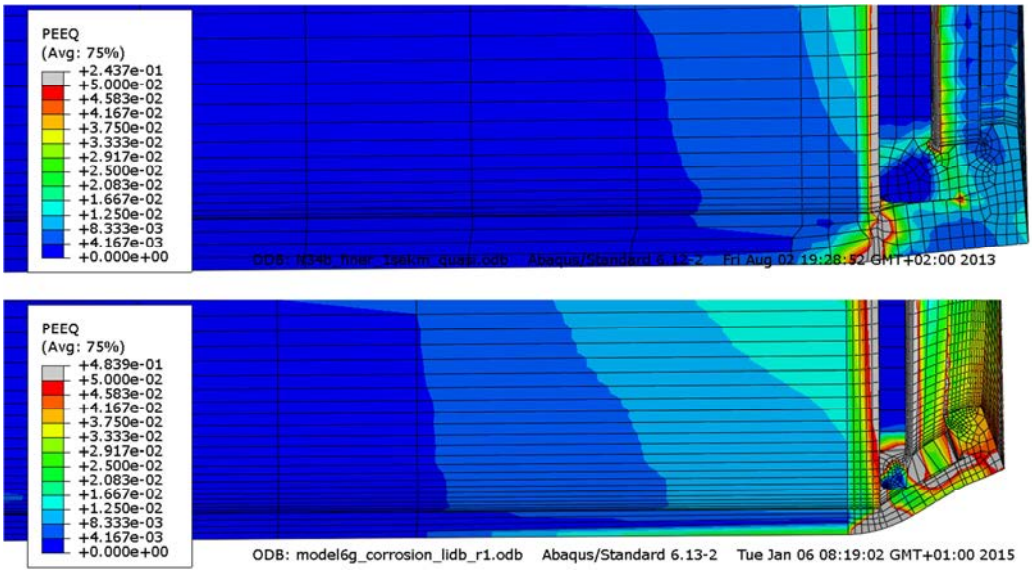

Figure 8-6. *Equivalent plastic strain (PEEQ) in the copper shell at 8 cm shearing for reference model, N34b_finer_1sekm_quasi (upper) and model6g_corrosion_lidb (lower) top right corner*

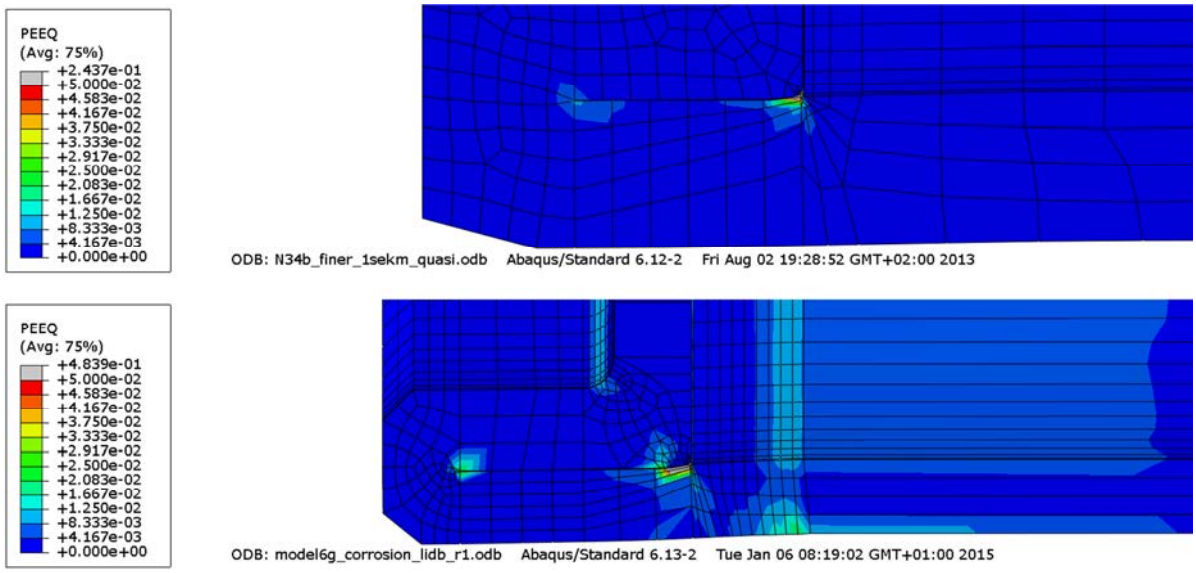

Figure 8-7. *Equivalent plastic strain (PEEQ) in the copper shell at 8 cm shearing for reference model, N34b_finer_1sekm_quasi (upper) and model6g_corrosion_lidb (lower) base right corner*

Figures 8-8 to 8-11 shows comparisons between the copper material model suggested by Unosson in SKBdoc 1393179 (model6g_corrosion_lidb_MU) and model6g_corrosion_lidb (Kimab copper material model) at 8 cm shearing. The Mises stresses differ due to different hardening rules (Figure 8-8). The plastic strains in Figure 8-9 are similar even though the maximum values differ slightly (39% using the model suggested by Unosson and 48% using the original model).

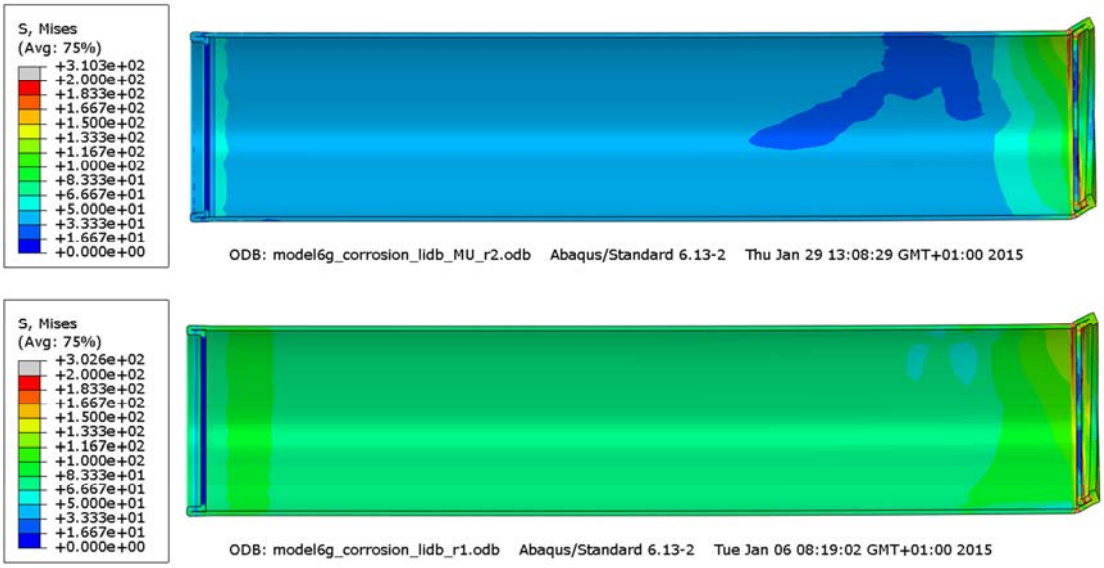

Figure 8-8. *Mises stress [MPa] in the copper shell at 8 cm shearing for model6g_corrosion_lidb_MU (upper) and model6g_corrosion_lidb (lower)*

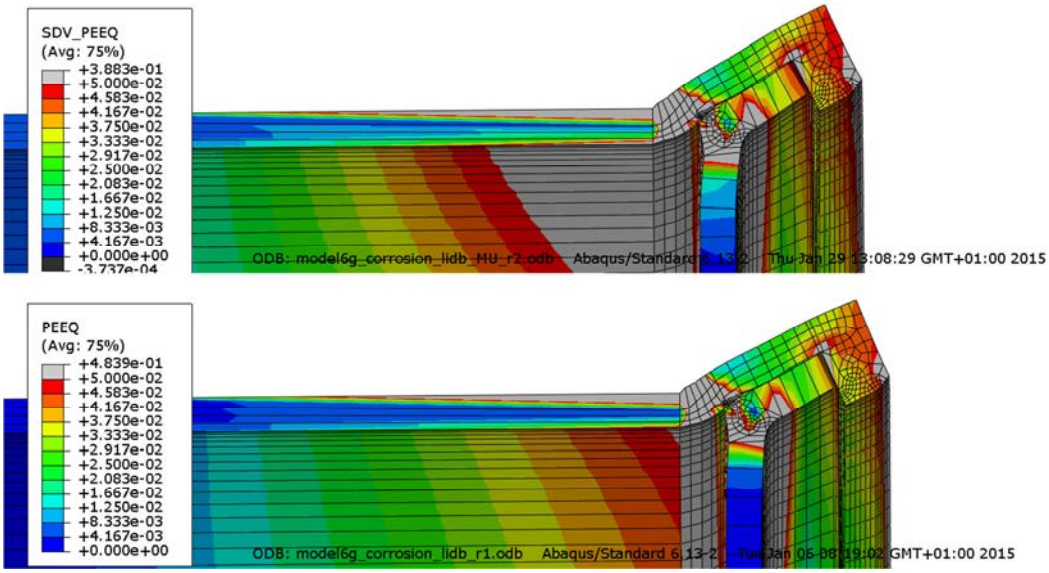

Figure 8-9. *Equivalent plastic strain (PEEQ) in the copper shell at 8 cm shearing for model6g_corrosion_lidb_MU (upper) and model6g_corrosion_lidb top left corner (lower)*

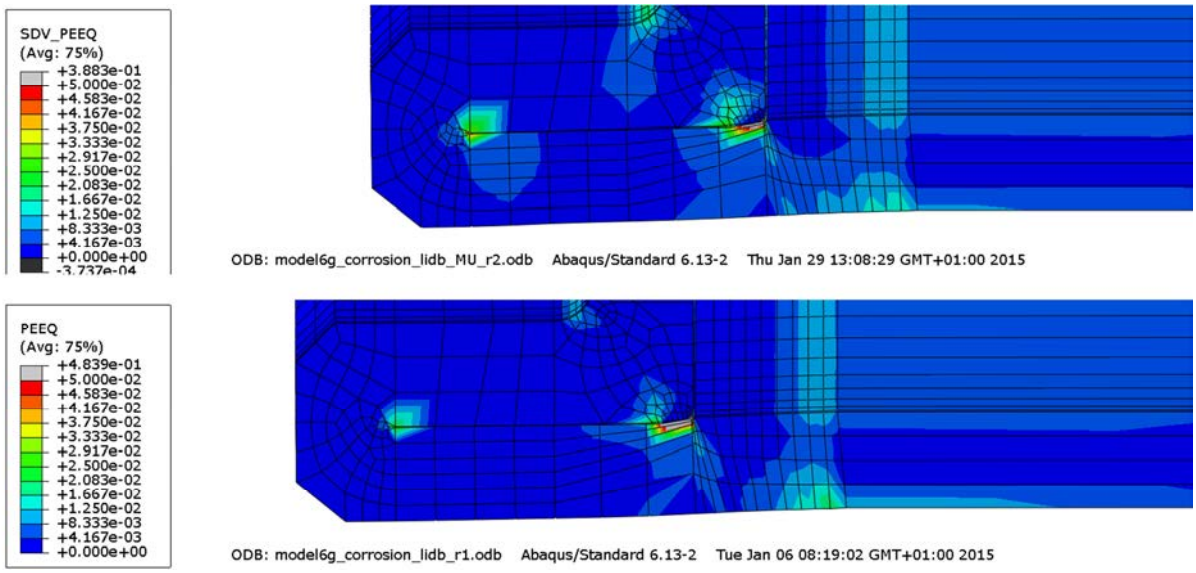

Figure 8-10. *Equivalent plastic strain (PEEQ) in the copper shell at 8 cm shearing for model6g_corrosion_lidb_MU (upper) and model6g_corrosion_lidb base right corner (lower)*

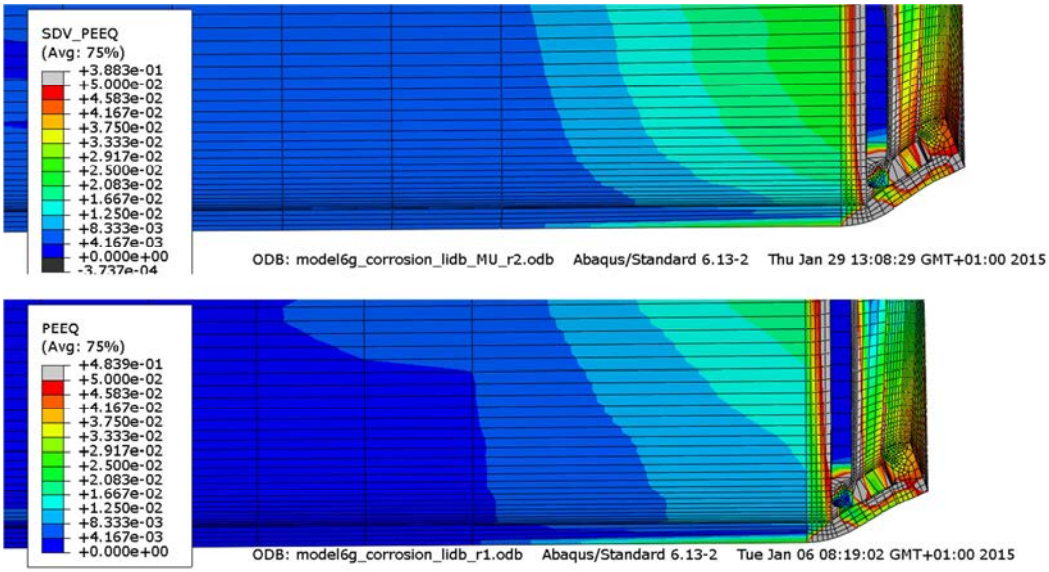

Figure 8-11. *Equivalent plastic strain (PEEQ) in the copper shell at 8 cm shearing for model6g_corrosion_lidb_MU (upper) and model6g_corrosion_lidb top right corner (lower)*

Figures 8-12 to 8-14 show comparisons at 5 cm shearing for shearing at the insert lid using the original copper material model and the copper material model suggested by Unosson. The plastic strains are similar even though the maximum values differ slightly (57% using the model suggested by Unosson and 50% using the original model).

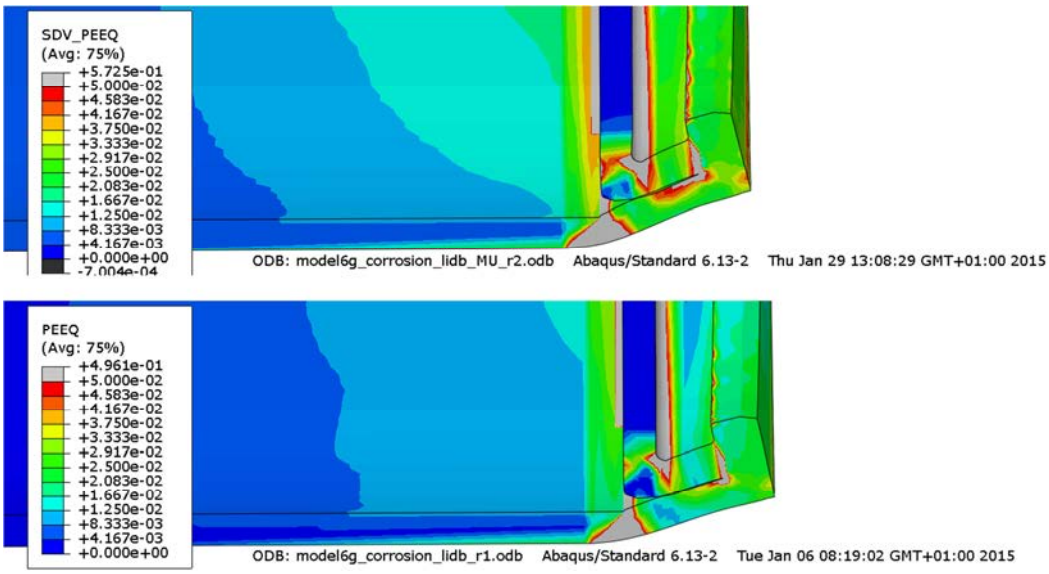

Figure 8-12. *Equivalent plastic strain (PEEQ) in the copper shell at 5 cm shearing for model6g_corrosion_lidb_MU (upper) and model6g_corrosion_lidb top right corner (lower)*

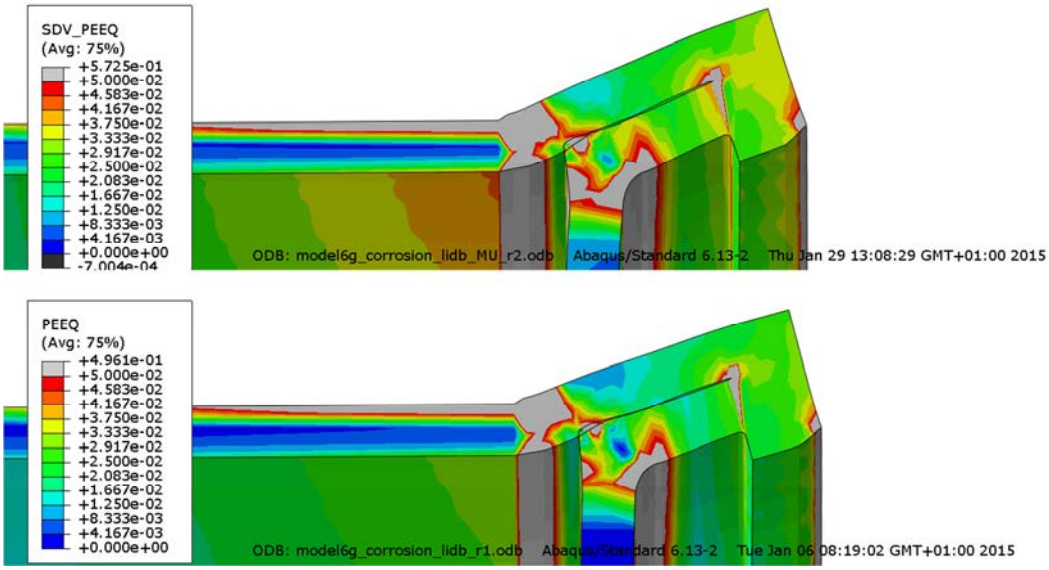

Figure 8-13. *Equivalent plastic strain (PEEQ) in the copper shell at 5 cm shearing for model6g_corrosion_lidb_MU (upper) and model6g_corrosion_lidb top left corner (lower)*

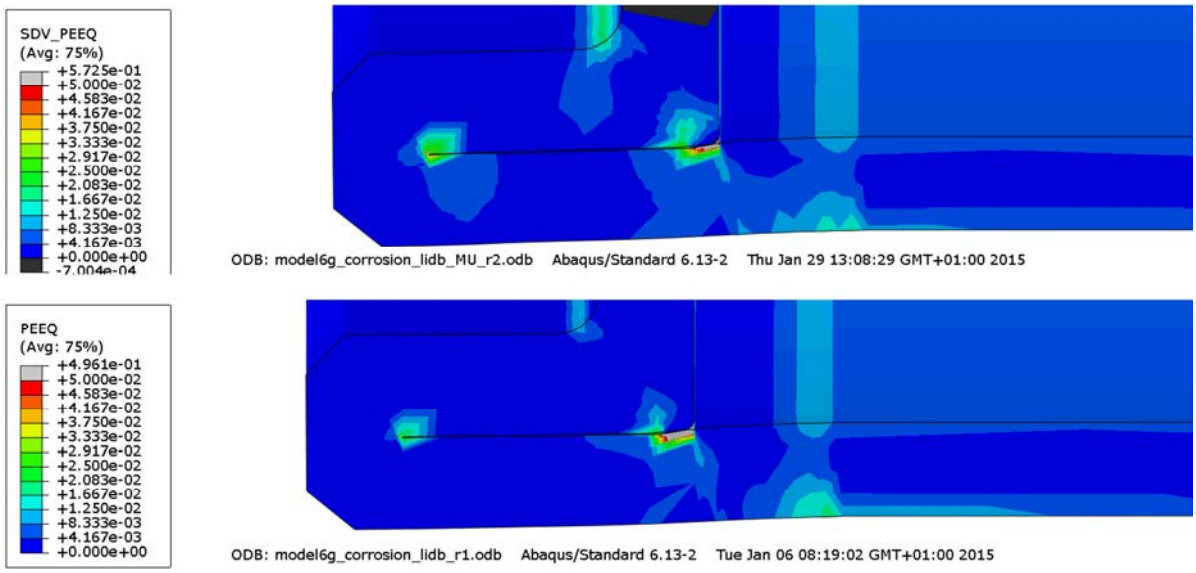

Figure 8-14. *Equivalent plastic strain (PEEQ) in the copper shell at 5 cm shearing for model6g_corrosion_lidb_MU (upper) and model6g_corrosion_lidb base right corner (lower)*

8.1.2 Shearing at 90% height of the insert

Figures 8-15 to 8-20 show comparisons for the reference case, N31b_finer_1sekm, and model6g_corrosion_90b at 6 cm shearing. Mises stresses are similar even though some differences can be observed which to some extent can be explained by a finer mesh for model6g_corrosion_90b (Figure 8-16). The plastic strains are almost zero for the insert (Figure 8-17).

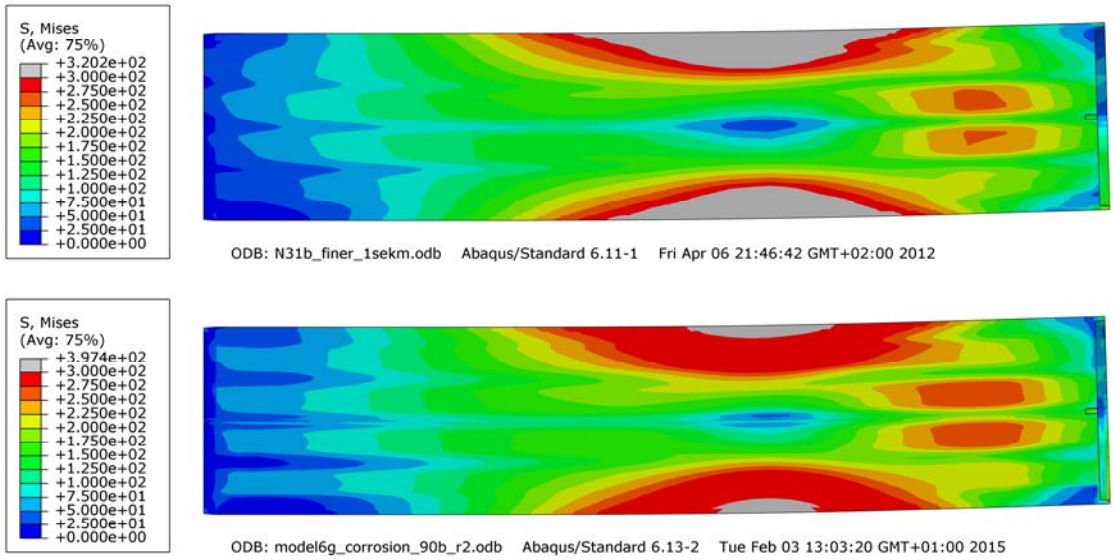

Figure 8-15. *Mises stress in the insert at 6 cm shearing for reference model, N31b_finer_1sekm (upper) and model6g_corrosion_90b (lower)*

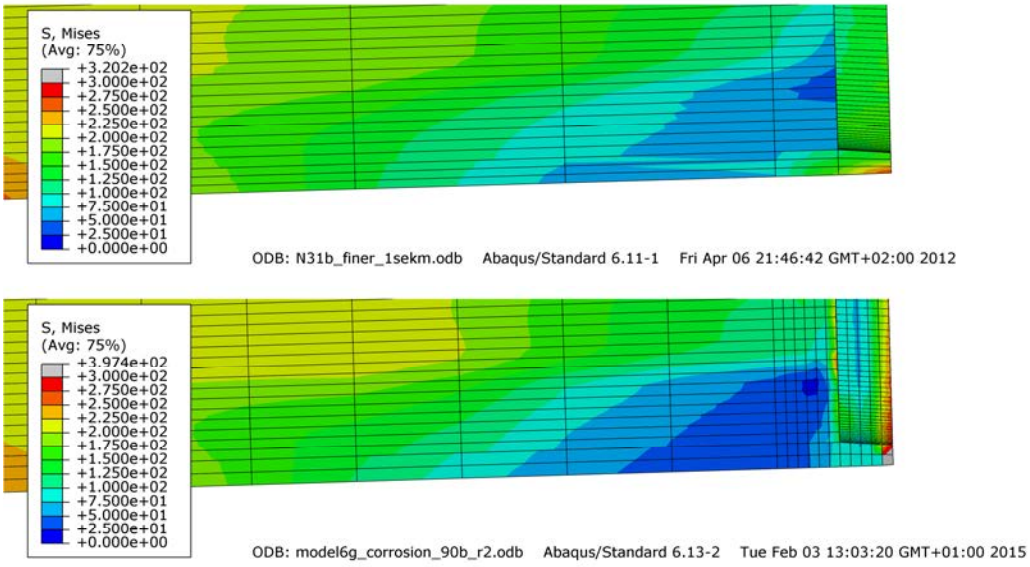

Figure 8-16. *Mises stress in the insert at 6 cm shearing for reference model, N31b_finer_1sekm (upper) and model6g_corrosion_90b (lower) at the top corner*

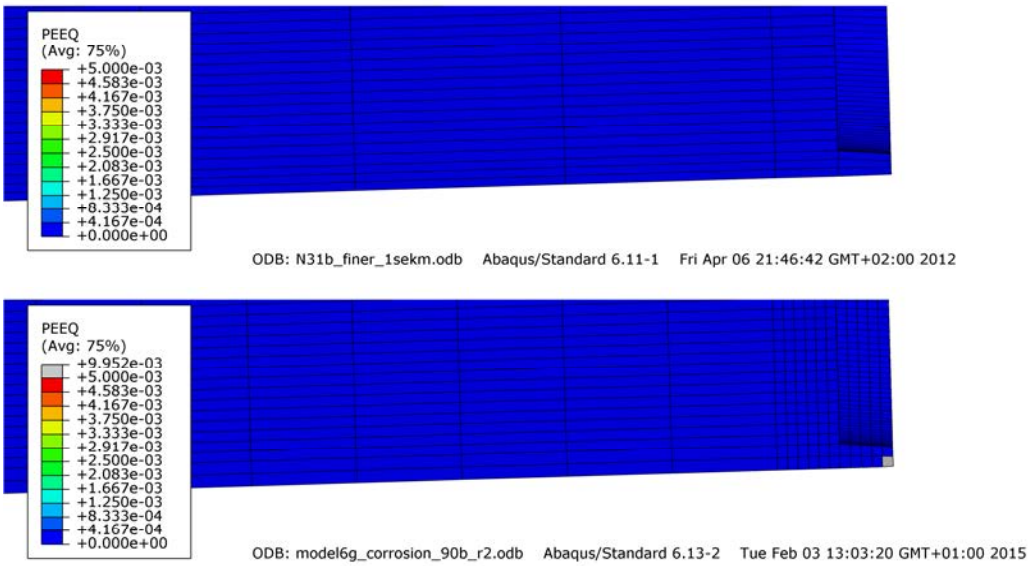

Figure 8-17. *Equivalent plastic strain (PEEQ) in the insert at 6 cm shearing for reference model, N31b_finer_1sekm (upper) and model6g_corrosion_90b (lower) top right corner*

Figures 8-18 to 8-20 shows comparisons for equivalent plastic strains (PEEQ) for reference model N31b_finer_1sekm and model6g_corrosion_90b. The maximum values differs a lot, 40% for the reference model and 50% for model6g_corrosion_90b.

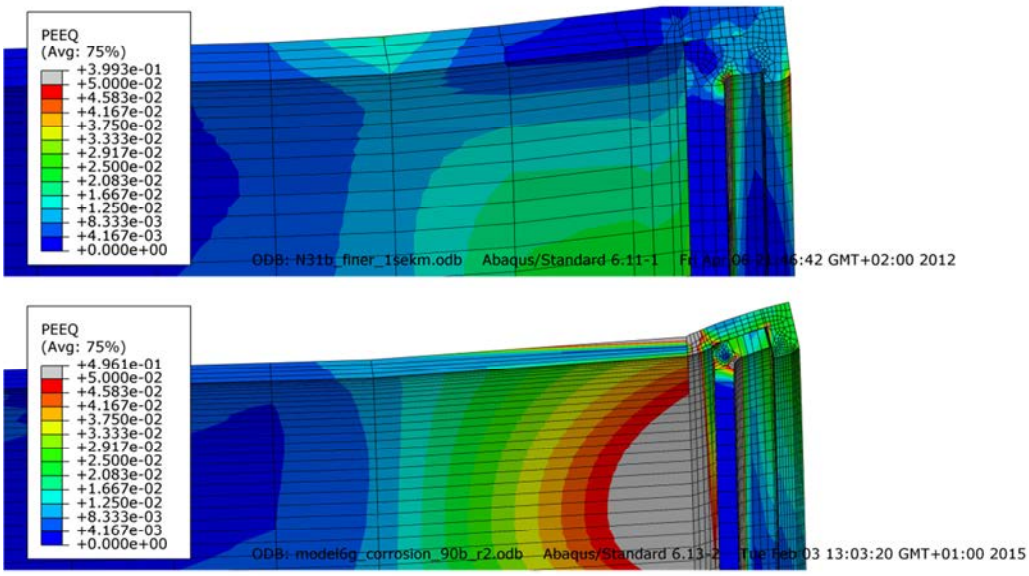

Figure 8-18. *Equivalent plastic strain (PEEQ) in the copper shell at 6 cm shearing for reference model, N31b_finer_1sekm (upper) and model6g_corrosion_90b (lower) top left corner*

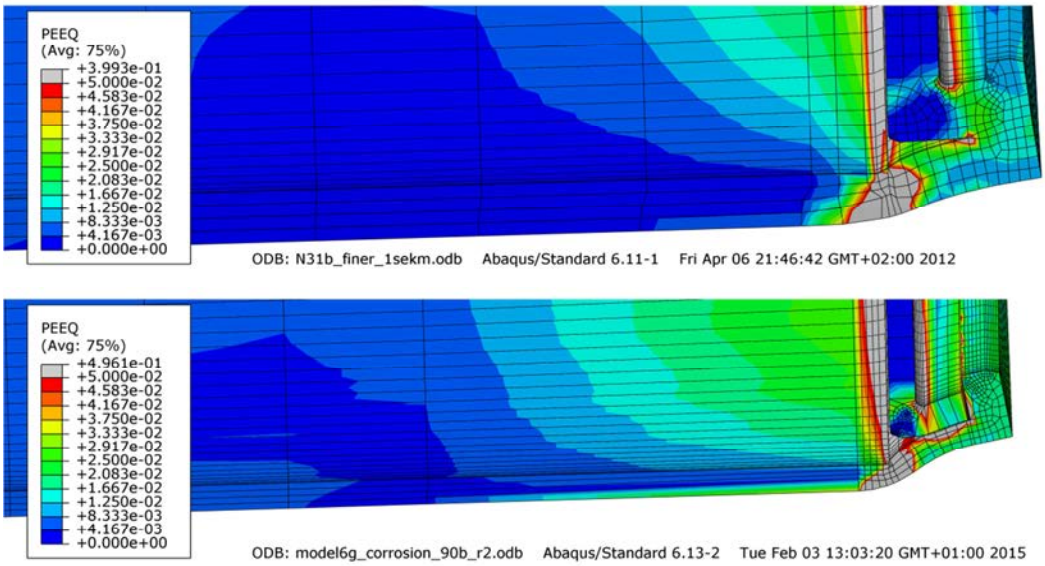

Figure 8-19. *Equivalent plastic strain (PEEQ) in the copper shell at 6 cm shearing for reference model, N31b_finer_1sekm (upper) and model6g_corrosion_90b (lower) top right corner*

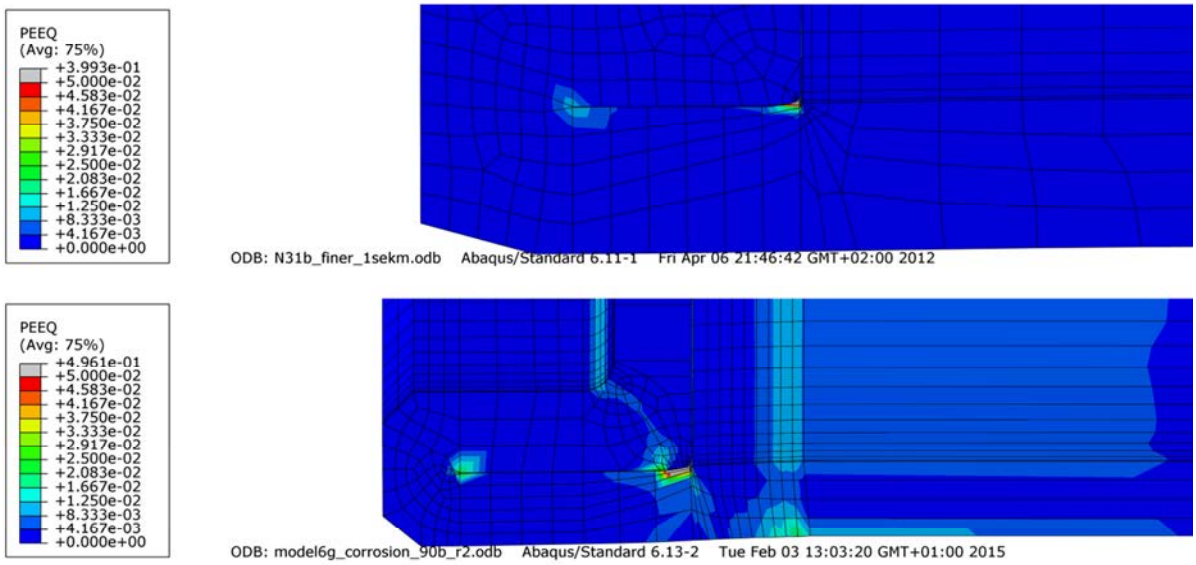

Figure 8-20. *Equivalent plastic strain (PEEQ) in the copper shell at 6 cm shearing for reference model, N31b_finer_1sekm (upper) and model6g_corrosion_90b (lower) base right corner*

Figures 8-21 to 8-24 shows comparisons between the copper material model suggested by Unosson (model6g_corrosion_90b_MU) and model6g_corrosion_90b (original copper material model) at 6 cm shearing (the last converged solution for model6g_corrosion_90b_MU). The Mises stresses differ due to different hardening rules (Figure 8-21) but the equivalent plastic strains (PEEQ) are similar even if the maximum values are rather high (about 75%). The elements in region 4, Figure 8-1, is removed before generating the contour plots of PEEQ.

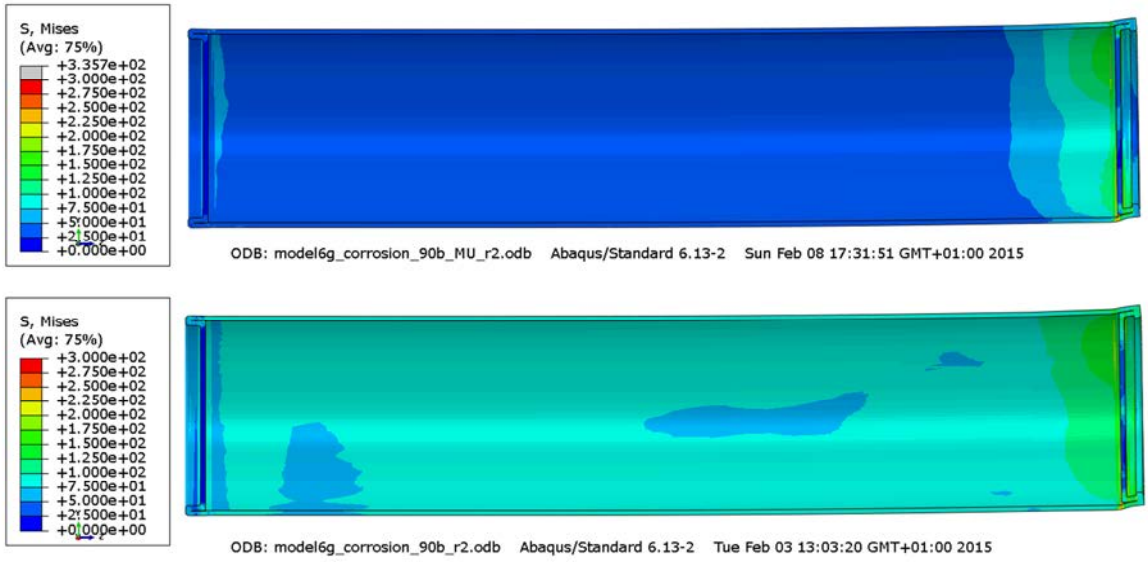

Figure 8-21. *Mises stress [MPa] in the copper shell at 6 cm shearing for model6g_corrosion_90b_MU (upper) and model6g_corrosion_90b (lower)*

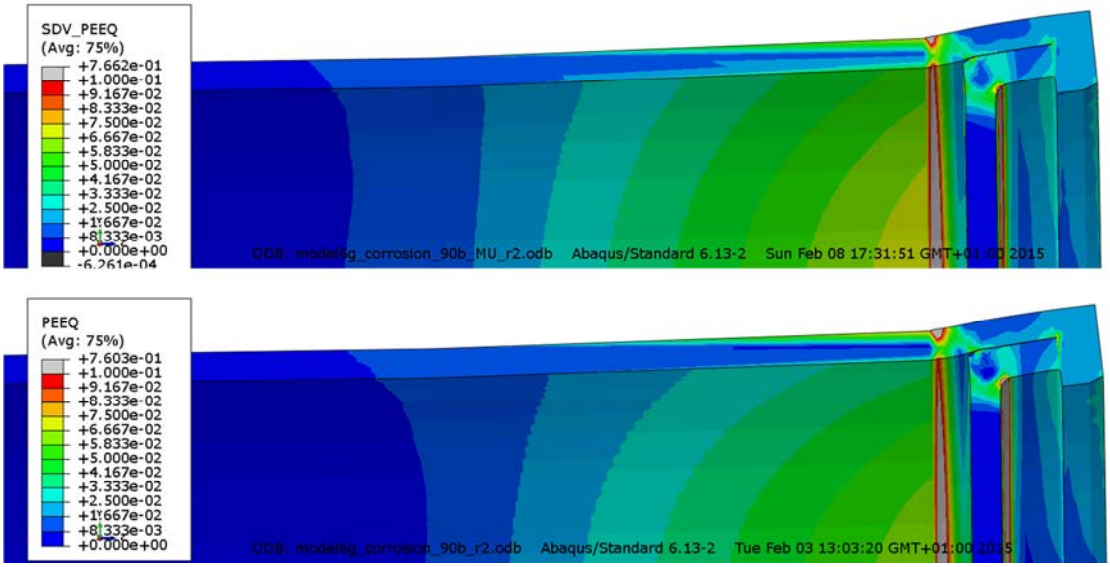

Figure 8-22. *Equivalent plastic strain (PEEQ) in the copper shell at 6 cm shearing for model6g_corrosion_90b_MU (upper) and model6g_corrosion_90b upper left corner (lower)*

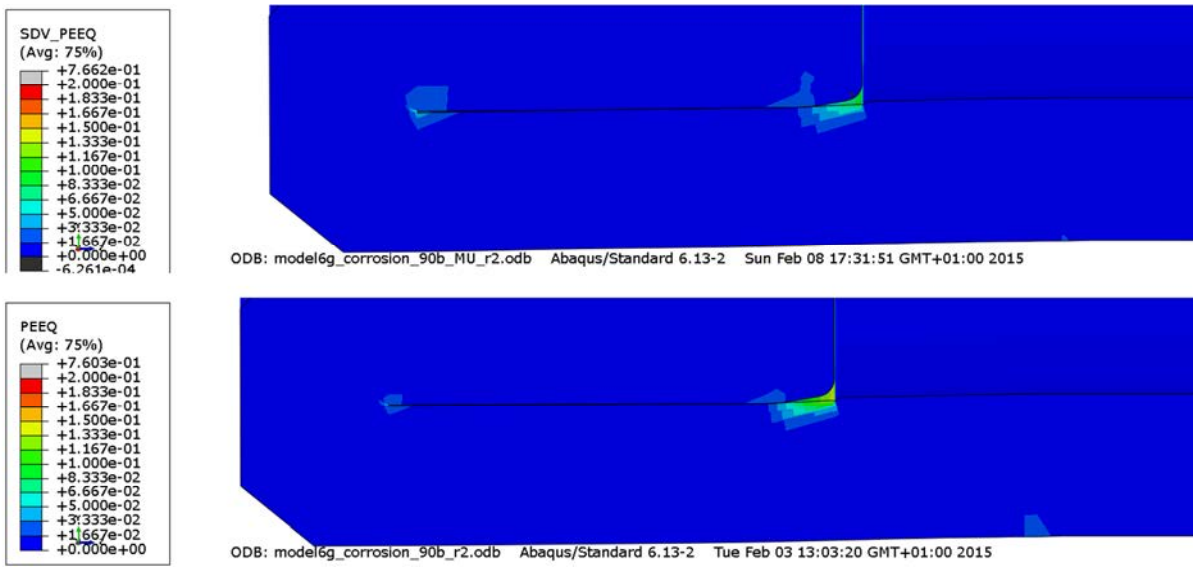

Figure 8-23. *Equivalent plastic strain (PEEQ) in the copper shell at 6 cm shearing for model6g_corrosion_90b_MU (upper) and model6g_corrosion_90b base right corner (lower)*

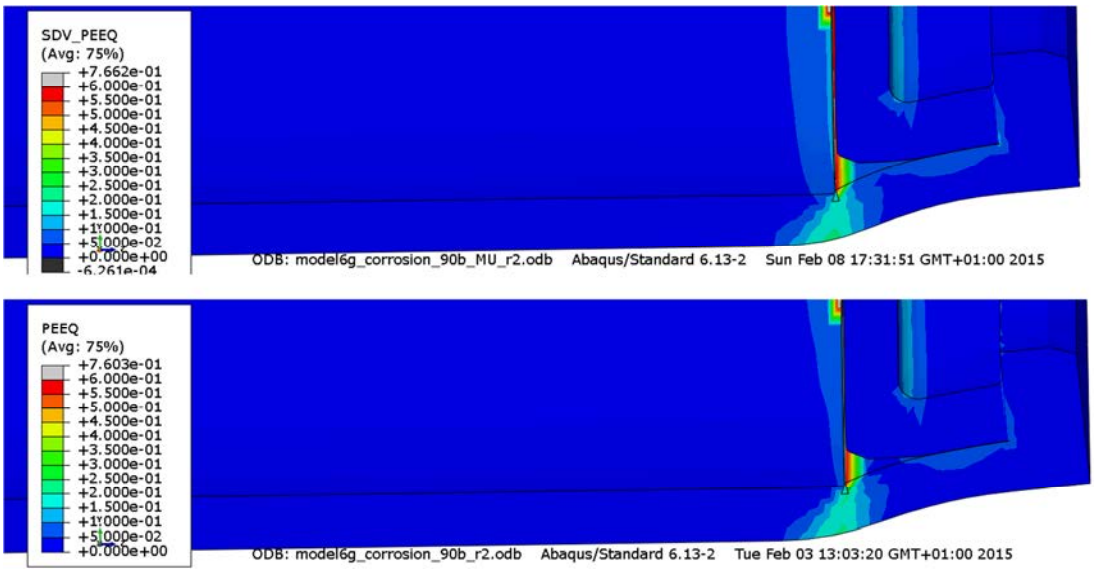

Figure 8-24. *Equivalent plastic strain (PEEQ) in the copper shell at 6 cm shearing for model6g_corrosion_90b_MU (upper) and model6g_corrosion_90b top right corner (lower)*

Table 8-1 shows results for the insert (Mises stress, axial stress (S33) and equivalent plastic strain (PEEQ) at 5 cm. Tables 8-2 to 8-5 show results for the copper shell (Mises stress and equivalent plastic strain (PEEQ) at 5 cm shearing displacement and at 6 cm shearing displacement when shearing at 90% of the insert height and at 8 cm when shearing at the insert lid (last converged solutions).

Region 4 (discontinuity at the top) is not reported since one row of elements at the discontinuity has deformed to have an almost singular Jacobian matrix which makes the results in this region non-representative.

Table 8-1. Summary of results for the insert

Model name	1 – iron insert 2 – steel channel tubes	PEEQ [%]				Mises [MPa]				S33 [MPa] maximum tension		Last converged shearing displacement and output result shearing [cm]		
	Shearing [cm]	5		8		5		8		5	8			
	Insert material	1	2	1	2	1	2	1	2	1	1			
model6g_corrosion_90b (6 cm)		0.3	0.2	0.7	0.3	380	481	397	511	294	298	6	5	6
model6g_corrosion_90b_MU (6 cm)		0.9	0.3	1.2	0.3	395	500	398	519	299	304	7.8	5	6
N31b_finer_1sekm (90%) (6 cm)		0.1	0.1	0.1	0.1	319	477	320	485	328	332	6	5	6
model6g_corrosion_lidb		0	0	0.3	0.1	276	425	312	457	66	75	8	5	8
model6g_corrosion_lidb_MU		0	0	0.6	0.1	299	439	324	449	70	86	8	5	8
n34b_finer_1sekm_quasi (lid)		0	0	0.2	0.0	228	215	330	392	117	119	10	5	8

Table 8-2. Summary of strain PEEQ (%) results for copper shell at 5 cm shearing.

Model name	1 – mid shell 2,3 – top/base welds 5 – base discontinuity 6,7 – top/base fillets						
	Copper shell region	1	2	3	5	6	7
model6g_corrosion_90b		7.51	6.57	5.32	14.43	14.41	3.13
model6g_corrosion_90b_MU		8.14	9.49	8.11	8.97	18.92	3.38
N31b_finer_1sekm (90%)		7.57	17.73	3.12	9.25	6.56	0.00
model6g_corrosion_lidb		8.26	14.68	5.03	14.43	23.52	3.08
model6g_corrosion_lidb_MU		8.53	18.64	7.31	8.87	22.33	3.29
n34b_finer_1sekm_quasi (lid)		3.11	11.44	2.63	2.09	7.59	0.00

Table 8-3. Summary of strain PEEQ (%) results for copper shell at 8 cm shearing.

Model name	1 – mid shell 2,3 – top/base welds 5 – base discontinuity 6,7 – top/base fillets						
	Copper shell region	1	2	3	5	6	7
model6g_corrosion_90b (6 cm)		10.27	10.97	5.64	14.43	19.44	3.19
model6g_corrosion_90b_MU (6cm)		9.26	13.37	8.29	8.98	20.30	3.41
N31b_finer_1sekm (90%) (6 cm)		9.59	24.37	3.16	11.30	8.80	0.00
model6g_corrosion_lidb		12.24	81.50	5.04	14.43	30.33	3.08
model6g_corrosion_lidb_MU		12.42	33.01	7.34	8.87	29.59	3.29
n34b_finer_1sekm_quasi (lid)		4.82	13.92	2.63	2.09	10.43	0.00

Table 8-4. Summary of Mises stress [MPa] results for copper shell at 5 cm shearing.

Model name	1 – mid shell 2,3 – top/base welds 5 – base discontinuity 6,7 – top/base fillets						
	Copper shell region	1	2	3	5	6	7
model6g_corrosion_90b		156	171	164	252	232	128
model6g_corrosion_90b_MU		152	182	173	255	272	109
N31b_finer_1sekm (90%)		163	156	131	147	149	65
model6g_corrosion_lidb		158	213	157	259	281	126
model6g_corrosion_lidb_MU		149	224	169	251	277	104
n34b_finer_1sekm_quasi (lid)		122	130	153	106	160	29

Table 8-5. Summary of Mises stress [MPa] results for copper shell at 8 cm shearing.

Model name	1 – mid shell 2,3 – top/base welds 5 – base discontinuity 6,7 – top/base fillets						
	Copper shell region	1	2	3	5	6	7
model6g_corrosion_90b (6 cm)		176	215	165	251	274	129
model6g_corrosion_90b_MU (6 cm)		162	209	175	256	276	112
N31b_finer_1sekm (90%) (6 cm)		180	175	129	157	167	70
model6g_corrosion_lidb		185	255	157	259	303	126
model6g_corrosion_lidb_MU		180	274	169	252	310	104
n34b_finer_1sekm_quasi (lid)		134	165	153	106	185	29

9 Uncertainties

The obtained results are based on several assumptions regarding loads and material properties. Also the discretization in the computer model will affect the results. The most important of these influencing factors are addressed below.

- Strain rate effects for bentonite, copper and iron will affect the results.
- All experiments used for material calibration have a spread which will imply a range for the properties defining each material model.
- Swelling pressure for the bentonite will affect the material stiffness. The experimental results have a spread in the results and the used data should be conservative in the sense that the obtained stress and strain magnitudes are overestimated.
- Element mesh is rather fine but nevertheless it is too coarse in some regions, especially at the welds and regions with geometric discontinuities. A more refined mesh will probably increase the maximum stress and strain levels. Fortunately, the use of non-linear material properties (such as plasticity) will decrease the sensitivity on the used mesh. The used mesh has been judged to be accurate enough considering also the required computer resources to obtain the results. Since several models have been executed with different mesh densities it has been possible to compare and the conclusion is that the mesh in a global sense is accurate.

10 Evaluation and conclusions

The results obtained from the rock shear analyses could be summarized as:

- The maximum plastic strain in copper shell occurs in the fillets (besides regions containing singularities). At the global level the plastic strains are much lower. The maximum plastic strains in the insert occur at the corners of a specific channel. However, the magnitude is small compared to ultimate strains and is considered not to cause any severe damage.
- Maximum principal stress in the insert mainly comes from bending of the shell – the level depends mainly on material properties (and dimensions) for the insert and buffer.
- Material dependency on strain rate has been considered for all parts except for copper, which uses an elastic-plastic model with an estimated strain rate.

The change of copper shell thickness due to assumed corrosion (half original thickness) affects the results. This could be summarized as:

- Stresses and strains in the insert are not affected except at some local regions due to a more refined mesh in the current study, see Figures 8-2 to 8-4. Maximum Mises stress increases from 232 MPa for the reference case to 316 MPa with reduced copper thickness when shearing at the lid with magnitude 8 cm.
- Deformation of the copper shell upper corners increases substantially when the copper thickness is reduced.
- Comparison of original copper material definition and copper material definition suggested by Unosson (SKBdoc 1393179) imply similar strain levels but Mises stress differs more due to different hardening rules.
- When 5 cm shear displacement occurs on a canister with copper thickness of 2.5 cm, results show that approximately 24 % plastic strain occurs in the copper shell at the shear plane at the insert steel lid and approximately 19 % plastic strain in the copper shell at the shear plane at 90 % position.
- The triaxiality dependent failure strain function of copper has been evaluated in the report "A constitutive model for texture dependent deformation hardening and pressure dependent initiation of ductile failure in metallic materials" (SKBdoc 1393179), from which it is clear that the strain at failure of copper in the canister exceeds 50 % even at high triaxiality.
- The obtained plastic strain in the copper shell in this analysis is below 50 %. In accordance with current design criterion maximum 80 % effective plastic strain for the copper shell and considering triaxiality effects, the conclusion is that the canister will maintain its mechanical integrity for the shear load case even with a copper shell thickness of 2.5 cm.

References

ABAQUS, 2013. Version 6.12.1. Dassault Systèmes Simulia Corp.

Börgesson L, 1988. Modelling of buffer material behaviour. Some examples of material models and performance calculations. SKB TR 88-29, Svensk Kärnbränslehantering AB.

Börgesson L, 1992. Interaction between rock, bentonite buffer and canister. FEM calculations of some mechanical effects on the canister in different disposal concepts. SKB TR 92-30, Svensk Kärnbränslehantering AB.

Börgesson L, Hernelind J, 2006. Earthquake induced rock shear through a deposition hole. Influence of shear plane inclination and location as well as buffer properties on the damage caused to the canister. SKB TR-06-43, Svensk Kärnbränslehantering AB.

Börgesson L, Johannesson L-E, Sandén T, Hernelind J, 1995. Modelling of the physical behaviour of water saturated clay barriers. Laboratory tests, material models and finite element application. SKB TR 95-20, Svensk Kärnbränslehantering AB.

Börgesson L, Johannesson L-E, Hernelind J, 2003. Earthquake induced rock shear through a deposition hole. Effect on the canister and the buffer. SKB TR-04-02, Svensk Kärnbränslehantering AB.

Börgesson L, Dueck A, Johannesson L-E, 2010. Material model for shear of the buffer – evaluation of laboratory test results. SKB TR-10-31, Svensk Kärnbränslehantering AB.

Hernelind J, 2010. Modelling and analysis of canister and buffer for earthquake induced rock shear and glacial load. SKB TR-10-34, Svensk Kärnbränslehantering AB.

Jin L-Z, Sandström R, 2008. Creep of copper canisters in power-law breakdown. Computational Materials Science 43, 403–416.

Raiko H, Sandström R, Rydén H, Johansson M, 2010. Design analysis report for the canister. SKB TR-10-28, Svensk Kärnbränslehantering AB.

Sandström R, Andersson H C M, 2008. Creep in phosphorus alloyed copper during power-law breakdown. Journal of Nuclear Materials 372, 76–88.

Sandström R, Hallgren J, Burman G, 2009. Stress strain flow curves for Cu-OFP. SKB R-09-14, Svensk Kärnbränslehantering AB.

SKB, 2010. Design, production and initial state of the canister. SKB TR-10-14, Stockholm: Svensk Kärnbränslehantering AB.

SSABDirekt, 2008. Steelfacts Domex 355 MC. Available at http://www.ssabdirect.com. [19 September 2008].

SS-EN 10025-2:2004. Varmvalsade konstruktionsstål – Del 2: Tekniska leveransbestämmelser för olegerade stål (Hot rolled products of structural steels – Part 2: Technical delivery conditions for non-alloy structural steels). Stockholm: Swedish Standards Institute.

SSM, 2014. Begäran om komplettering av ansökan om slutförvaring av använt kärnbränsle och kärnavfall – Inverkan av koppartjocklek på kapselns designanalys. SSM2011-2426-172, Strålsäkerhetsmyndigheten. (In Swedish.)

Unpublished documents

SKBdoc id, version	Title	Issuer, year
1201865 ver 1.0	Dragprovning av gjutjärn. (In Swedish.)	KTH, 2009
1203875 ver 2.0	Ritningsförteckning för kapselkomponenter. (In Swedish.)	SKB, 2014
1339902 ver 1.0	Global simulation of copper canister – final deposition	5T Engineering, 2013
1393179 ver 2.0	A constitutive model for texture dependent deformation hardening and pressure dependent initiation of ductile failure in metallic materials	True Stress Engineering, 2015
1403930 ver 1.0	Shearing of copper canister at top and base	5T Engineering, 2013
1407337 ver 1.0	Earthquake induced rock shear through a deposition hole – Part 2. Additional calculations of the influence of inhomogeneous buffer on the stresses in the canister.	Clay Technology/5T Engineering, 2013

Appendix 1 –Rock shear perpendicular to canister axis at 90% of the insert height – copper with Kimab material model

Plots A1-1 to A1-16 showing deformed geometry, plastic strain (PEEQ), Mises stress (MISES) for shearing magnitudes 5 and 6 cm. Deformations scaled by factor 2.

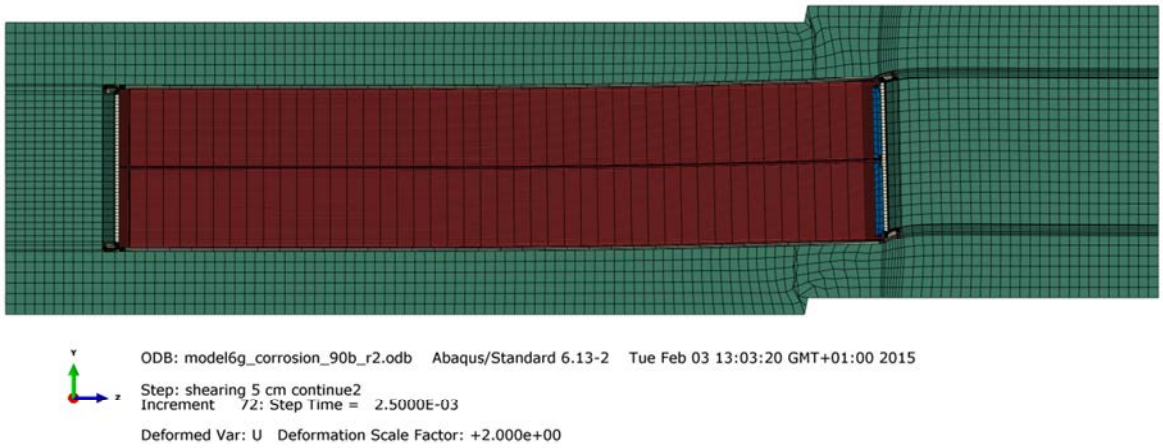

Figure A1-1. *Deformed geometry at 5 cm shearing.*

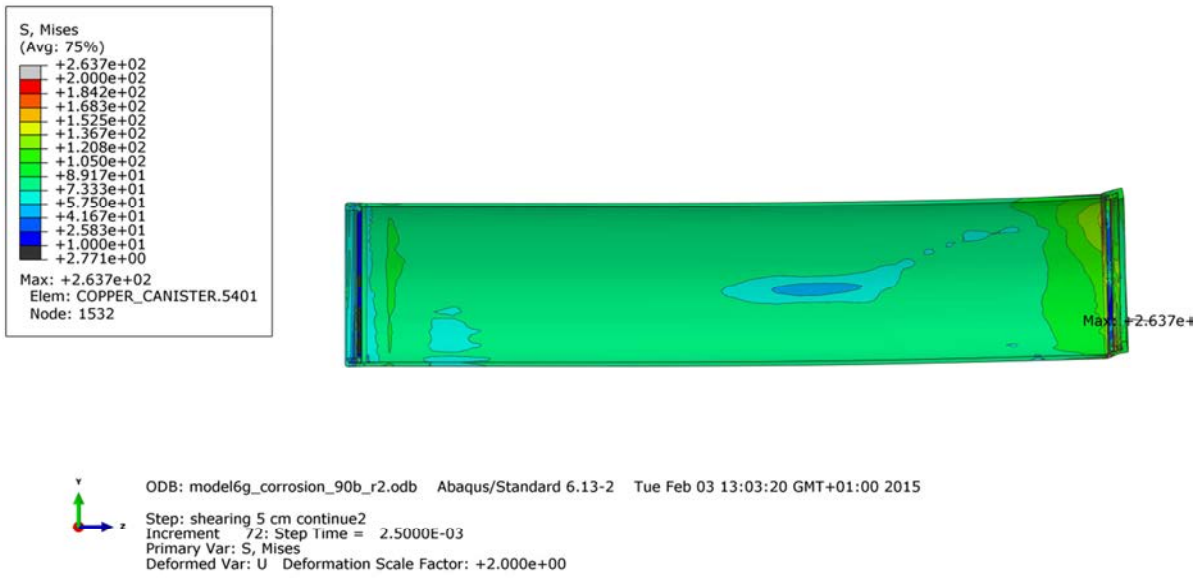

Figure A1-2. *Mises stress [MPa] in the copper shell at 5 cm shearing.*

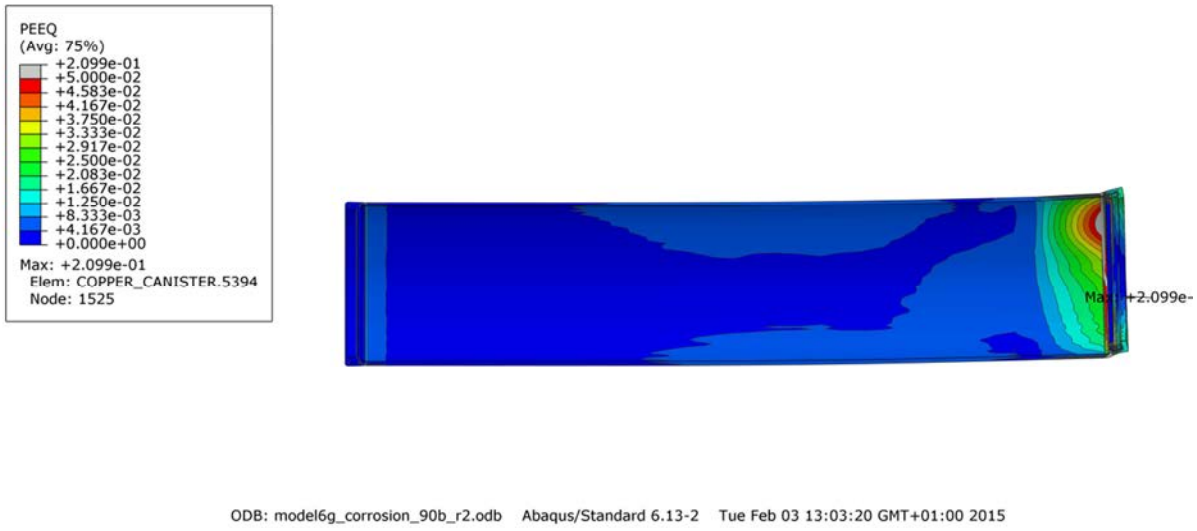

Figure A1-3. *Equivalent plastic strain (PEEQ) in the copper shell at 5 cm shearing.*

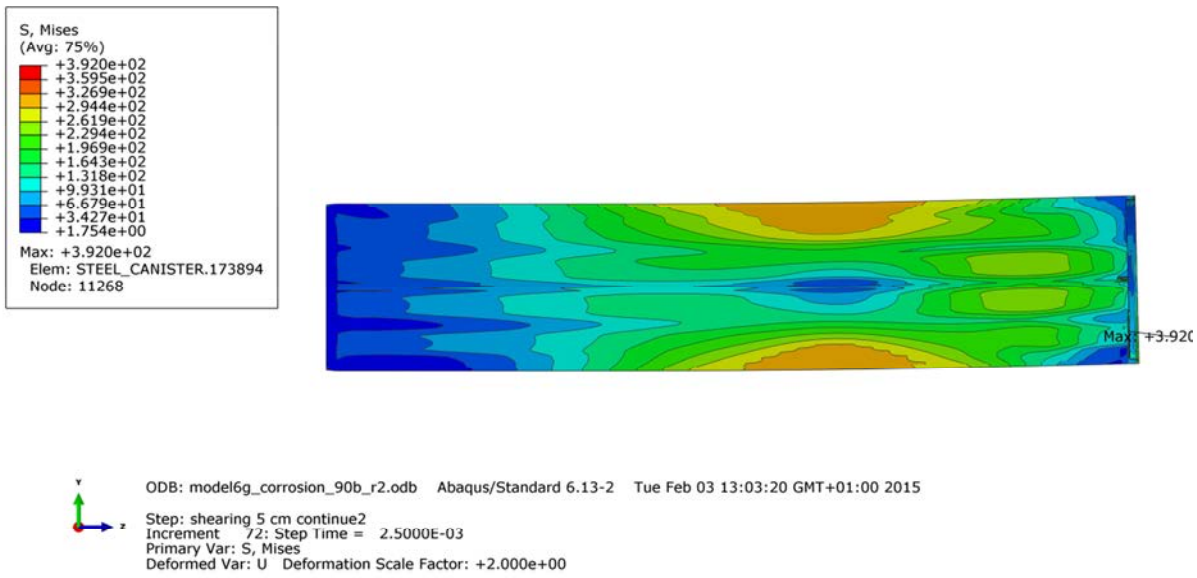

Figure A1-4. *Mises stress [MPa] in the insert at 5 cm shearing.*

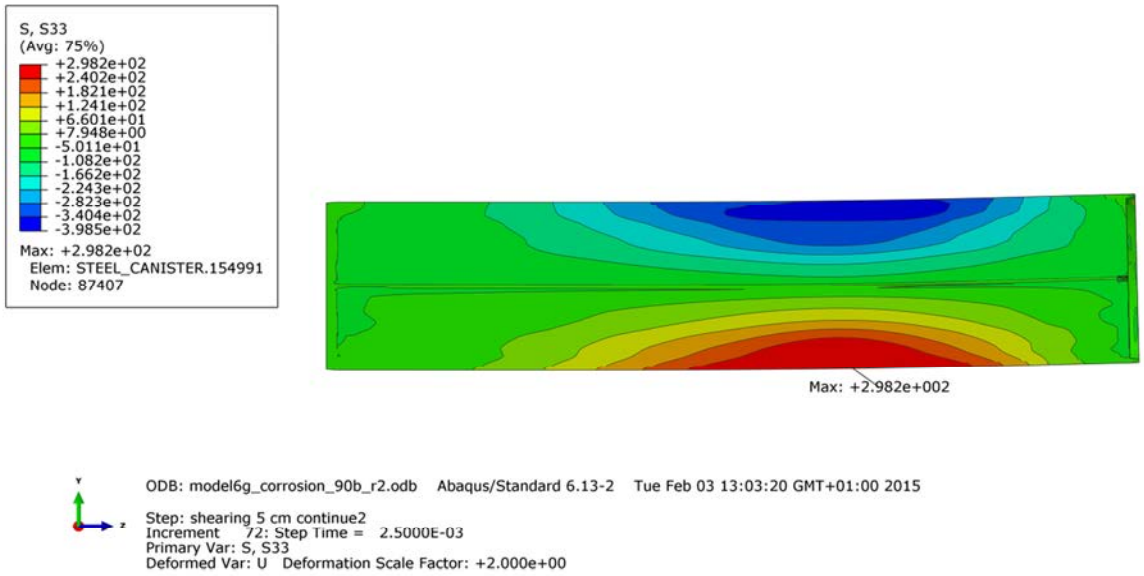

Figure A1-5. *Axial stress [MPa] in the insert at 5 cm shearing.*

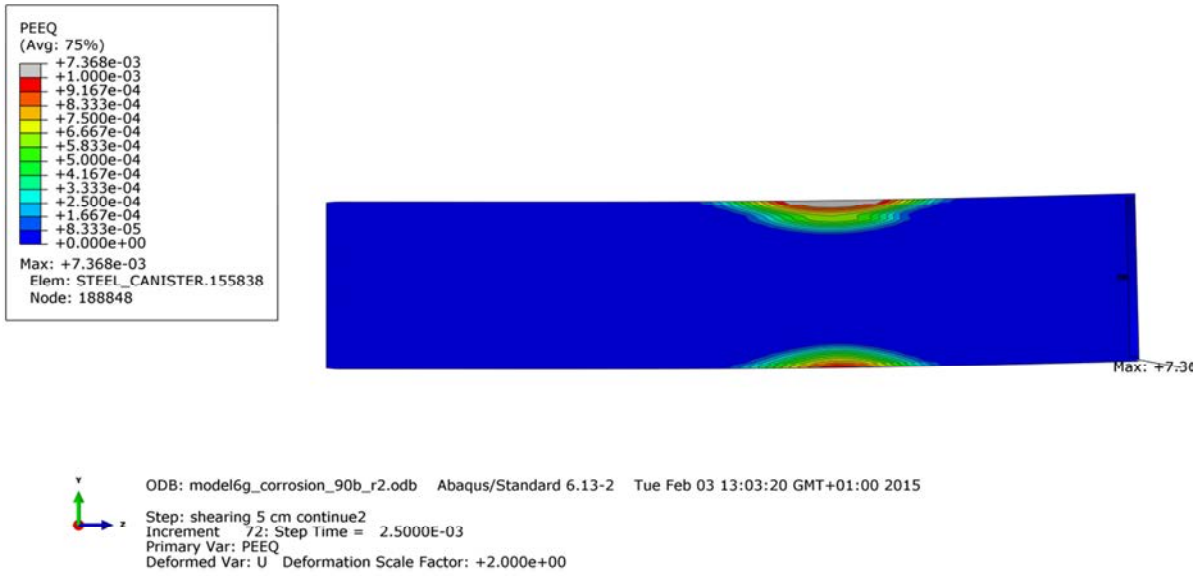

Figure A1-6. *Equivalent plastic strain (PEEQ) in the insert at 5 cm shearing.*

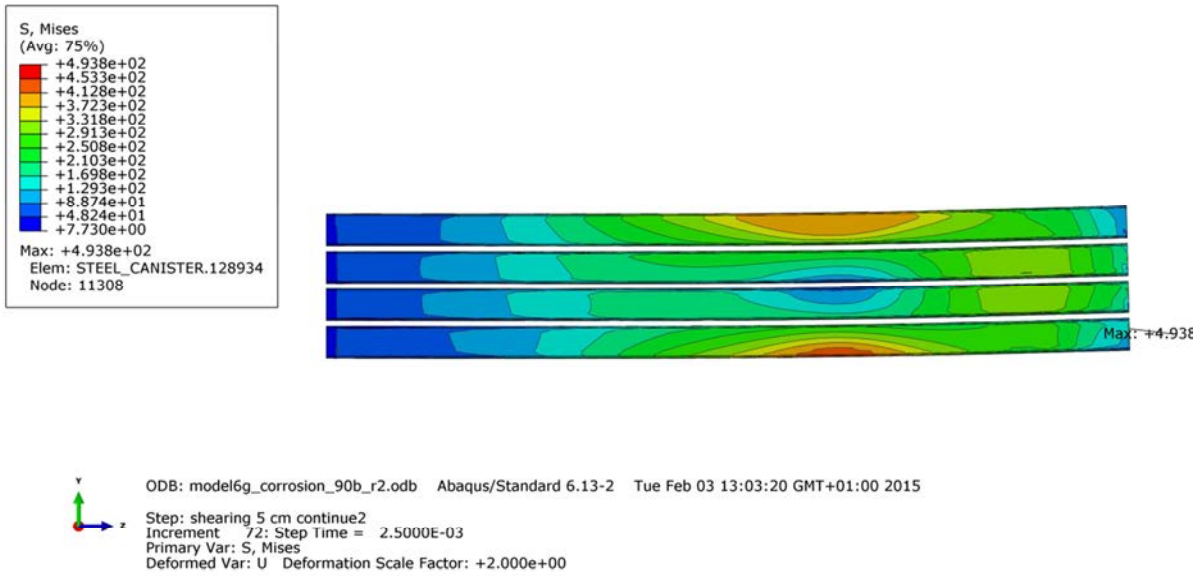

Figure A1-7. *Mises stress [MPa] in the channel tubes at 5 cm shearing.*

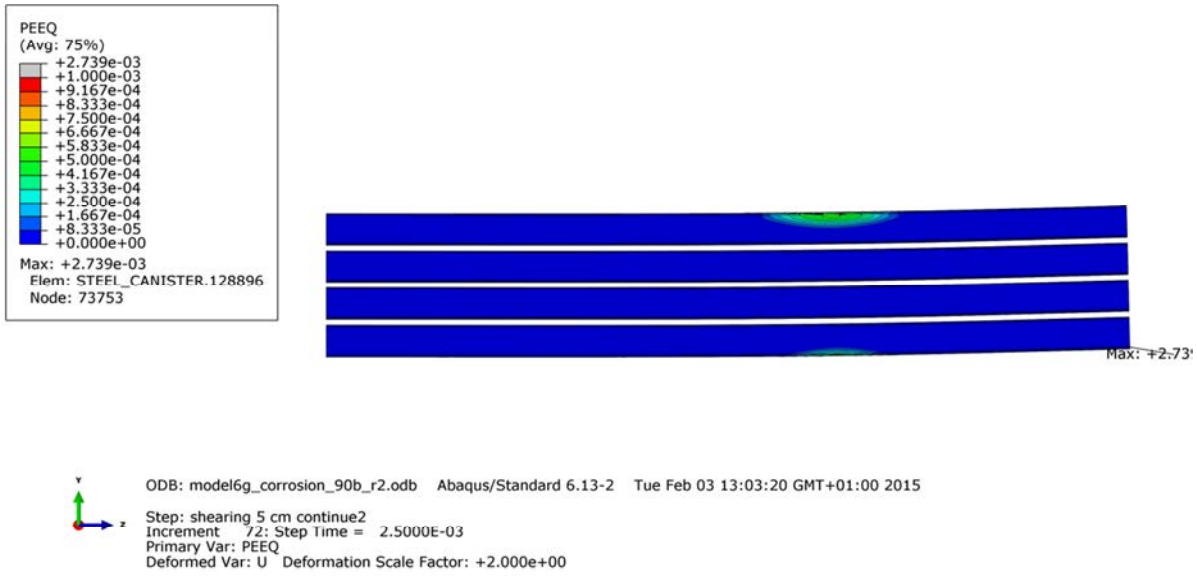

Figure A1-8. *Equivalent plastic strain (PEEQ) in the channel tubes at 5 cm shearing.*

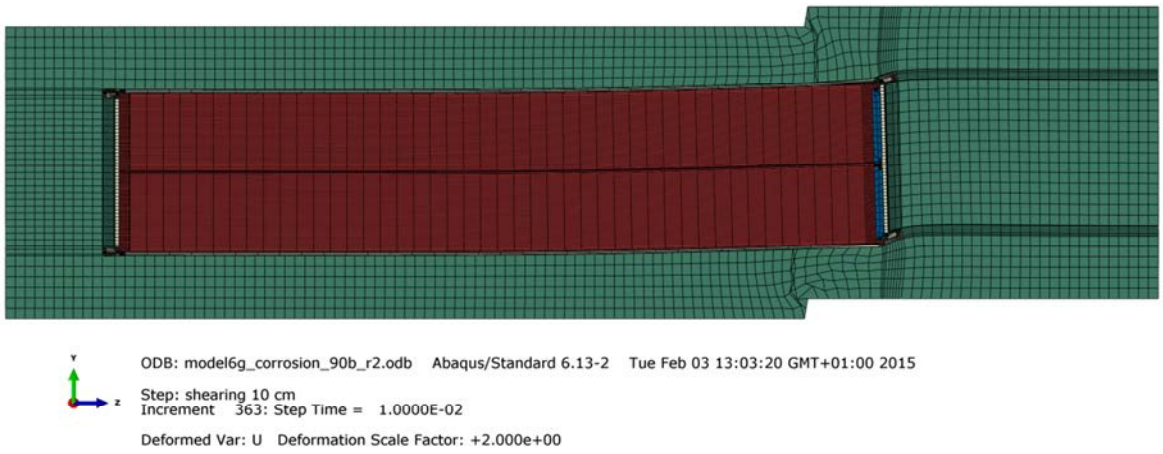

Figure A1-9. *Deformed geometry at 6 cm shearing.*

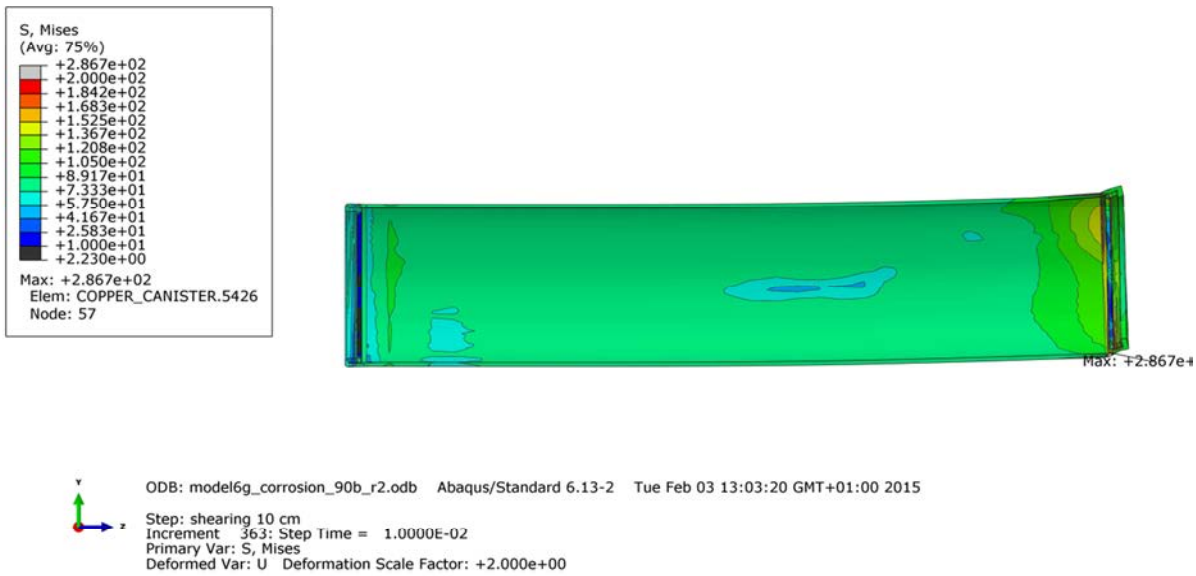

Figure A1-10. *Mises stress [MPa] in the copper shell at 6 cm shearing.*

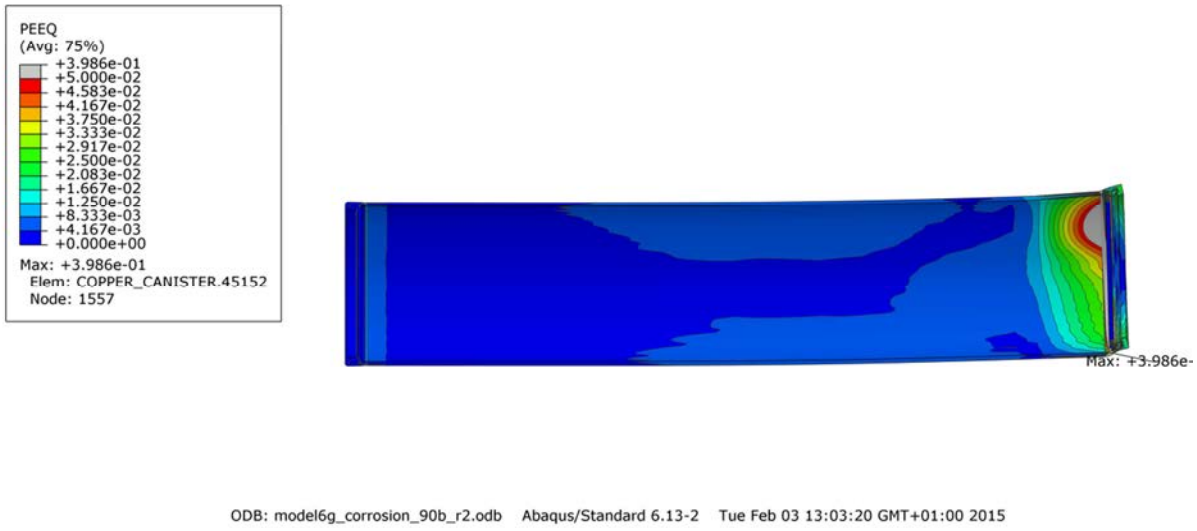

Figure A1-11. *Equivalent plastic strain (PEEQ) in the copper shell at 6 cm shearing.*

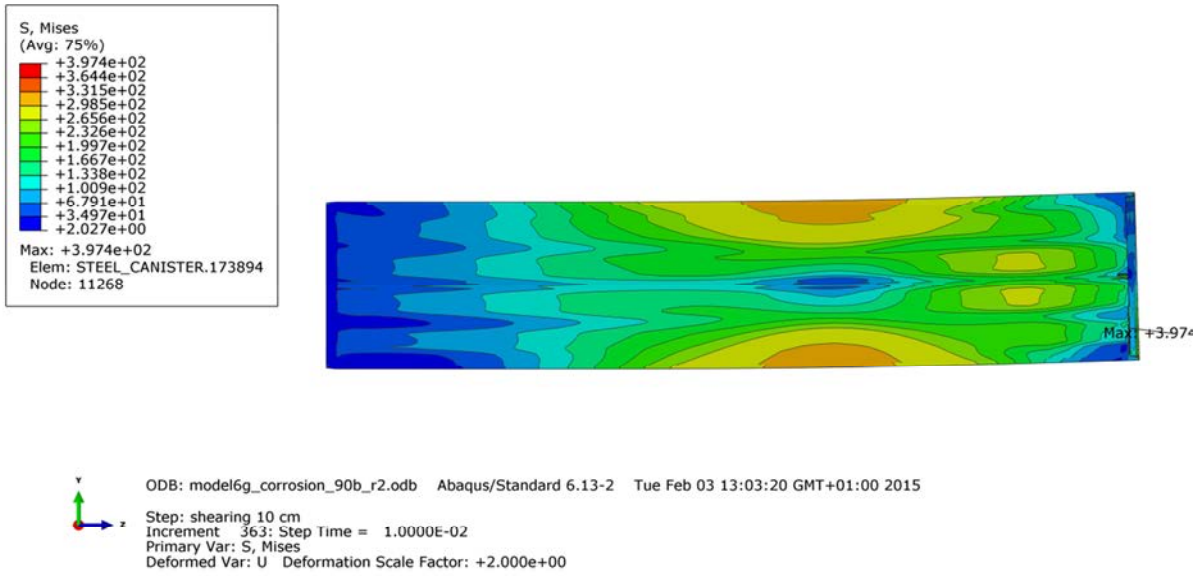

Figure A1-12. *Mises stress [MPa] in the insert at 6 cm shearing.*

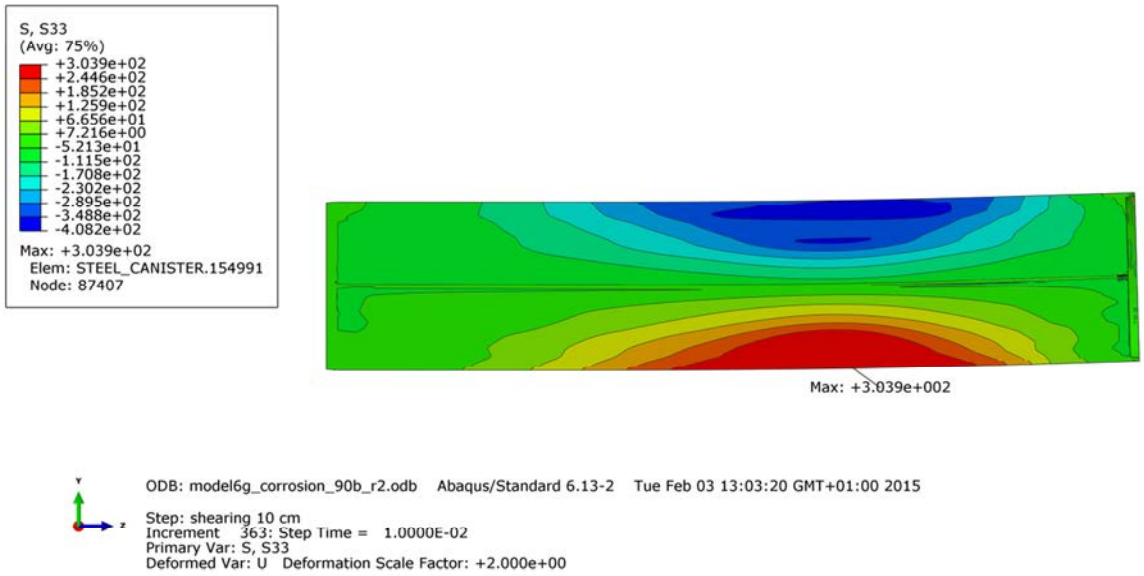

Figure A1-13. *Axial stress [MPa] in the insert at 6 cm shearing.*

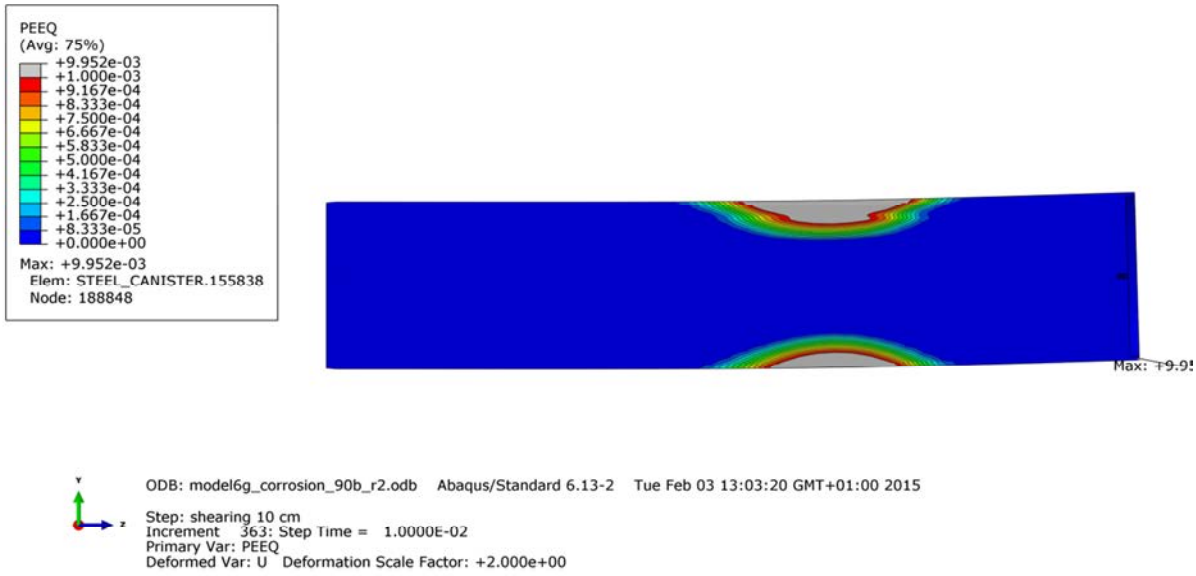

Figure A1-14. *Equivalent plastic strain (PEEQ) in the insert at 6 cm shearing.*

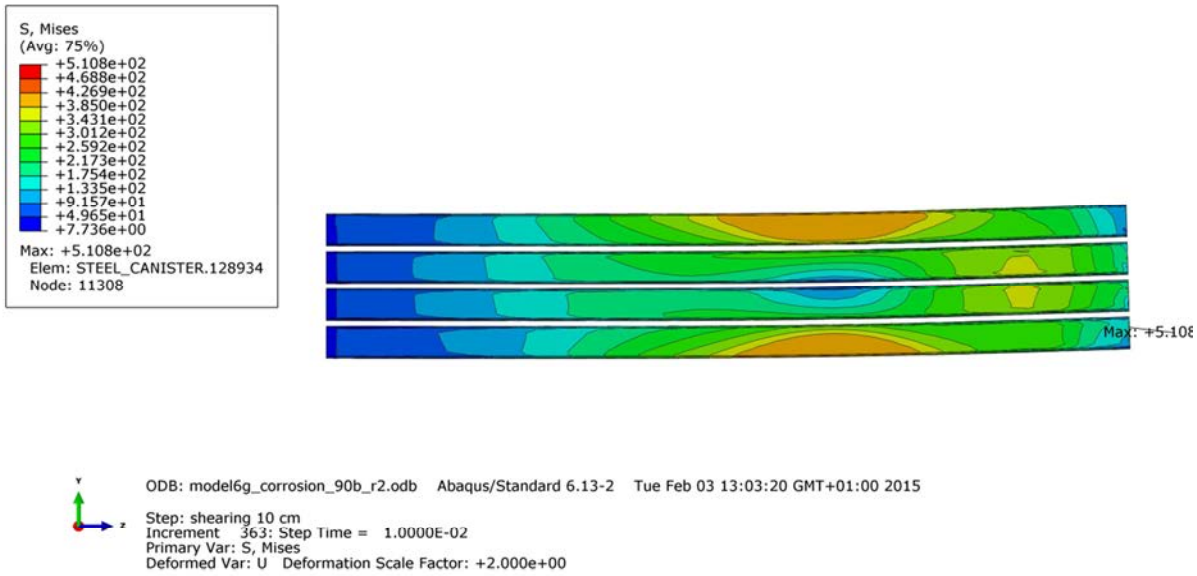

Figure A1-15. *Mises stress [MPa] in the channel tubes at 6 cm shearing.*

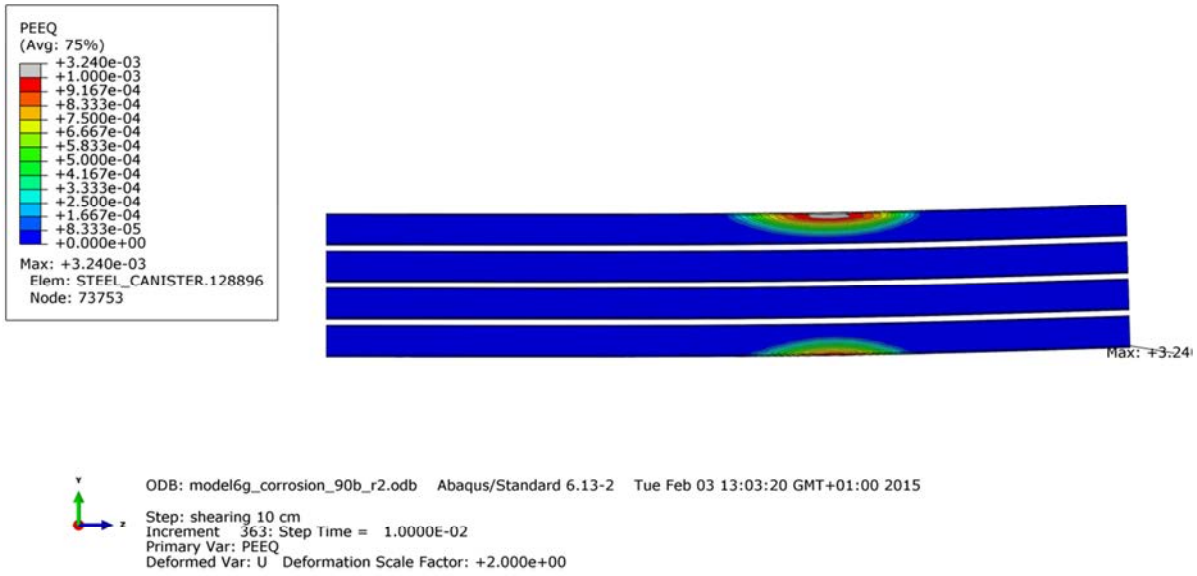

Figure A1-16. *Equivalent plastic strain (PEEQ) in the channel tubes at 6 cm shearing.*

Appendix 2 –Rock shear perpendicular to canister axis at 90% of the insert height – copper with Unosson material model, SKBdoc 1393179

Plots A2-1 to A2-16 showing deformed geometry, plastic strain (PEEQ), Mises stress (MISES) for shearing magnitudes 5 and 6 cm. Deformations scaled by factor 2.

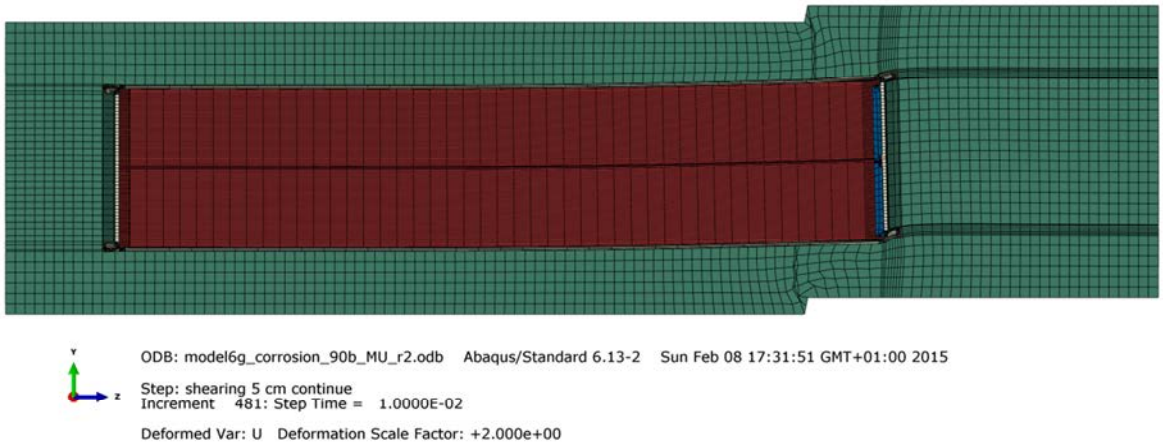

Figure A2-1. *Deformed geometry at 5 cm shearing.*

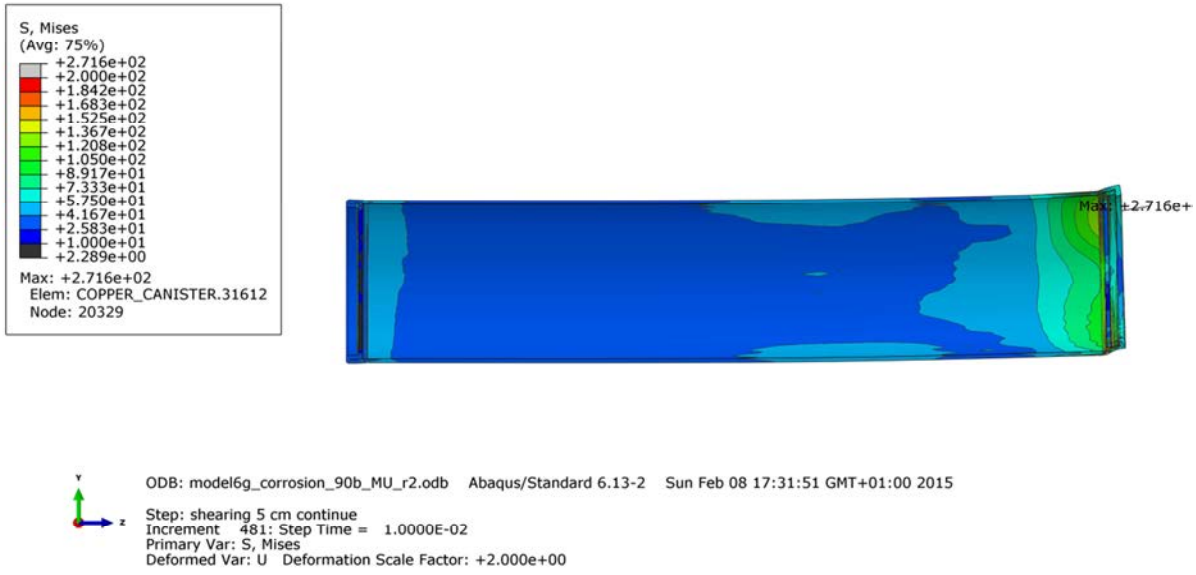

Figure A2-2. *Mises stress [MPa] in the copper shell at 5 cm shearing.*

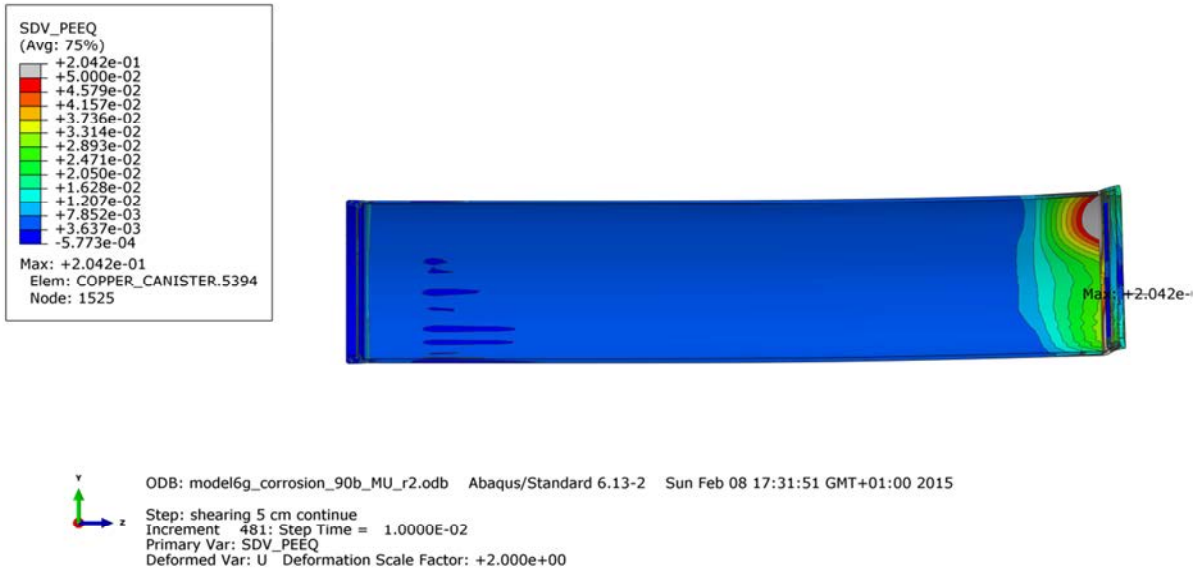

Figure A2-3. *Equivalent plastic strain (PEEQ) in the copper shell at 5 cm shearing.*

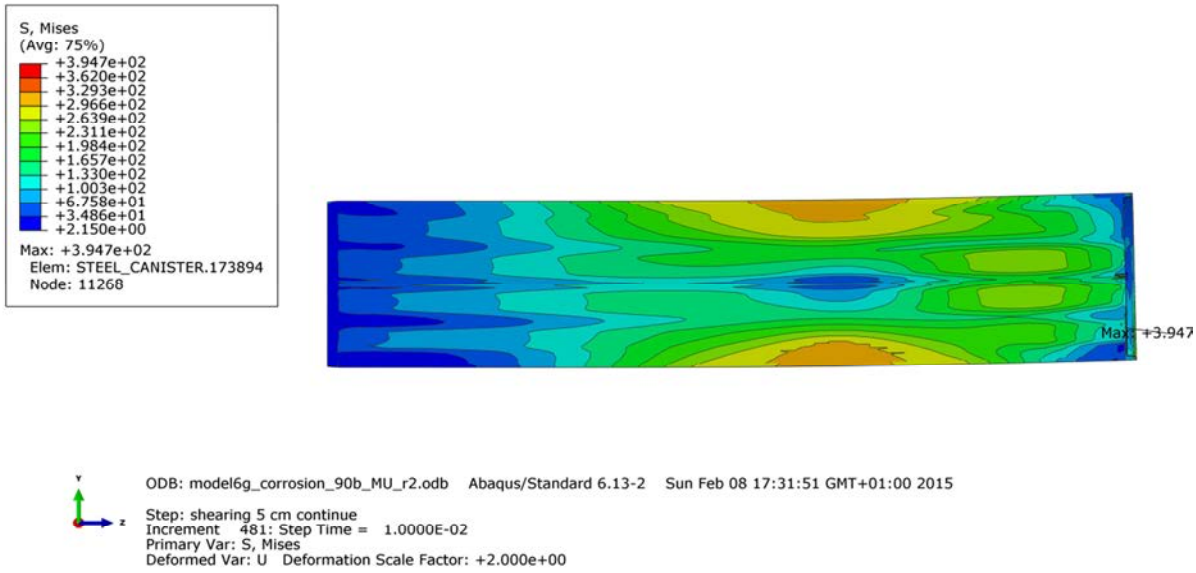

Figure A2-4. *Mises stress [MPa] in the insert at 5 cm shearing.*

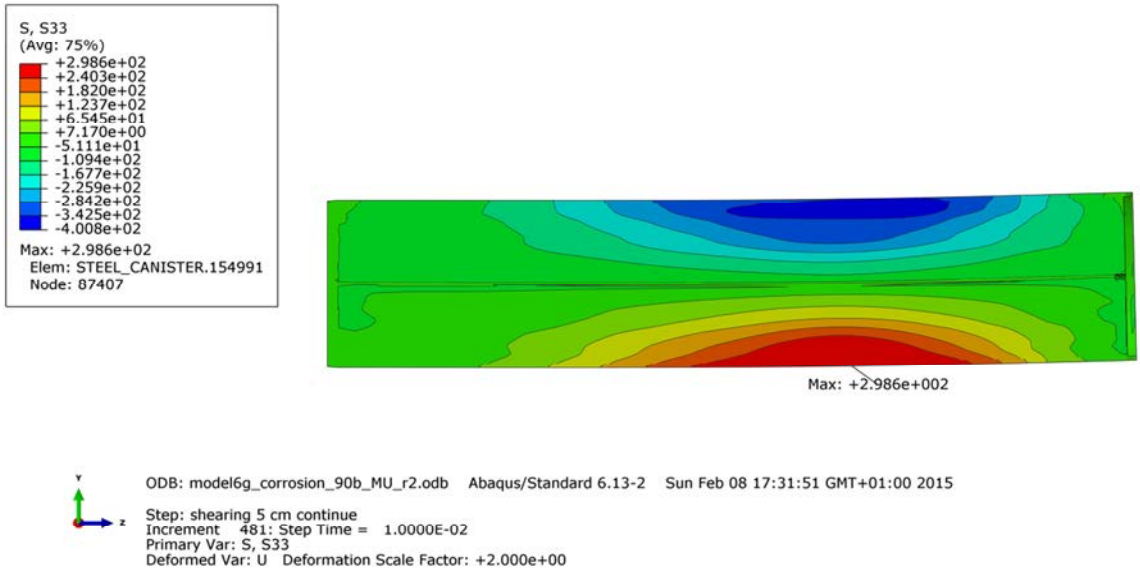

Figure A2-5. *Axial stress [MPa] in the insert at 5 cm shearing.*

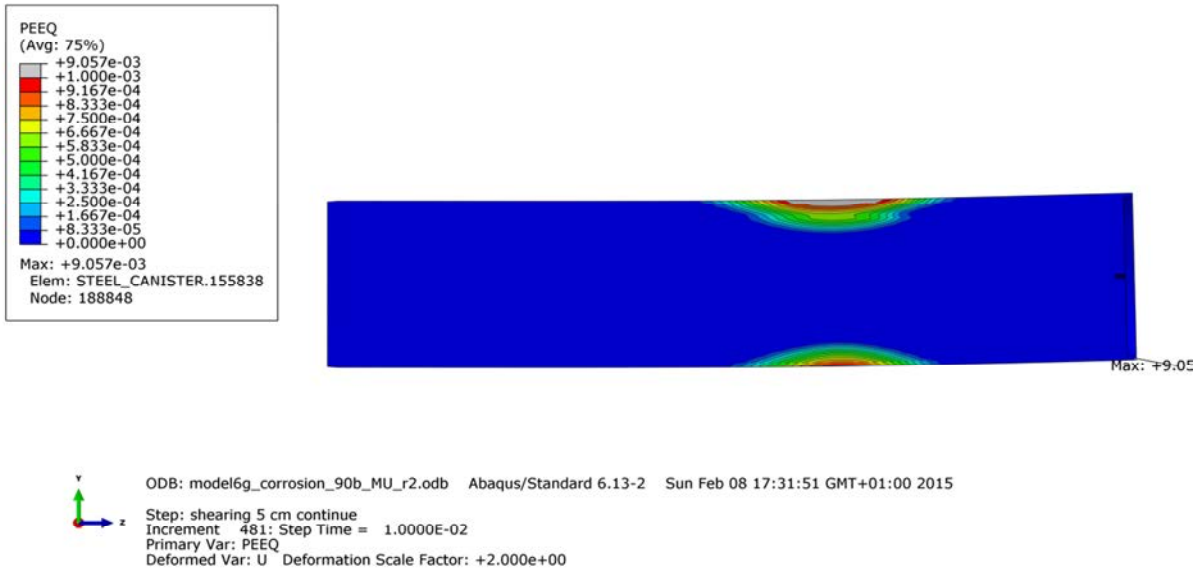

Figure A2-6. *Equivalent plastic strain (PEEQ) in the insert at 5 cm shearing.*

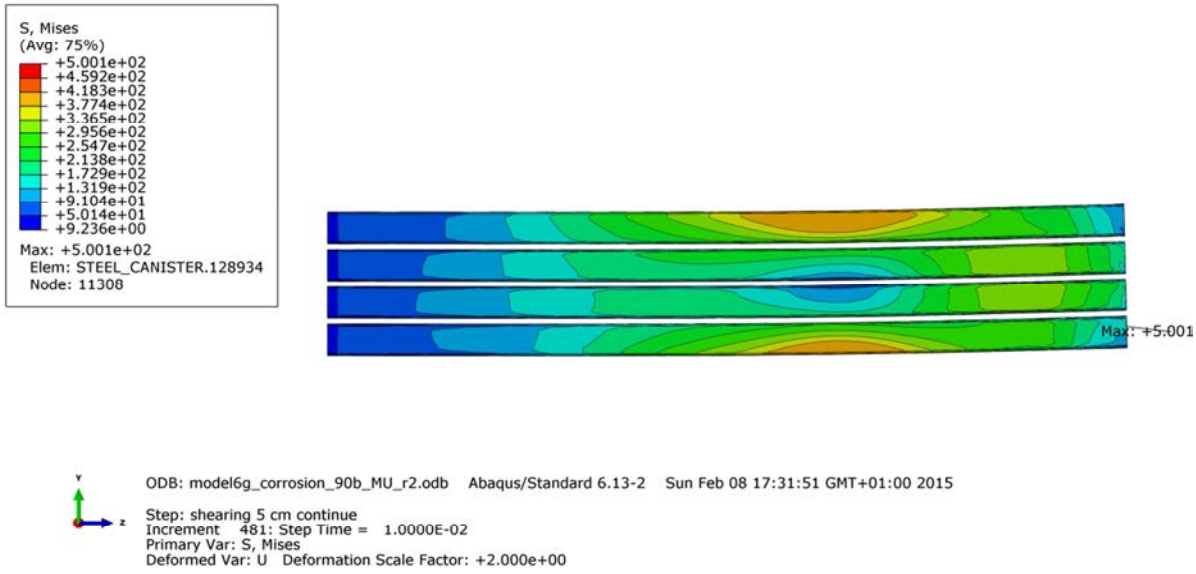

Figure A2-7. *Mises stress [MPa] in the channel tubes at 5 cm shearing.*

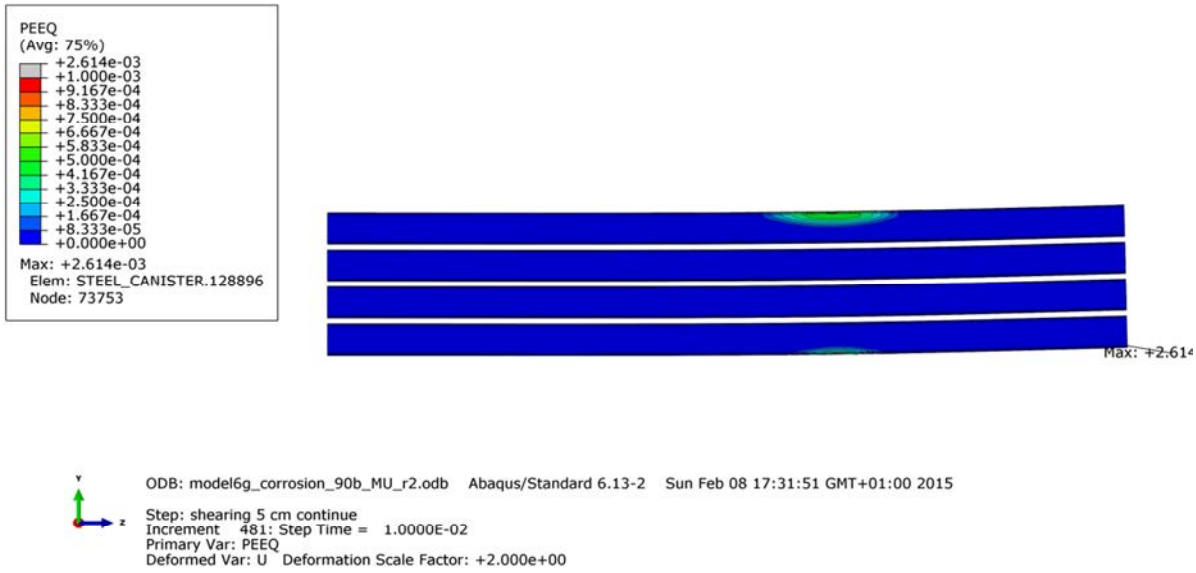

Figure A2-8. *Equivalent plastic strain (PEEQ) in the channel tubes at 5 cm shearing.*

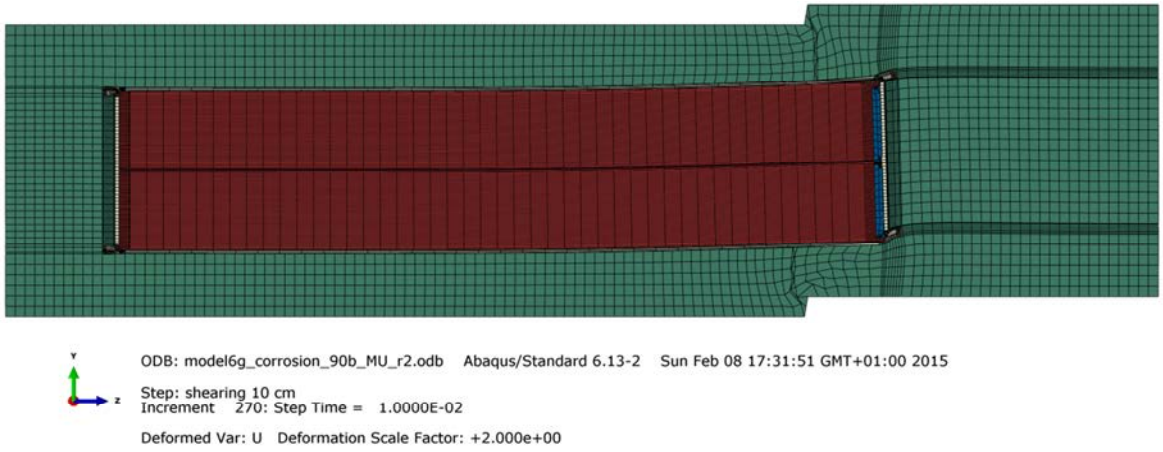

Figure A2-9. *Deformed geometry at 6 cm shearing.*

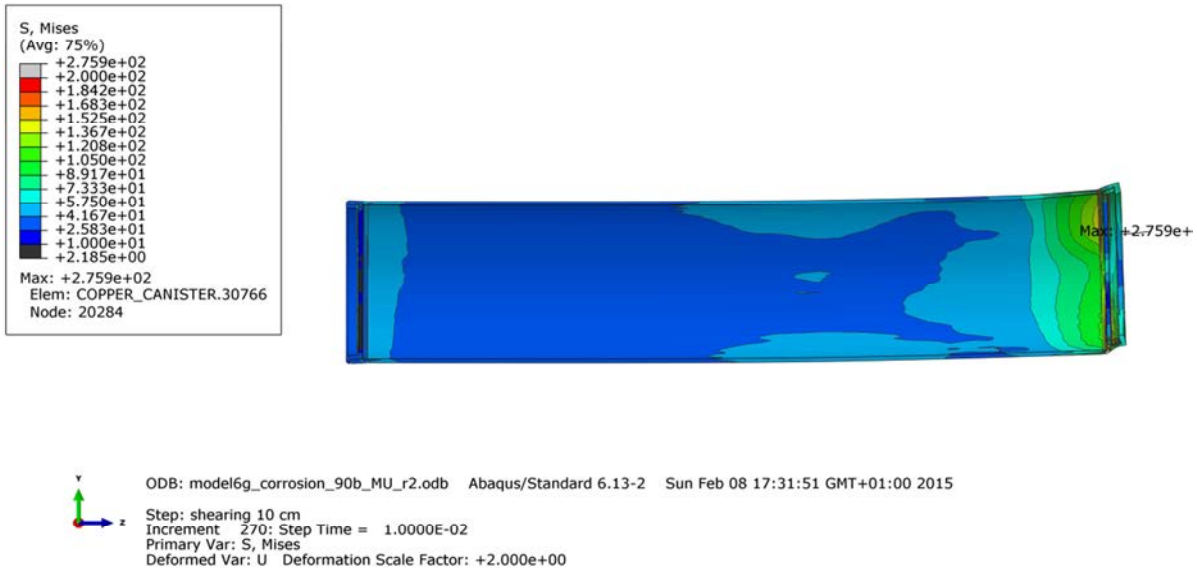

Figure A2-10. *Mises stress [MPa] in the copper shell at 6 cm shearing.*

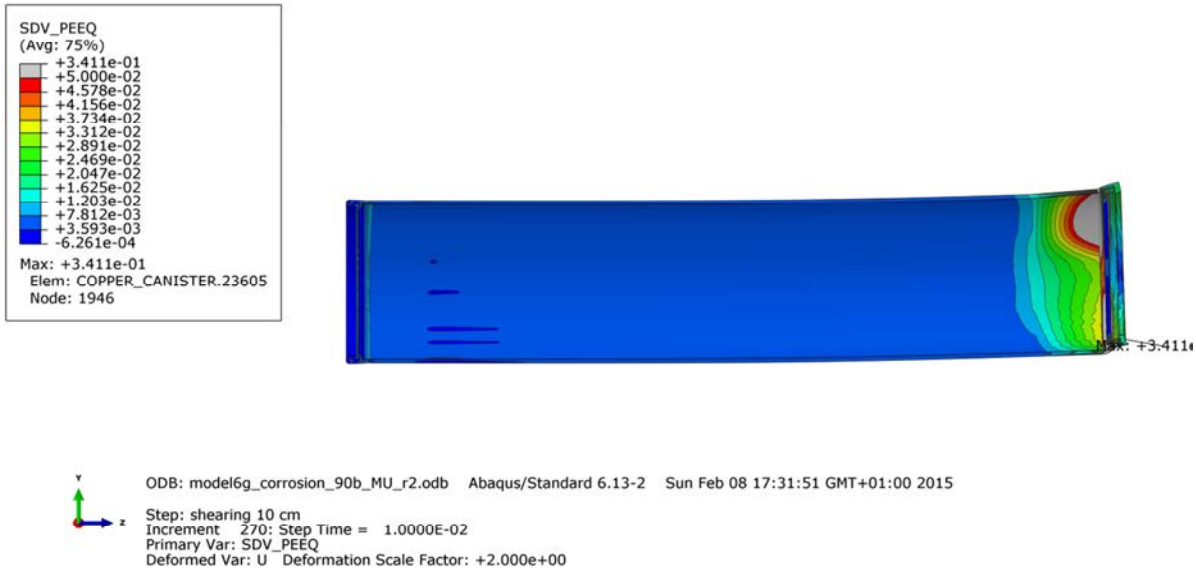

Figure A2-11. *Equivalent plastic strain (PEEQ) in the copper shell at 6 cm shearing.*

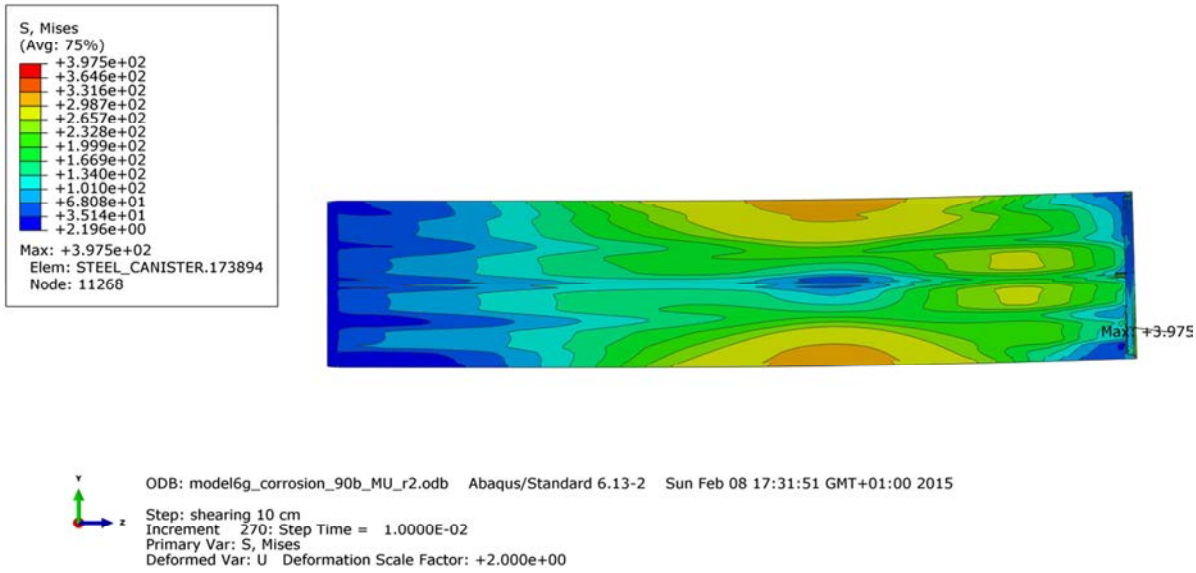

Figure A2-12. *Mises stress [MPa] in the insert at 6 cm shearing.*

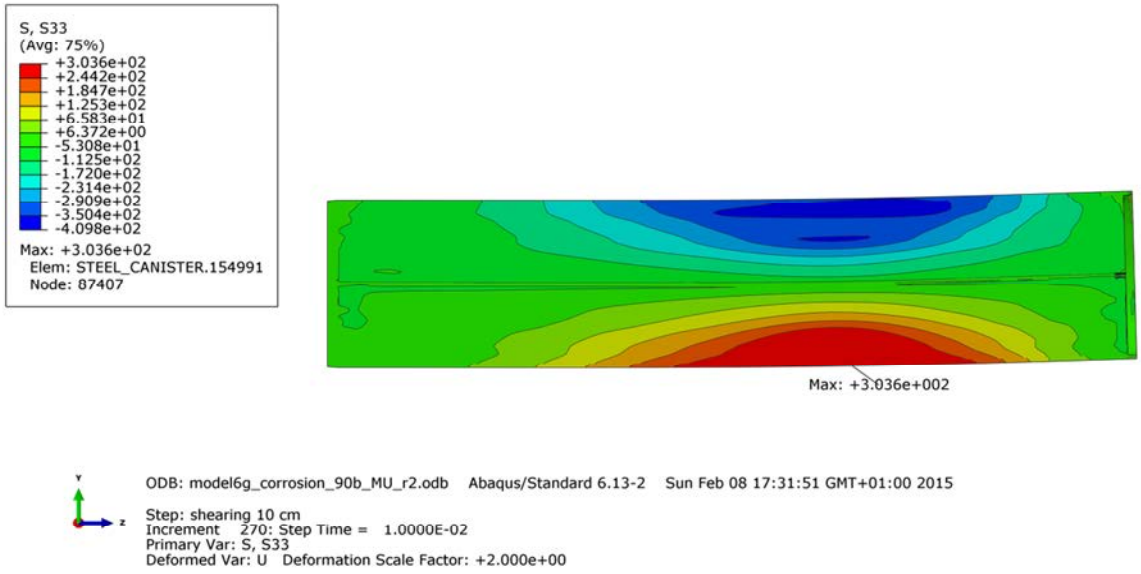

Figure A2-13. *Axial stress [MPa] in the insert at 6 cm shearing.*

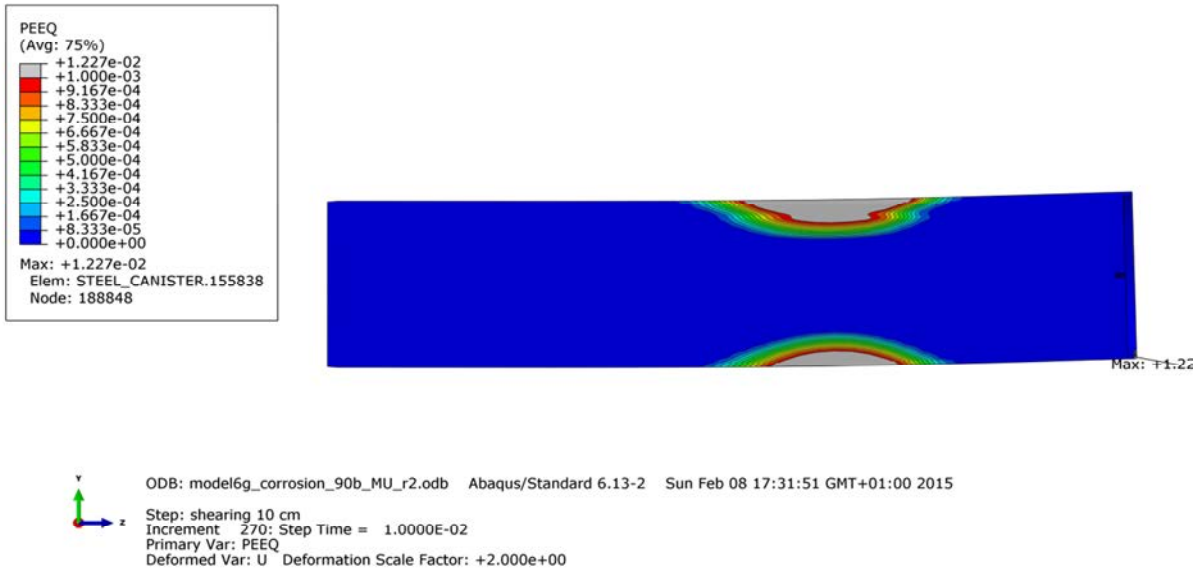

Figure A2-14. *Equivalent plastic strain (PEEQ) in the insert at 6 cm shearing.*

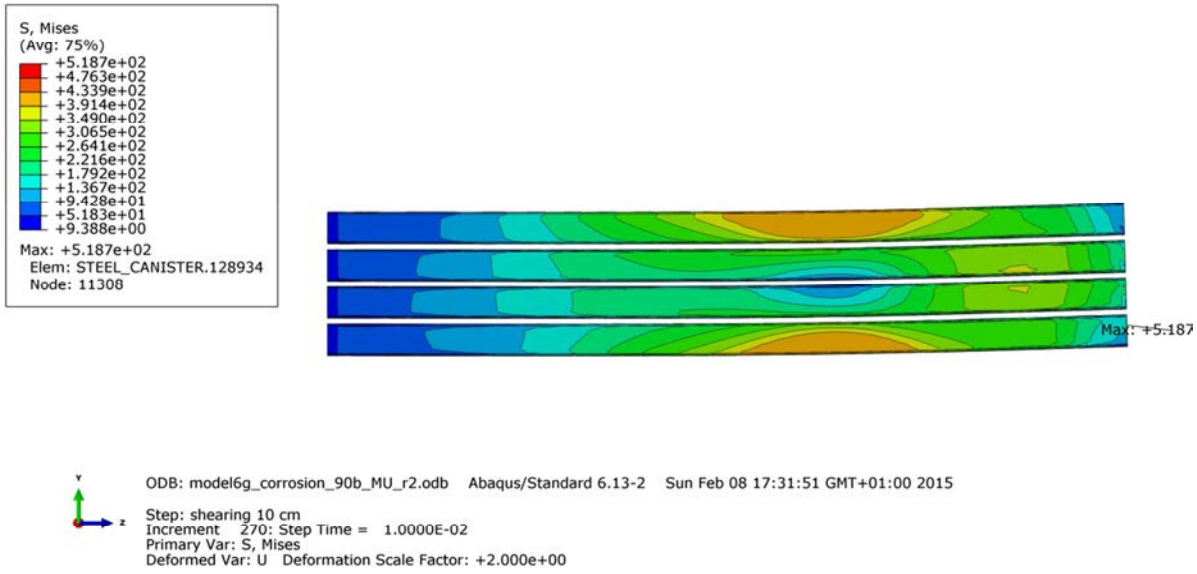

Figure A2-15. *Mises stress [MPa] in the channel tubes at 6 cm shearing.*

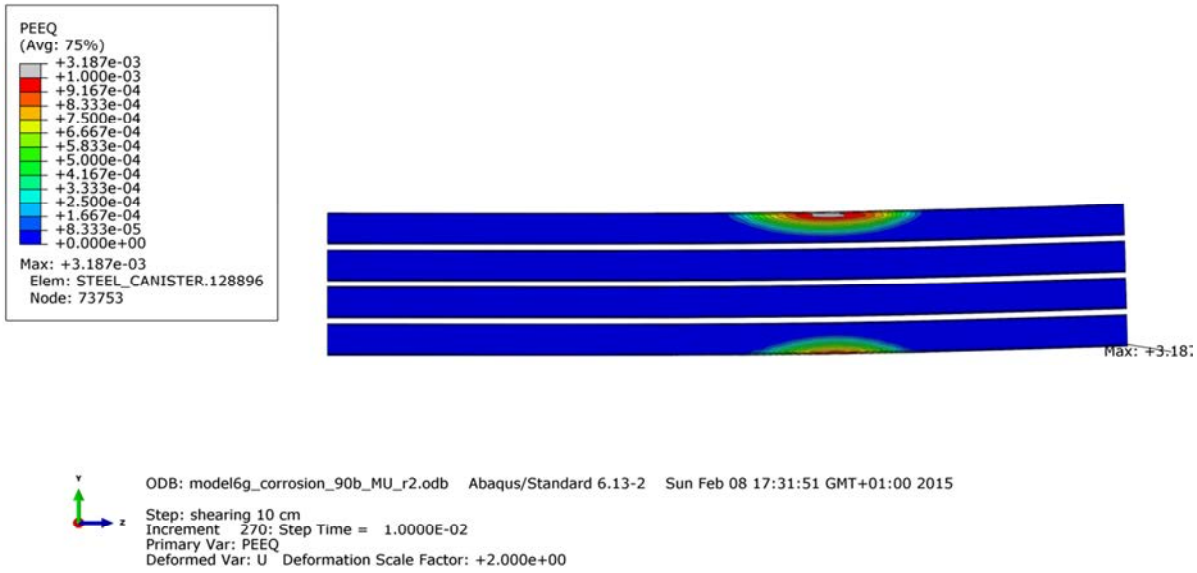

Figure A2-16. *Equivalent plastic strain (PEEQ) in the channel tubes at 6 cm shearing.*

Appendix 3 –Rock shear perpendicular to canister axis at the insert lid – copper with Kimab material model

Plots A3-1 to A3-16 showing deformed geometry, plastic strain (PEEQ), Mises stress (MISES) for shearing magnitudes 5 and 8 cm. Deformations scaled by factor 2.

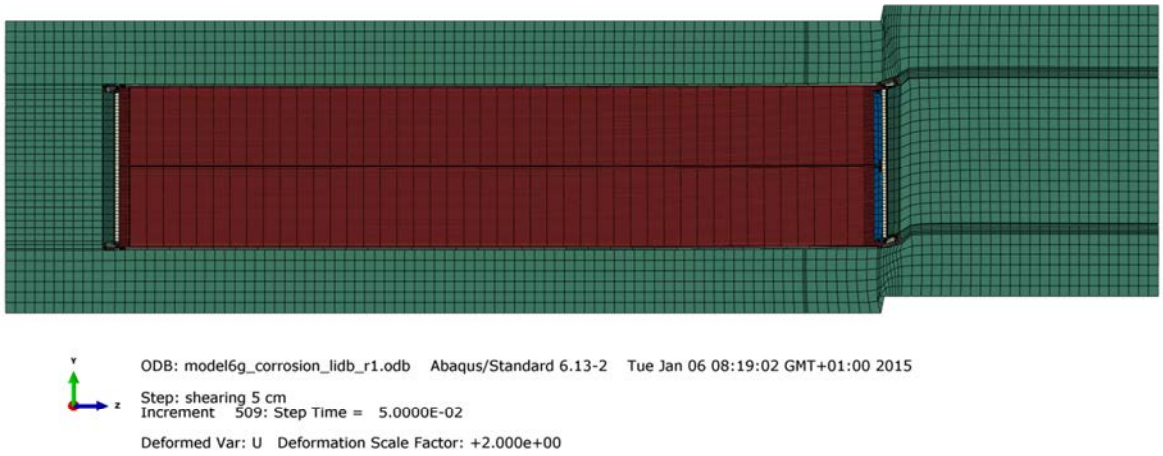

Figure A3-1. *Deformed geometry at 5 cm shearing.*

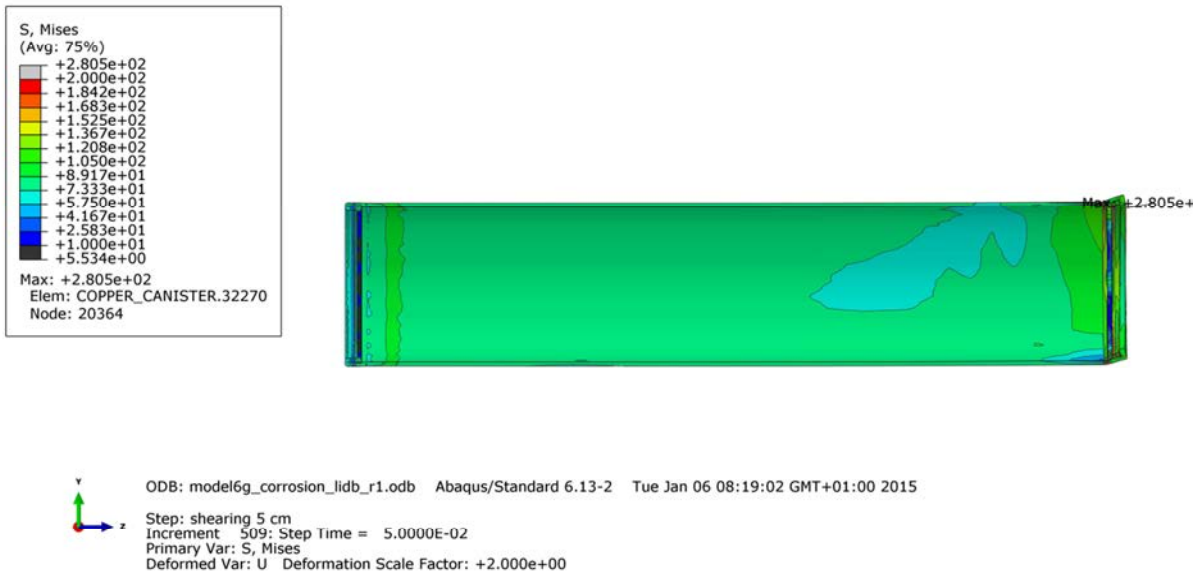

Figure A3-2. *Mises stress [MPa] in the copper shell at 5 cm shearing.*

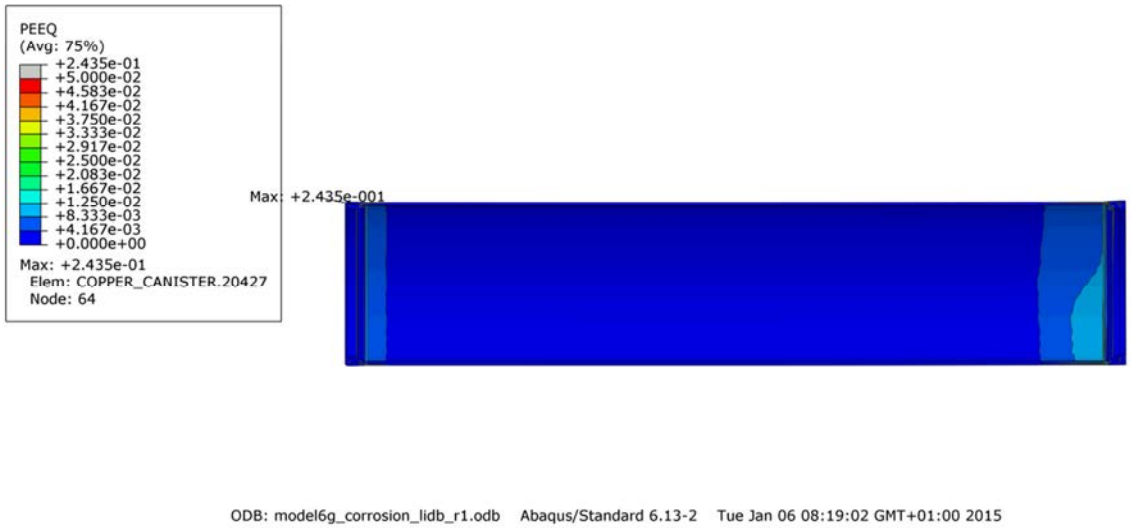

Figure A3-3. *Equivalent plastic strain (PEEQ) in the copper shell at 5 cm shearing.*

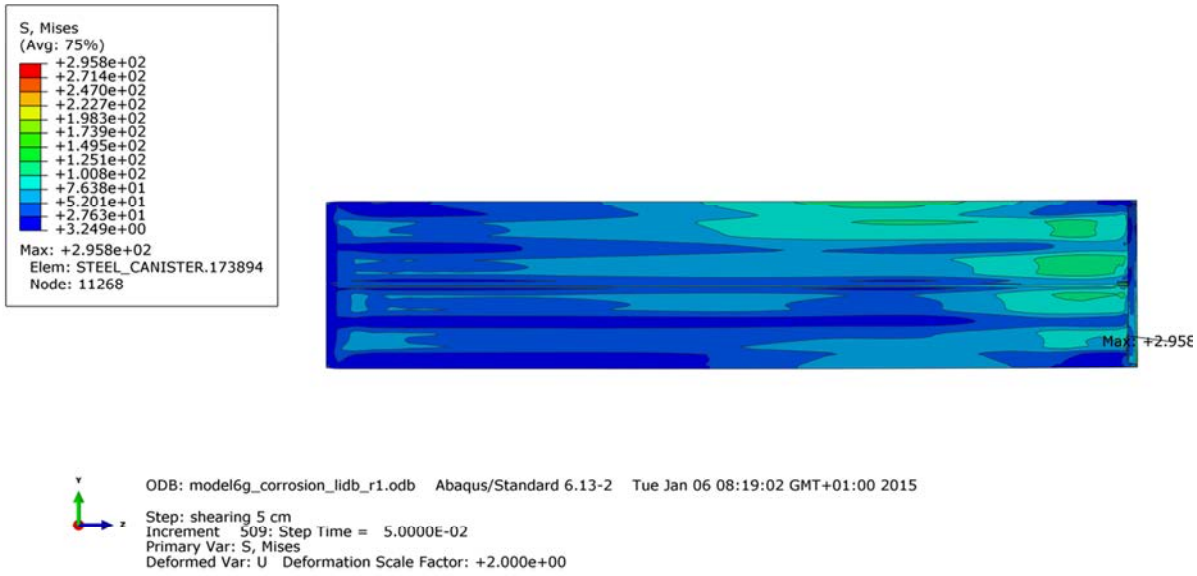

Figure A3-4. *Mises stress [MPa] in the insert at 5 cm shearing.*

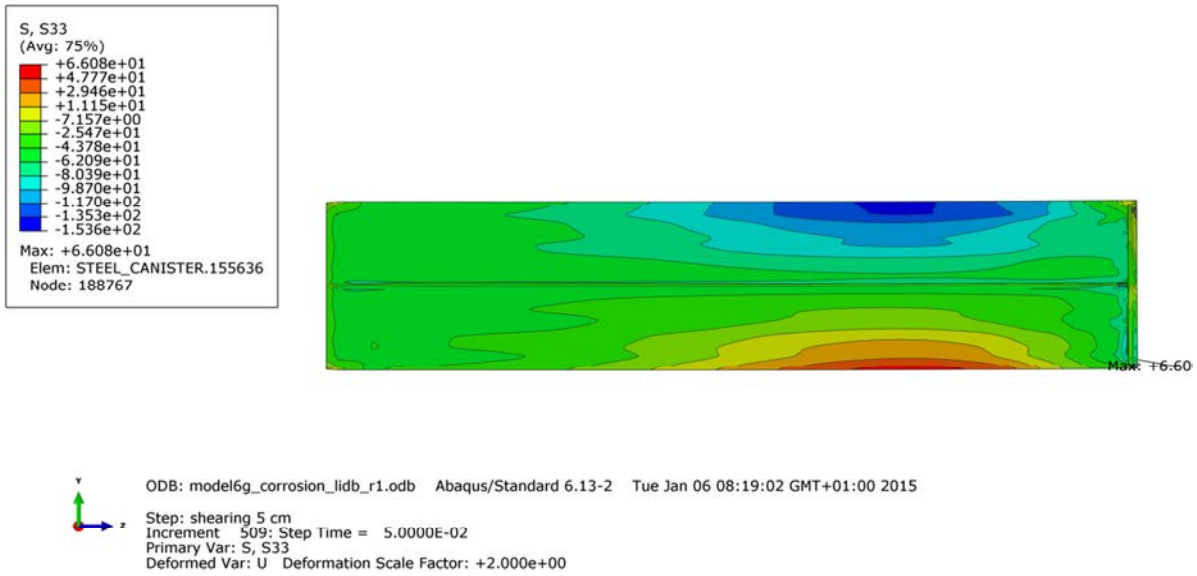

Figure A3-5. *Axial stress [MPa] in the insert at 5 cm shearing.*

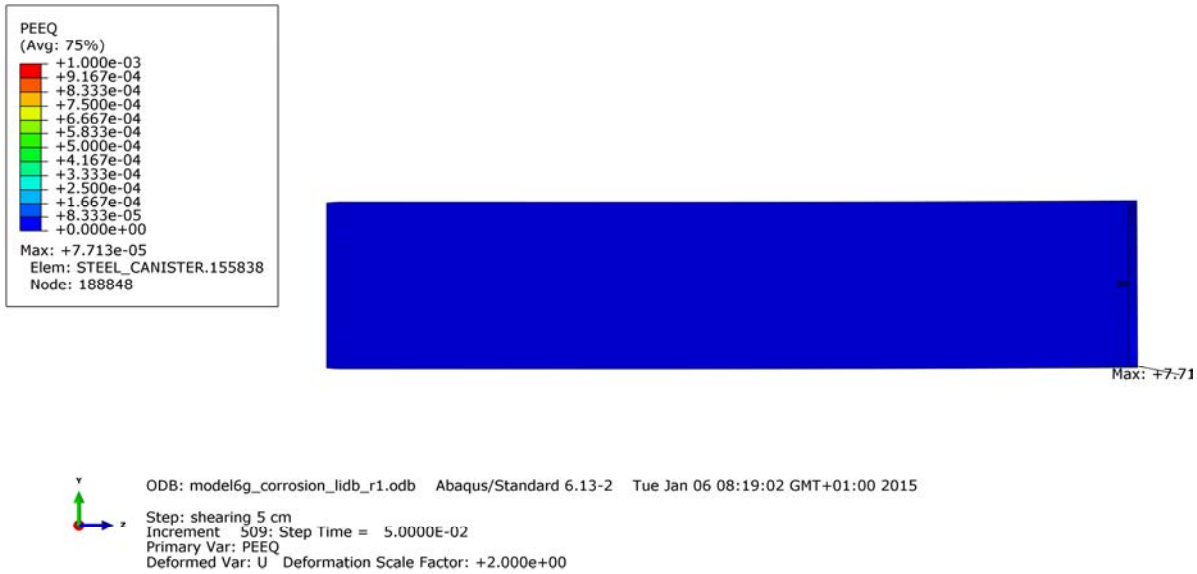

Figure A3-6. *Equivalent plastic strain (PEEQ) in the insert at 5 cm shearing.*

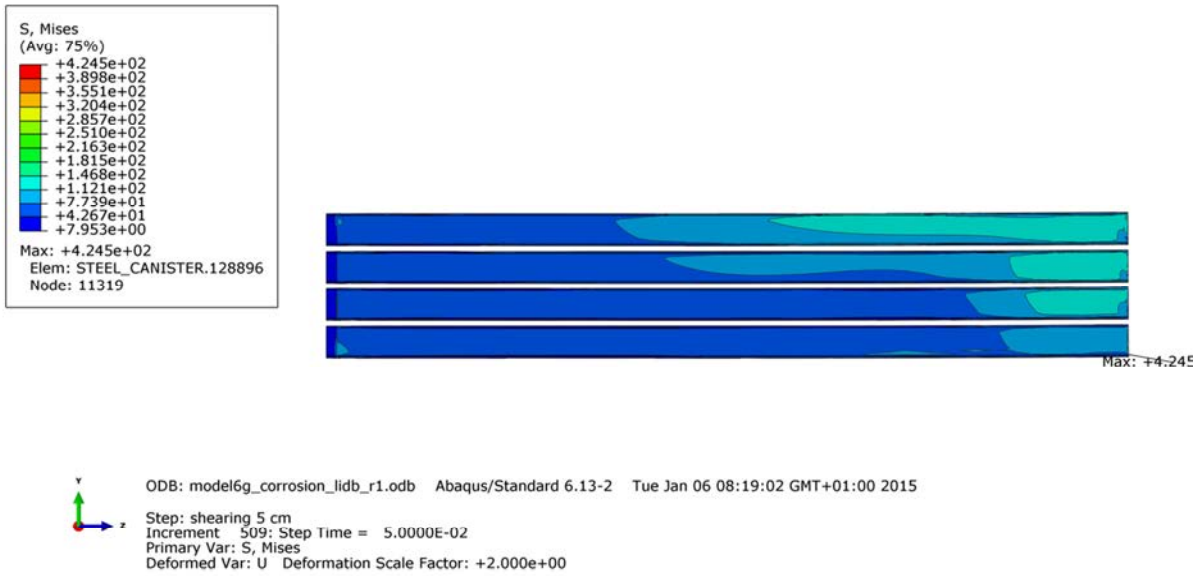

Figure A3-7. *Mises stress [MPa] in the channel tubes at 5 cm shearing.*

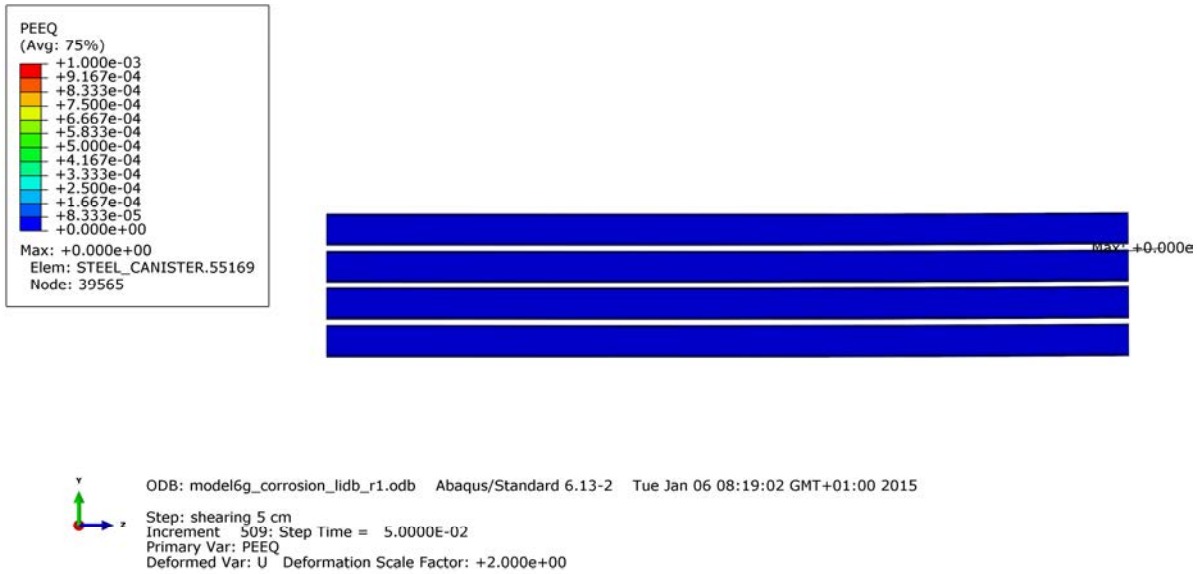

Figure A3-8. *Equivalent plastic strain (PEEQ) in the channel tubes at 5 cm shearing.*

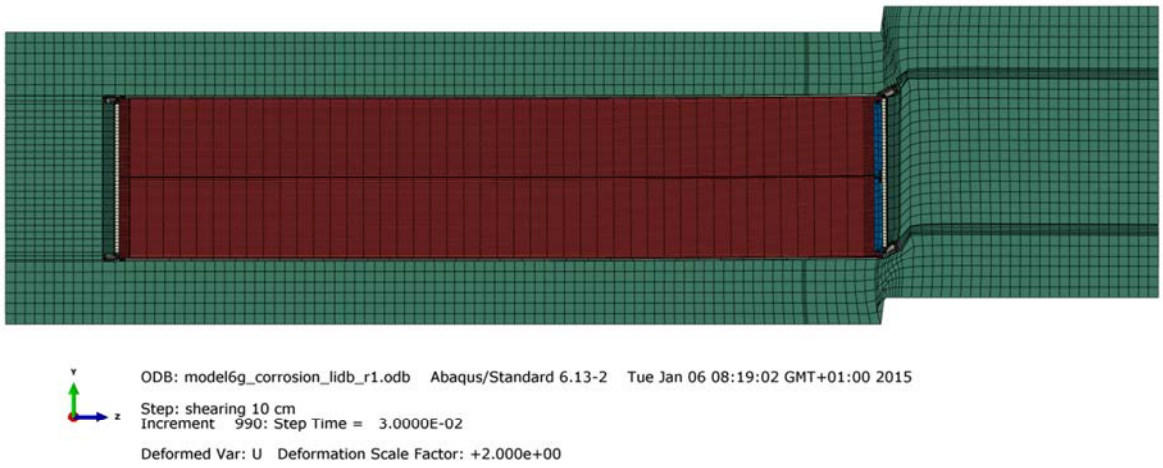

Figure A3-9. *Deformed geometry at 8 cm shearing.*

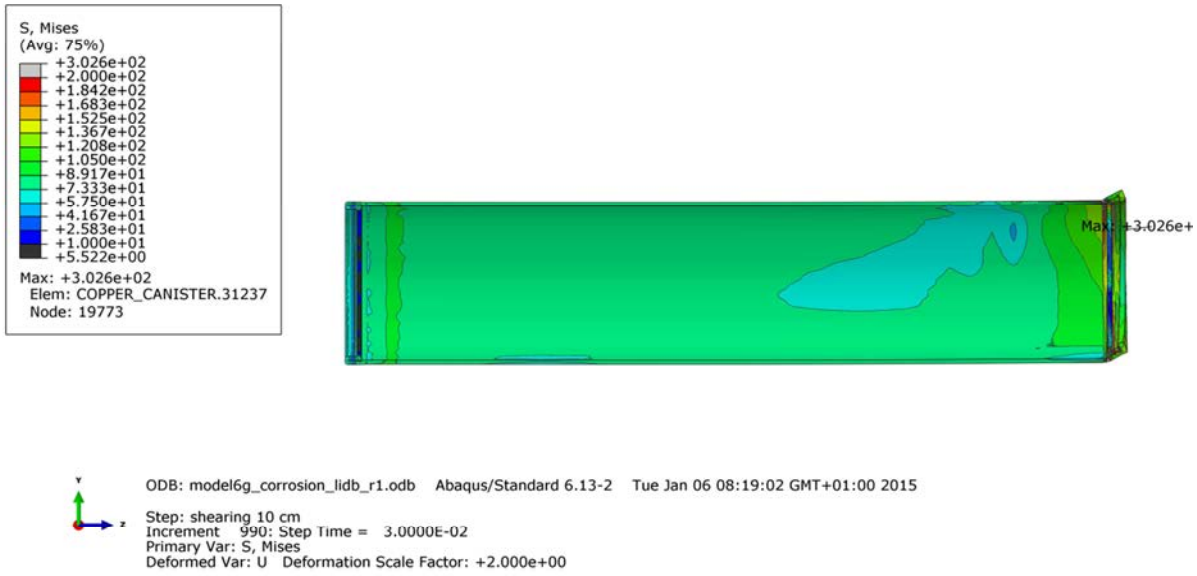

Figure A3-10. *Mises stress [MPa] in the copper shell at 8 cm shearing.*

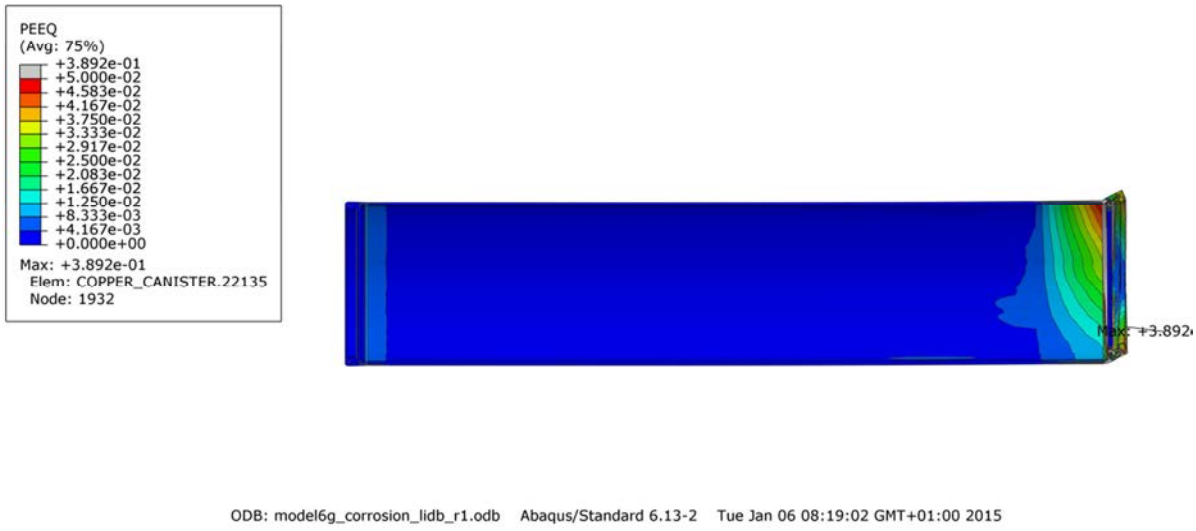

Figure A3-11. *Equivalent plastic strain (PEEQ) in the copper shell at 8 cm shearing.*

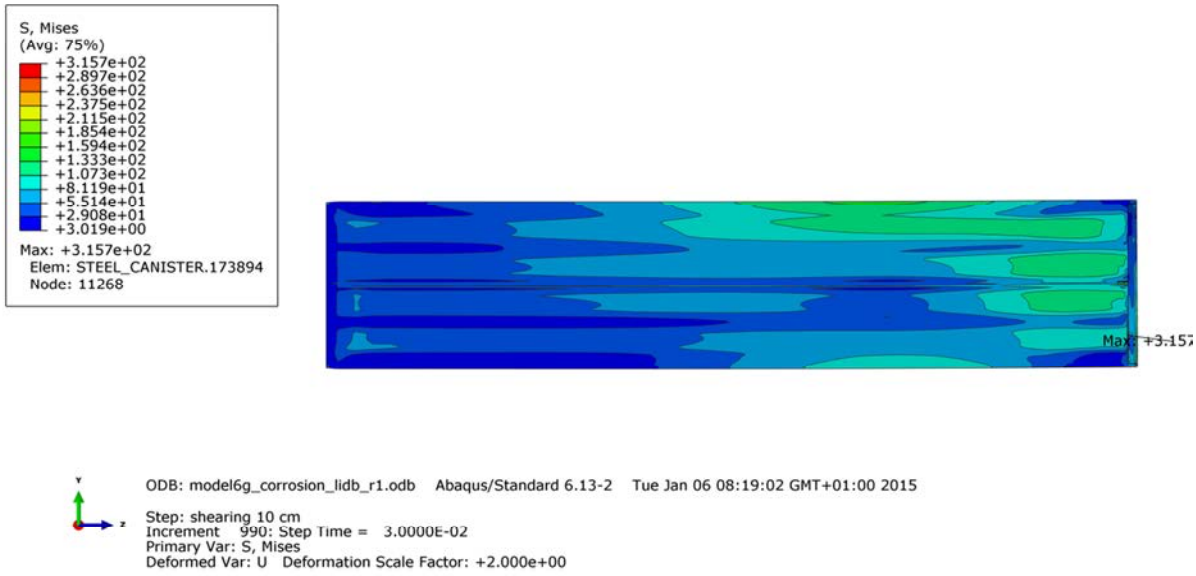

Figure A3-12. *Mises stress [MPa] in the insert at 8 cm shearing.*

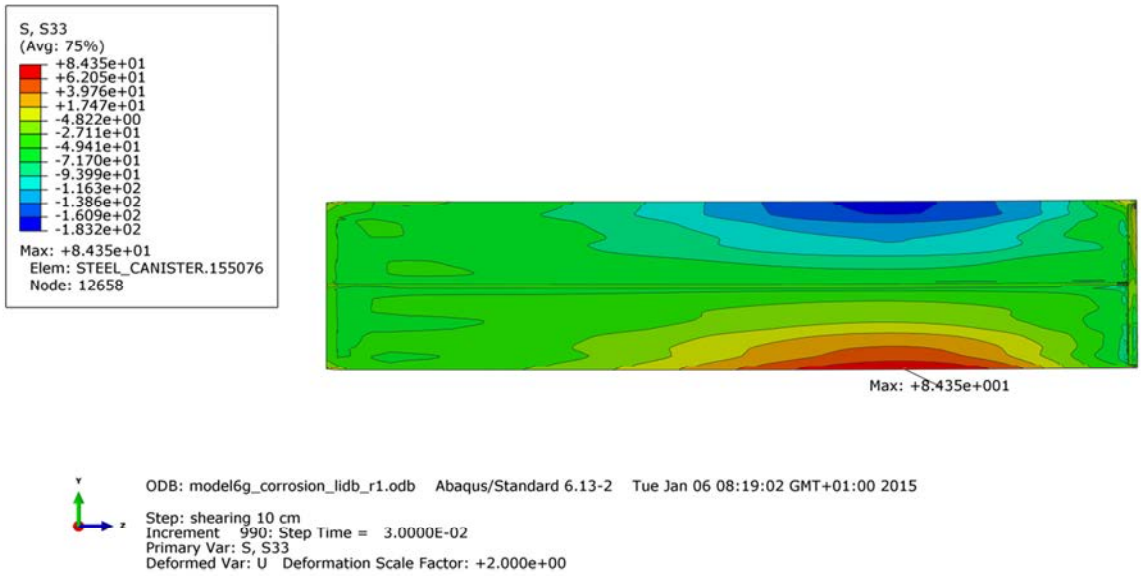

Figure A3-13. *Axial stress [MPa] in the insert at 8 cm shearing.*

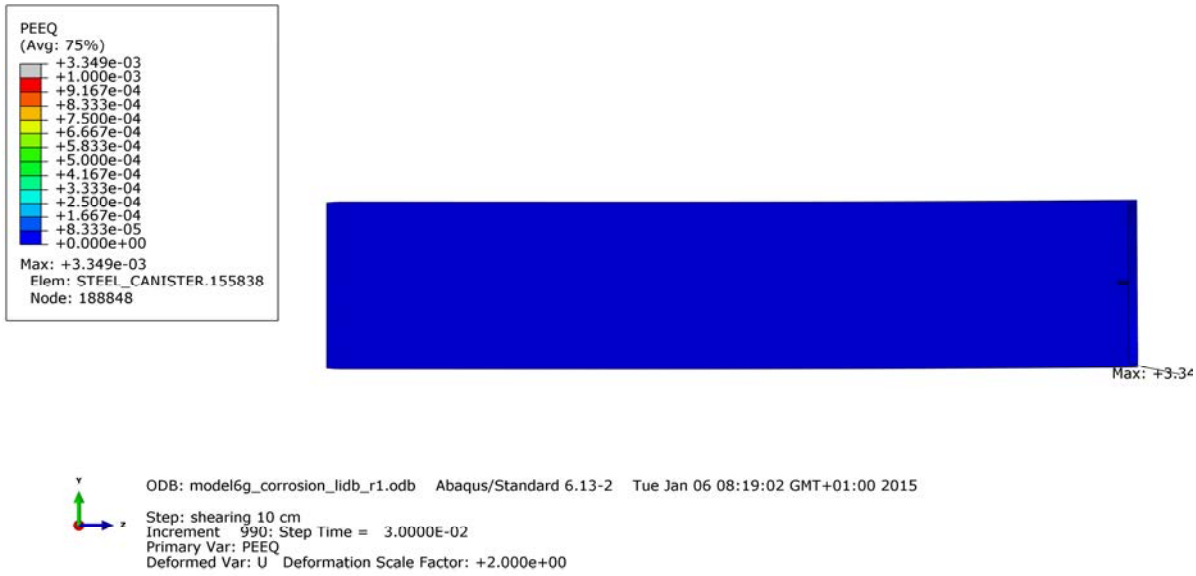

Figure A3-14. *Equivalent plastic strain (PEEQ) in the insert at 8 cm shearing.*

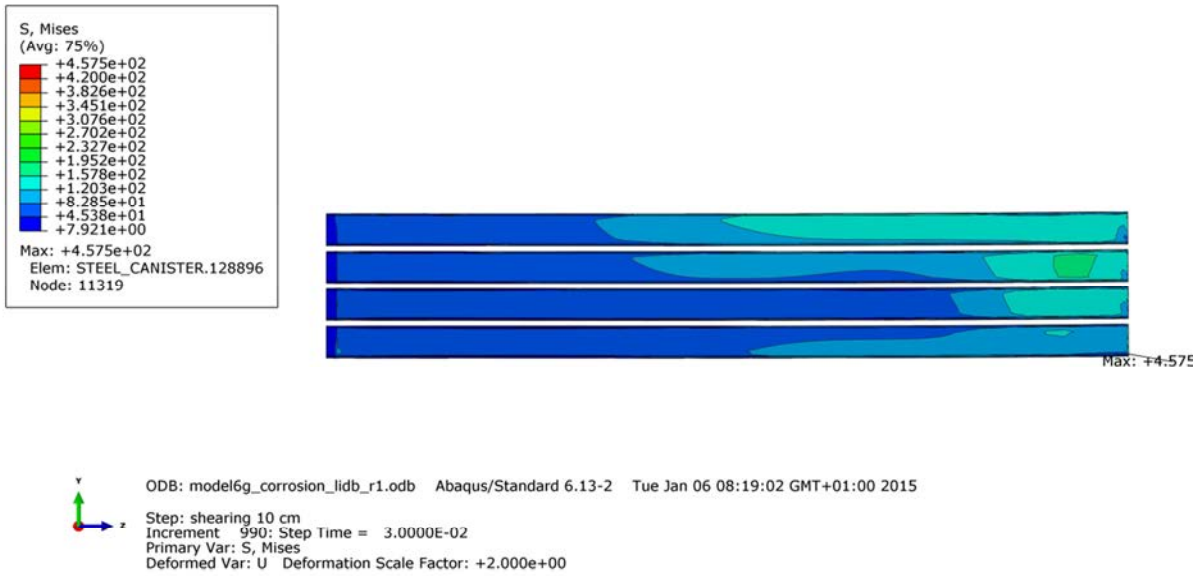

Figure A3-15. *Mises stress [MPa] in the channel tubes at 8 cm shearing.*

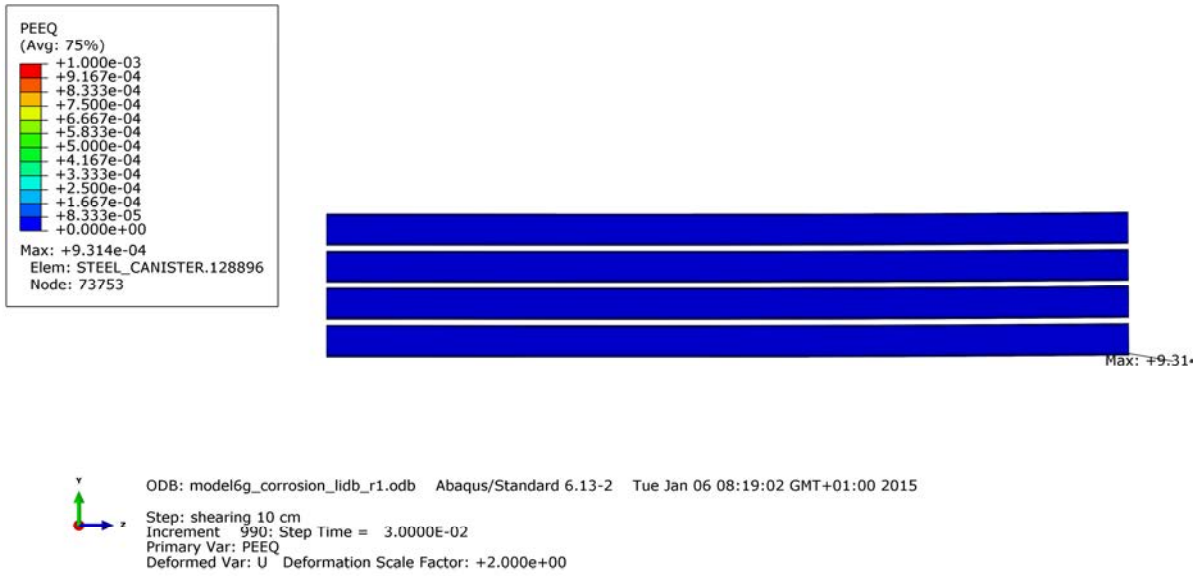

Figure A3-16. *Equivalent plastic strain (PEEQ) in the channel tubes at 8 cm shearing.*

Appendix 4 –Rock shear perpendicular to canister axis at the insert lid – copper with Unosson material model, (SKBdoc 1393179)

Plots A4-1 to A4-16 showing deformed geometry, plastic strain (PEEQ), Mises stress (MISES) for shearing magnitudes 5 and 8 cm. Deformations scaled by factor 2.

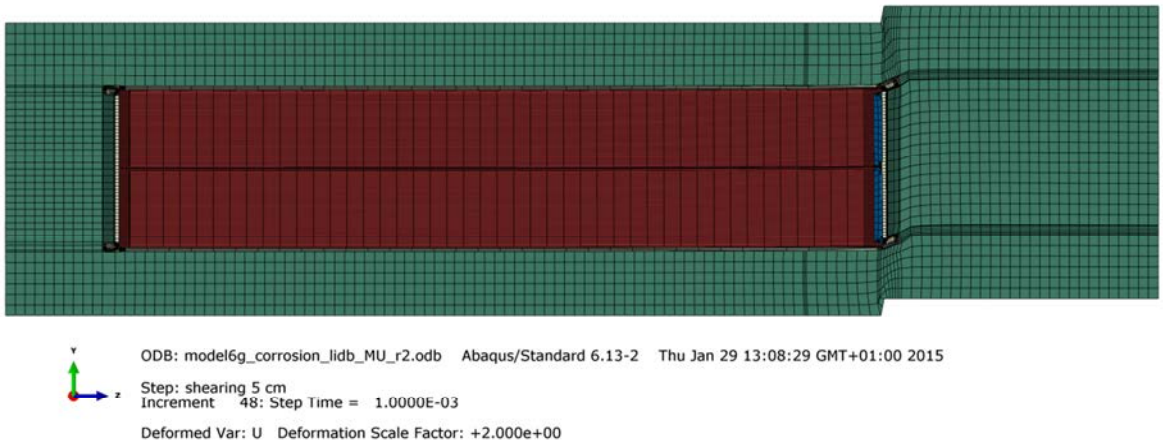

Figure A4-1. *Deformed geometry at 5 cm shearing.*

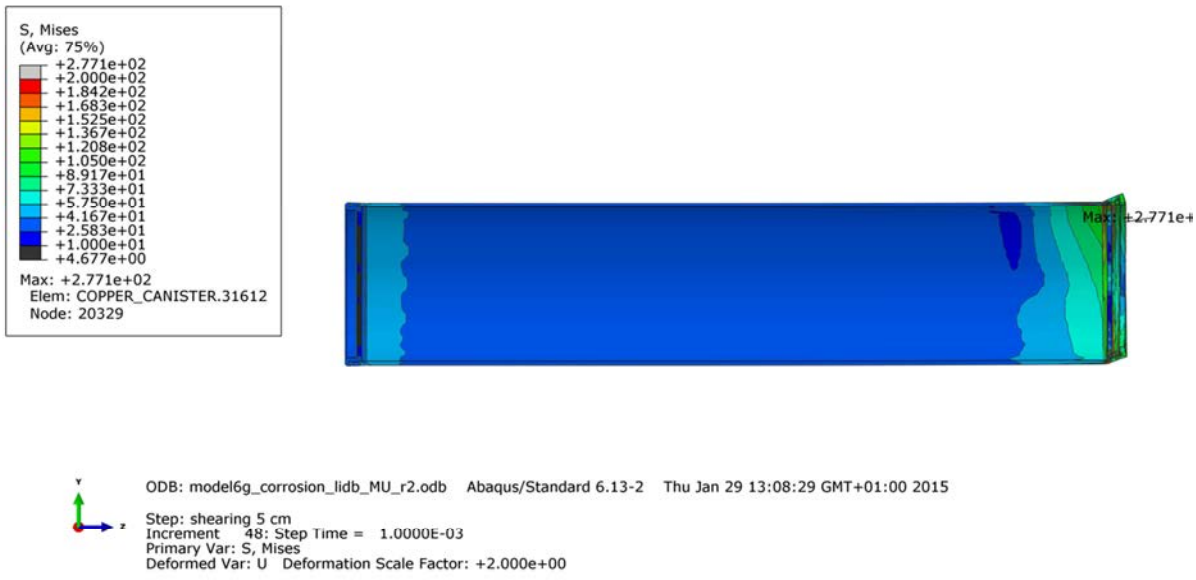

Figure A4-2. *Mises stress [MPa] in the copper shell at 5 cm shearing.*

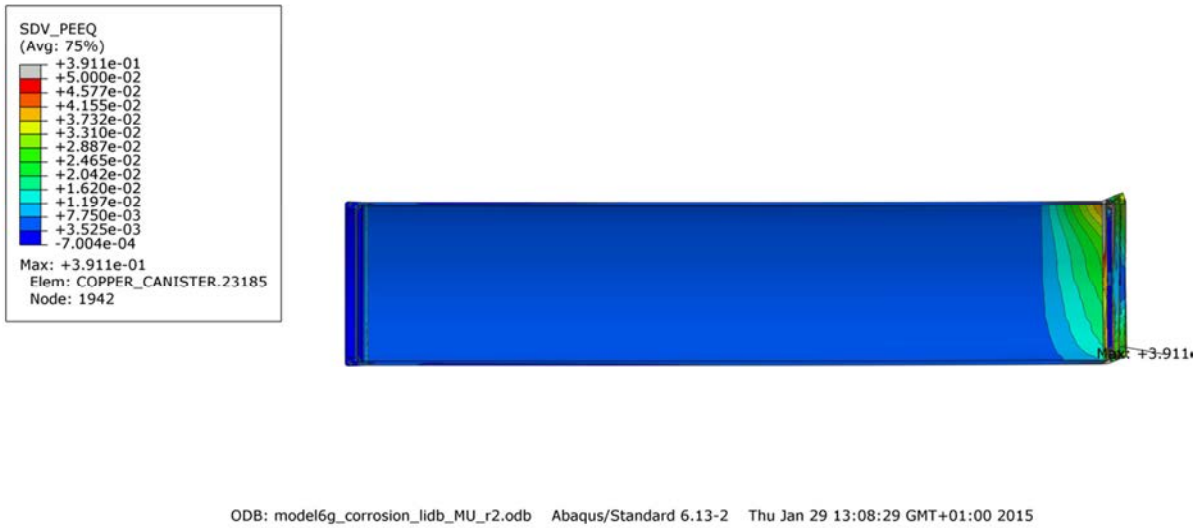

Figure A4-3. *Equivalent plastic strain (PEEQ) in the copper shell at 5 cm shearing.*

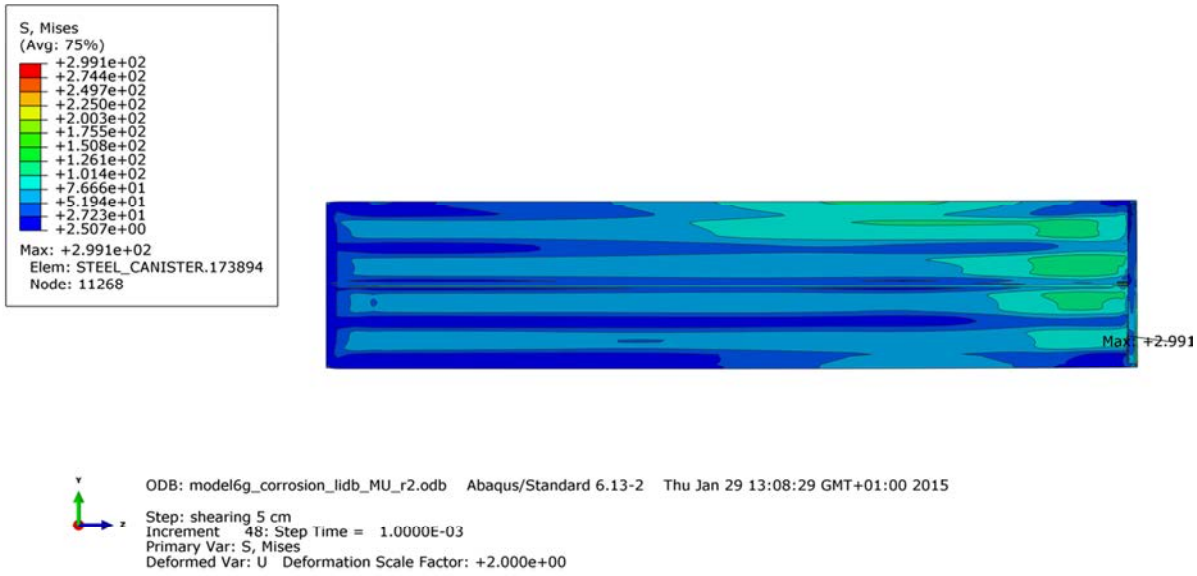

Figure A4-4. *Mises stress [MPa] in the insert at 5 cm shearing.*

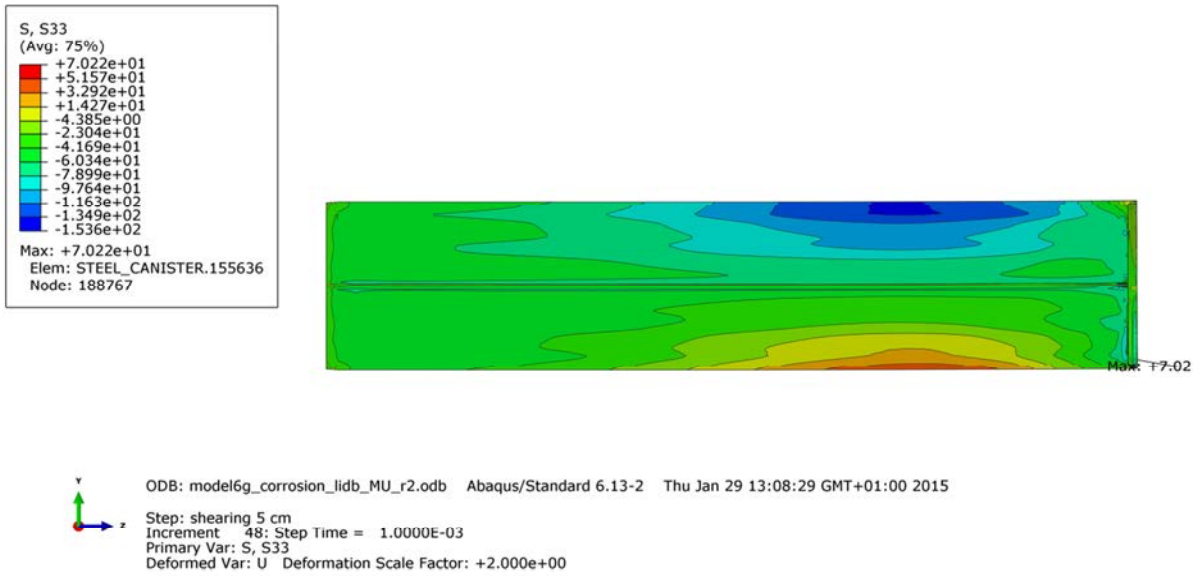

Figure A4-5. *Axial stress [MPa] in the insert at 5 cm shearing.*

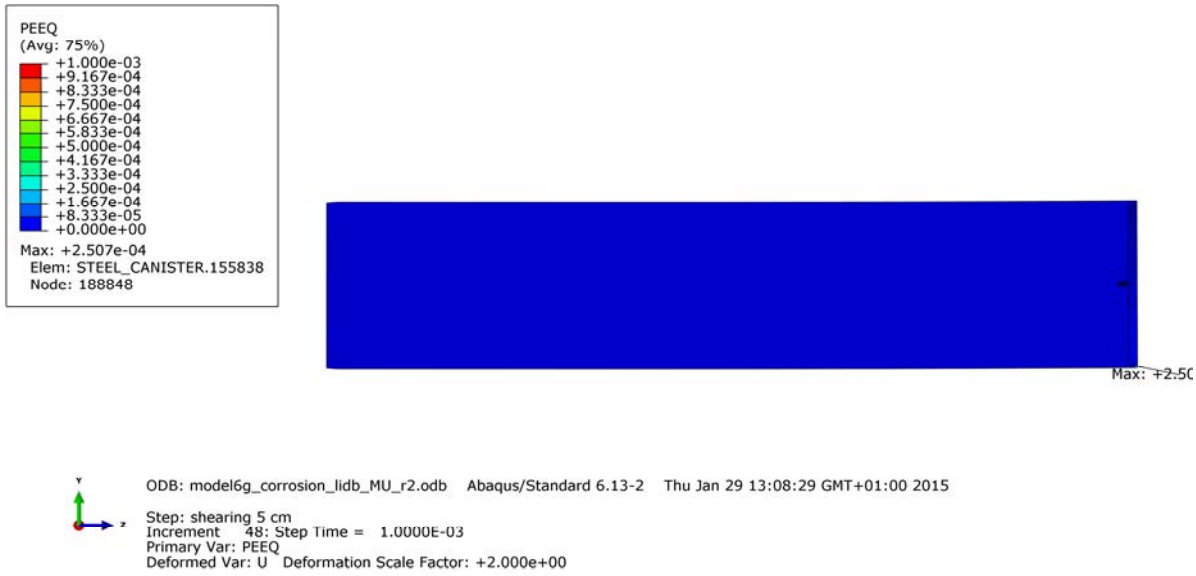

Figure A4-6. *Equivalent plastic strain (PEEQ) in the insert at 5 cm shearing.*

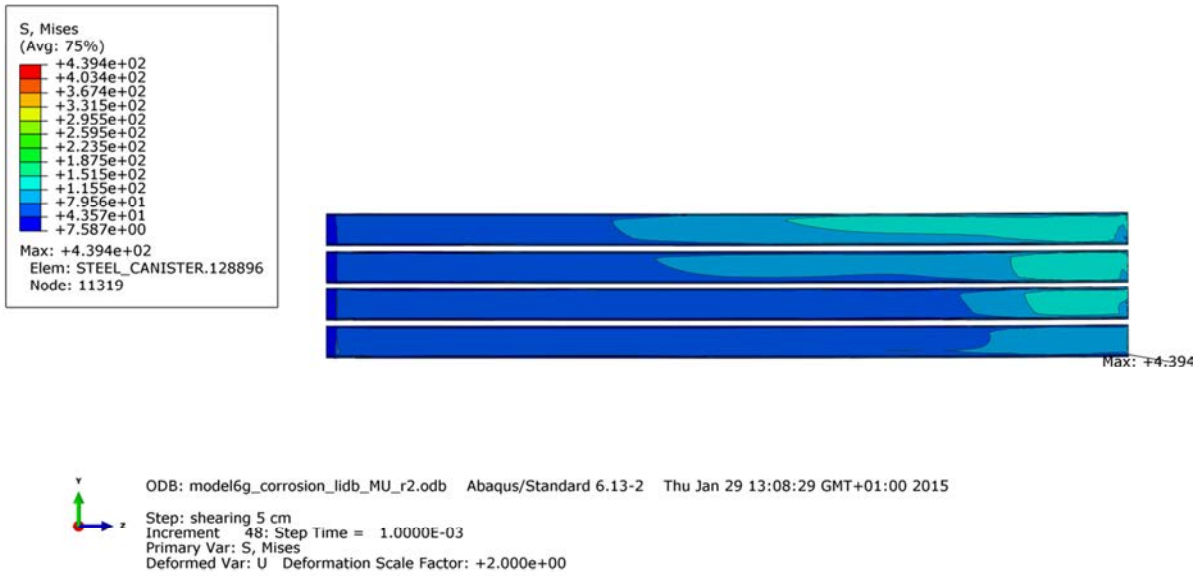

Figure A4-7. *Mises stress [MPa] in the channel tubes at 5 cm shearing.*

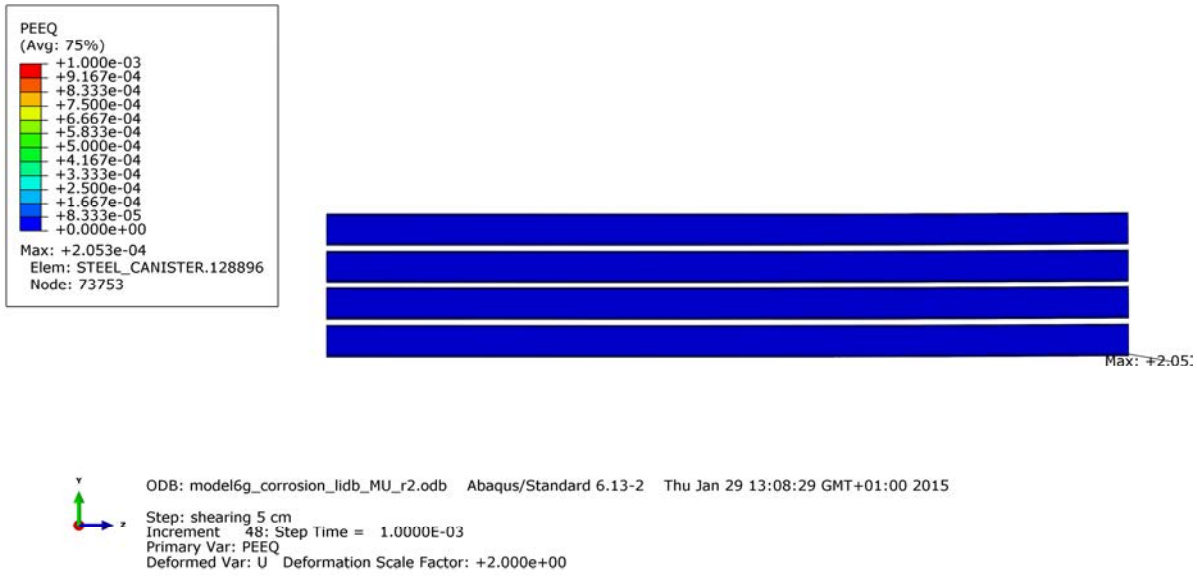

Figure A4-8. *Equivalent plastic strain (PEEQ) in the channel tubes at 5 cm shearing.*

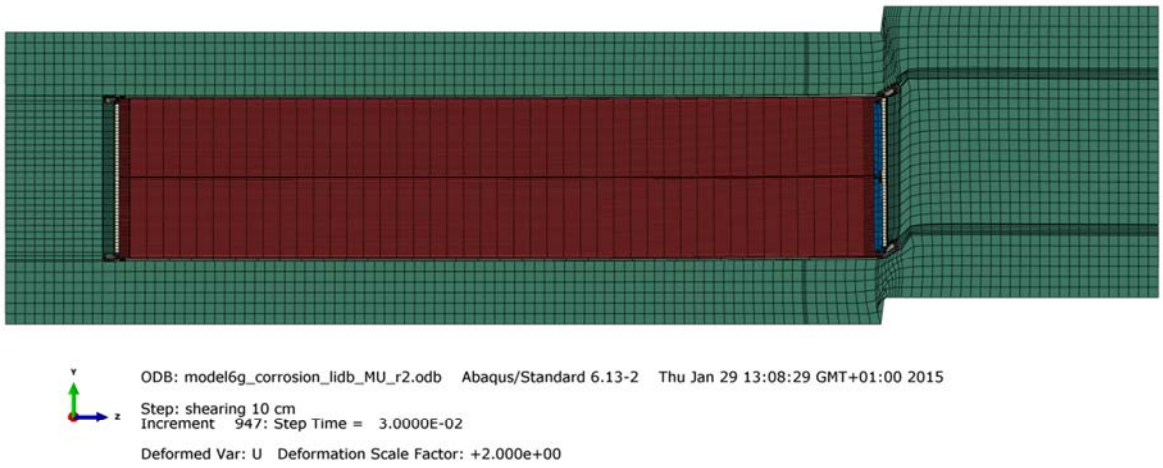

Figure A4-9. *Deformed geometry at 8 cm shearing.*

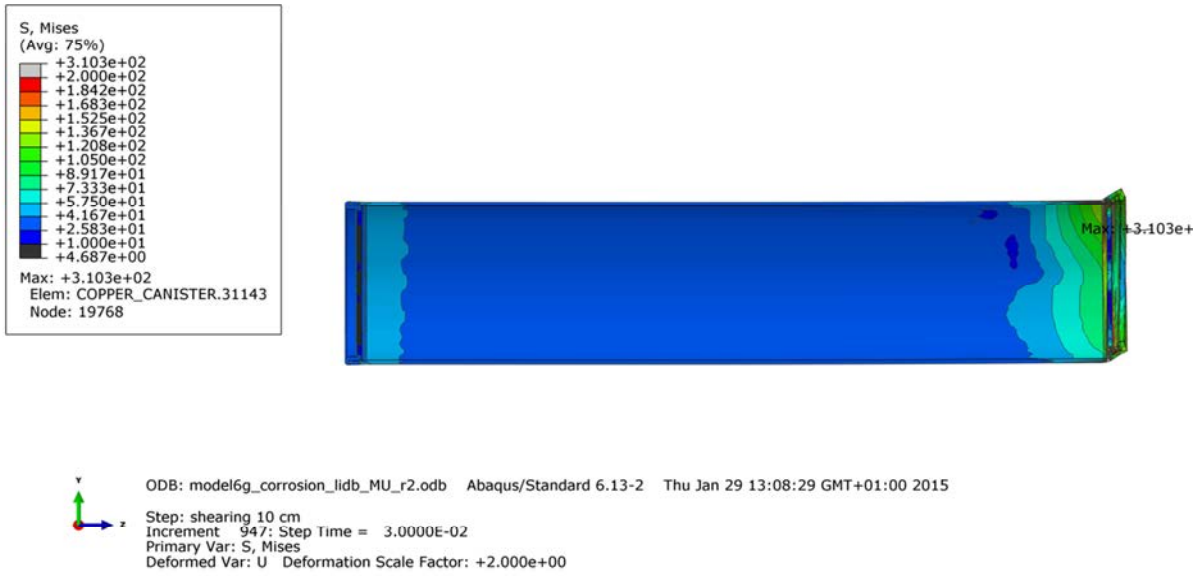

Figure A4-10. *Mises stress [MPa] in the copper shell at 8 cm shearing.*

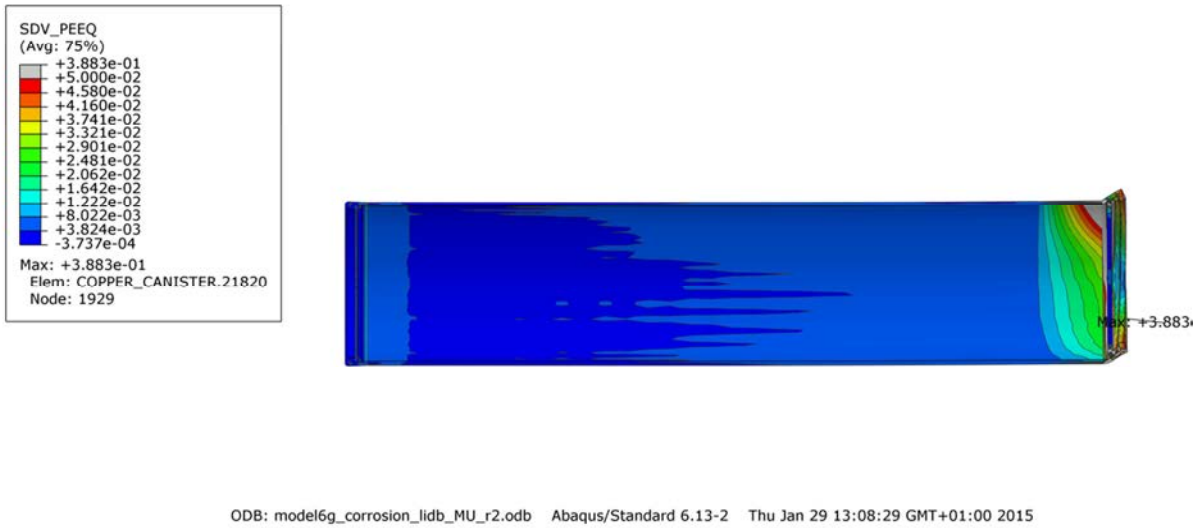

Figure A4-11. *Equivalent plastic strain (PEEQ) in the copper shell at 8 cm shearing.*

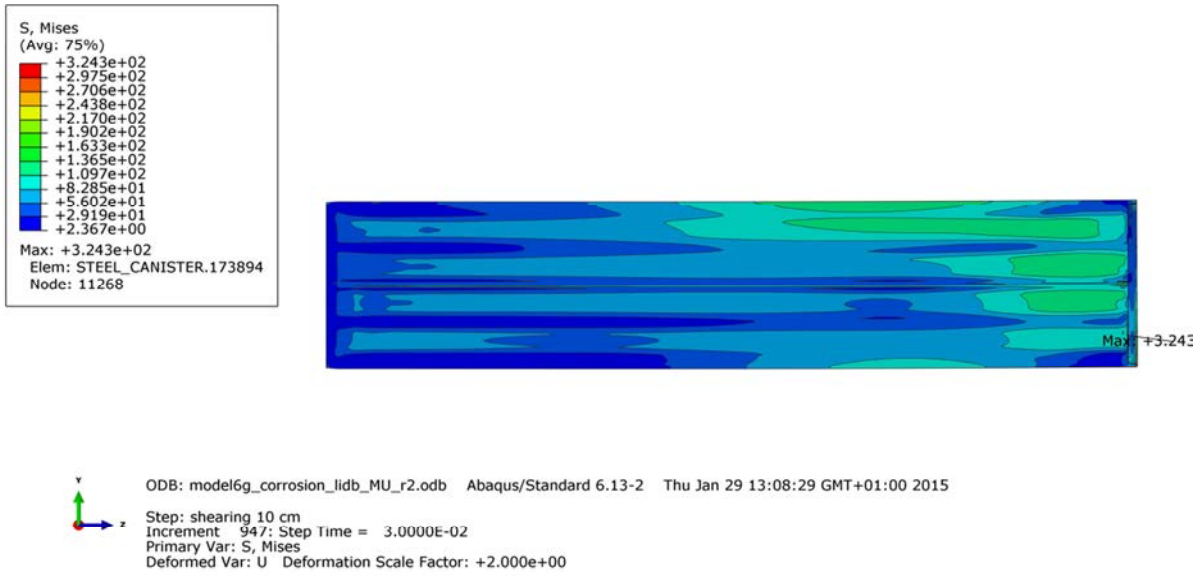

Figure A4-12. *Mises stress [MPa] in the insert at 8 cm shearing.*

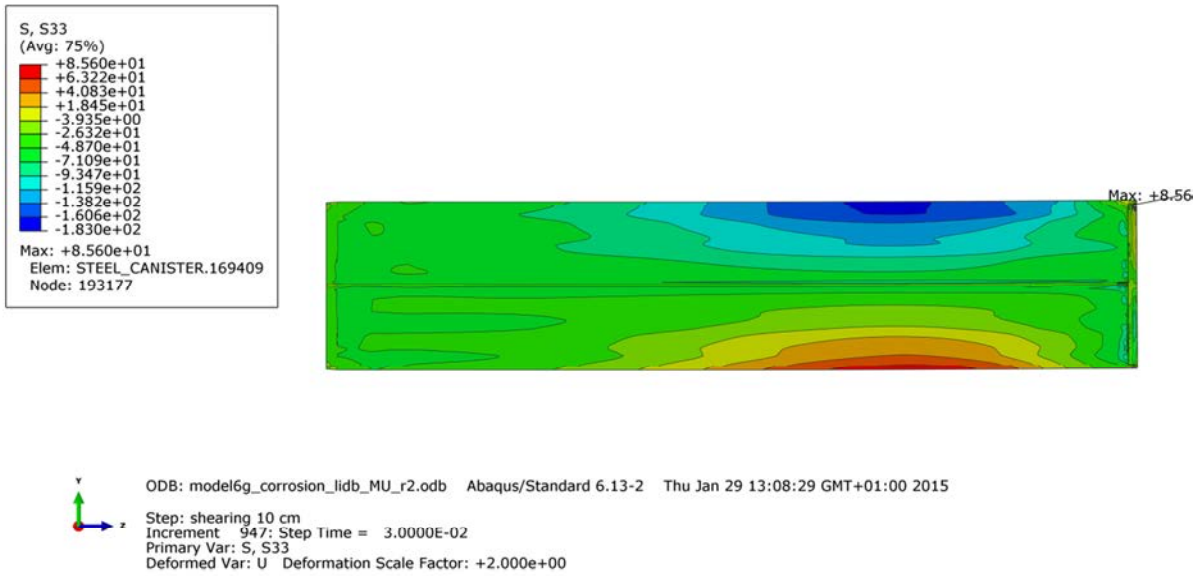

Figure A4-13. *Axial stress [MPa] in the insert at 8 cm shearing.*

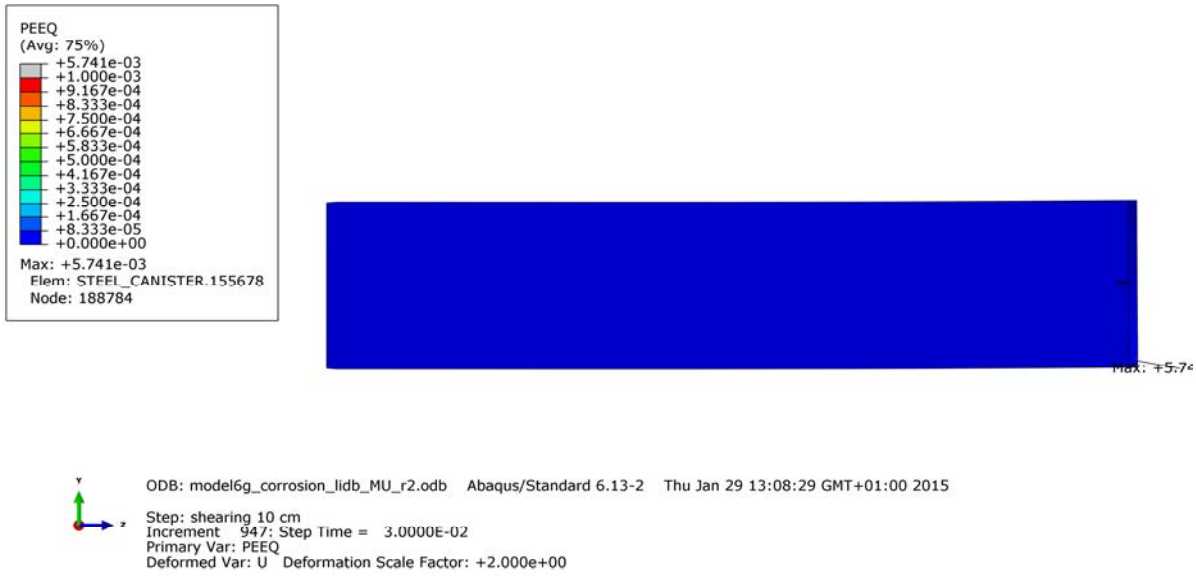

Figure A4-14. *Equivalent plastic strain (PEEQ) in the insert at 8 cm shearing.*

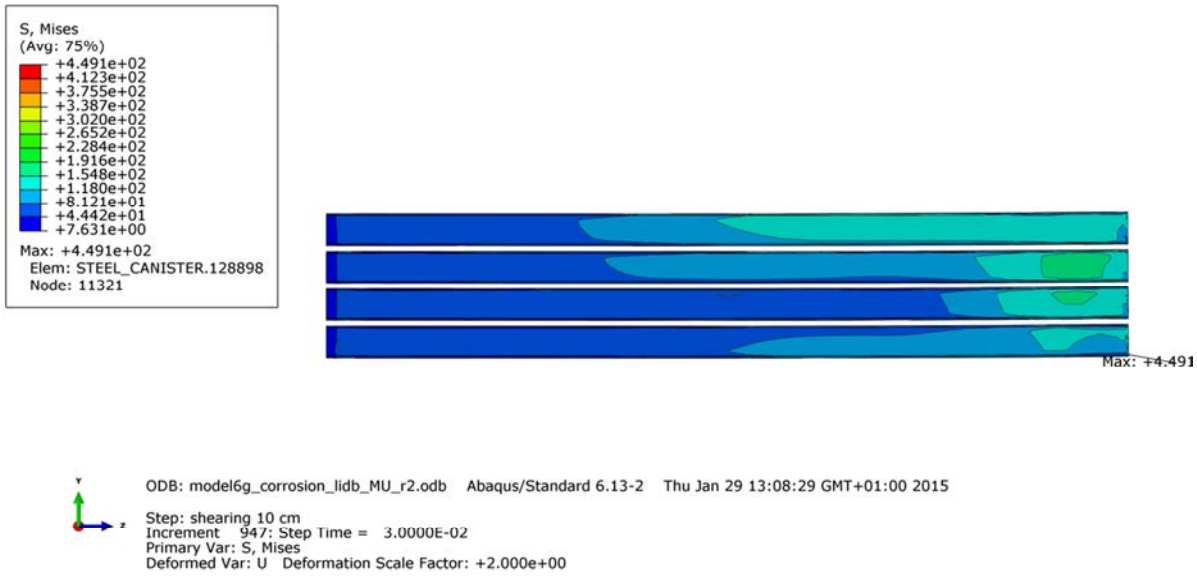

Figure A4-15. *Mises stress [MPa] in the channel tubes at 8 cm shearing.*

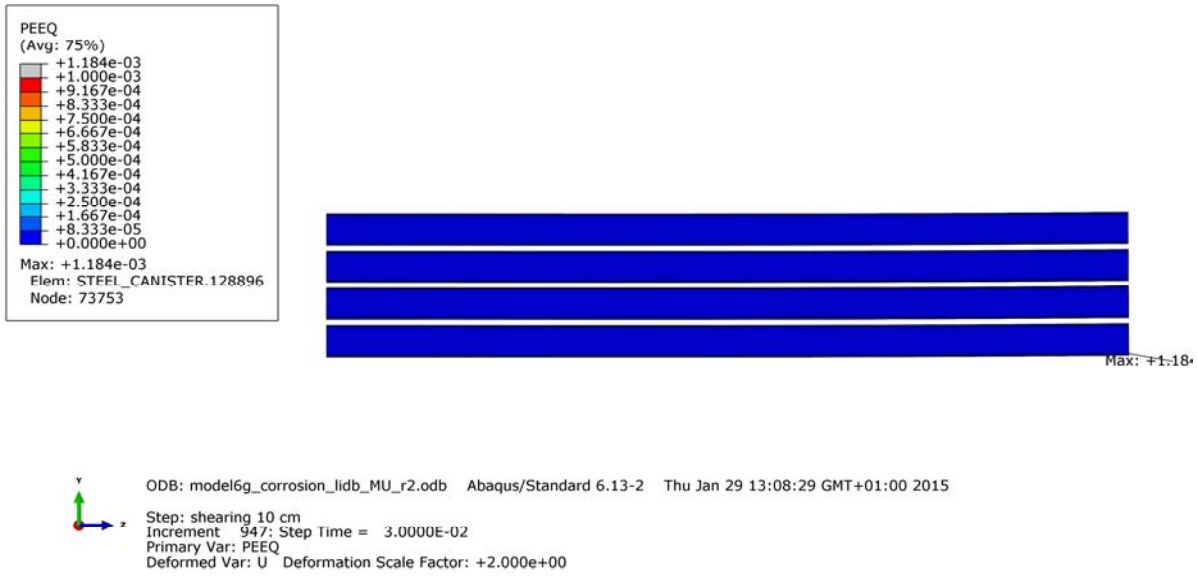

Figure A4-16. *Equivalent plastic strain (PEEQ) in the channel tubes at 8 cm shearing.*

Appendix 5 – Storage of files

This report is based on the results from a lot of FE-simulations using ABAQUS which is a commercial available code and is thus not stored as part of the work. Below is a short description of files used in the project and directories for storage of these. These files are also stored at SKB.

The files are stored in directories as:

geometry
Input-files
plots
Report_global_model_shear_test_modelling-version100305.doc - this report
scripts

1 – Plot-files used in the report

Contents in C:\Users\jhd\mappar\skb\kapsel\design_report_final\plots

model6g_normal-mesh.png	- Fig 1
model6g_normal-corner_mesh.png	- Fig 3
model6g_lid_mesh.png	- Fig 6
model6g_copper_mesh.png	- Fig 7
model5_2_2050ca3_nobentonite-bc_xsymm.png	- Fig 11
model5_2_2050ca3_nobentonite-bc_rigid.png	- Fig 12
model6g_copper_materials.png	- Fig 14
modelg6_copper_output_regions.png	- Fig 15
model6g_normal_half_2050ca3-copper_peeq_5cm_detailbot.png	- Fig 16
model6g_normal_half_2050ca3-peeq_bot.png	- Fig 16
model6g_normal_half_2050ca3-copper_peeq_5cm_detail.png	- Fig 17
model6g_normal_half_2050ca3-peeq_top.png	- Fig 17
model6g_normal_half_2050ca3_copper_peeq_5cm_detailbot2.png	- Fig 18
model6g_normal_half_2050ca3-peeq_bot_fillet.png	- Fig 18
model6g_normal_half_2050ca3_copper_peeq_5cm_detailtop2.png	Fig 19
model6g_normal_half_2050ca3-peeq_top_fillet.png	- Fig 19
model6g_normal_quarter_2050ca3-insert_iron-peeq_5cm_detail.png	- Fig 20
model6g_normal_half_2050ca3-peeq_iron_insert..png	- Fig 20
model6g_normal_half_2050ca3_channel_peeq_5cm_detail.png	- Fig 21
model6g_normal_half_2050ca3-peeq_steel_channel..png	- Fig 21

Plot files used in the report

Appendix 1
model6g_normal_quarter_2050ca3- 5cm_deformed.png
model6g_normal_quarter_2050ca3- 5cm_maxPrin_insert.png
model6g_normal_quarter_2050ca3- 5cm_mises_copper.png
model6g_normal_quarter_2050ca3- 5cm_mises_insert.png
model6g_normal_quarter_2050ca3- 5cm_peeq_copper.png
model6g_normal_quarter_2050ca3- 5cm_peeq_insert.png
model6g_normal_quarter_2050ca3-10cm_deformed.png
model6g_normal_quarter_2050ca3-10cm_maxPrin_insert.png
model6g_normal_quarter_2050ca3-10cm_mises_copper.png
model6g_normal_quarter_2050ca3-10cm_mises_insert.png
model6g_normal_quarter_2050ca3-10cm_peeq_copper.png
model6g_normal_quarter_2050ca3-10cm_peeq_insert.png
model6g_normal_quarter_2050ca3-peeq_iron_insert.png
model6g_normal_quarter_2050ca3-peeq_steel_channel.png
model6g_normal_quarter_2050ca3-s33_castiron.png
model6g_normal_quarter_2050ca3-s33_steelchannels.png

Appendix 2
model6g_normal_half_2050ca3- 5cm_deformed.png
model6g_normal_half_2050ca3- 5cm_maxPrin_insert.png
model6g_normal_half_2050ca3- 5cm_mises_copper.png
model6g_normal_half_2050ca3- 5cm_mises_insert.png
model6g_normal_half_2050ca3- 5cm_peeq_copper.png
model6g_normal_half_2050ca3- 5cm_peeq_insert.png
model6g_normal_half_2050ca3-10cm_deformed.png
model6g_normal_half_2050ca3-10cm_maxPrin_insert.png
model6g_normal_half_2050ca3-10cm_mises_copper.png
model6g_normal_half_2050ca3-10cm_mises_insert.png
model6g_normal_half_2050ca3-10cm_peeq_copper.png
model6g_normal_half_2050ca3-10cm_peeq_insert.png

2 – Input files used for the simulations
Each analysis is started by abaqus job=input-file (w/o .inp).

Files with extension “incl” are referenced by some of the input-files (extension “inp”).

Contents in C:\Users\jhd\mappar\skb\kapsel\design_report_final\Input-files

model6g_axial_mid_2050ca3.inp
model6g_axial_quarter_2050ca3.inp
model6g_hori_2050ca3.inp
model6g_hori_quarter_2050ca3.inp
model6g_normal_half_2050ca3.inp
model6g_normal_quarter_2050ca3.inp - global model with density 2050

model6g_material.incl - material definitions used by all input-files
model6g_normal_quarter_pressure1a_2050ca3_cload.incl - load definition used
model6g_normal_quarter_pressure2a_2050ca3_cload.incl

4 – Scripts used for post-processing

Used inside ABAQUS/CAE or by abaqus cae startup=script.py after appropriate editing of job-name inside the script-file.

Contents in C:\Users\jhd\mappar\skb\kapsel\design_report_final\scripts

active_elements.py
model6g_copper_material.py
model6g_displaygroups.py
model6g_full_display.py
model6g_full_post.py
model6g_geom.py
model6g_special.py
model6_nobentonite.py
model_2step_vp1.py

5 – Geometry definitions

Contents in C:\Users\jhd\mappar\skb\kapsel\design_report_final\geometry

model6g.cae model6g.jnl - ABAQUS/CAE-database and journal files

CAD-geometries received from SKB:

IDE-00015-111-CALC_plan_top.igs
IDE-00015-111-CALC_plan_top.stp
IDE-00015-111-CALC_plan_top_R02.igs
IDE-00015-111-CALC_plan_top_R02.stp
IDE-00015-111-CALC_R03.stp

PWR_INSATS_CALK.stp
Ritningar_kapsel.pdf
sammanst„llning svetsad kopparcylinder_m†tt fr†n IDE-00015_sheet 1.pdf
sammanst„llning svetsad kopparcylinder_m†tt fr†n IDE-00015_sheet 2.pdf
sammanst„llning svetsad kopparcylinder_m†tt fr†n IDE-00015_sheet 3.pdf

SKB00-IDE-00015-CALC.igs
SKB00-IDE-00015-CALC.stp
SKB00-IDE-00015-CALC_02.stp
SKB00-IDE-00015-CALC_old.stp
SKB00-IDE-00015.igs
SKB00-IDE-00015.stp
_0816123248_001.pdf
_0903090815_001.pdf